UNIVERSITY OF MISKOLC

MIKOVINY SÁMUEL DOCTORAL SCHOOL OF EARTH SCIENCES

Head of the Doctoral School:

Prof. Dr. Péter Szűcs

AN INTEGRATED GEO-HYDRO-INFORMATICS APPROACH FOR GROUNDWATER POTENTIAL ASSESSMENT IN THE HIGHLAND OF ERITREA

PhD Thesis By:

Kabral Mogos Asghede

Scientific supervisor:

Dr. János Vágó

Miskolc, 2026

HUNGARY

Dedication

With heartfelt gratitude, I dedicate this work to my family, friends, and colleagues, whose unwavering support, love, and encouragement from my earliest days to the present have shaped who I am. I am endlessly thankful for the strength, warmth, and belief each of you has given me, making this journey possible.

Most especially, to my beloved wife, Yordanos Yohannes (Engineer), who carried the full weight of parenthood to our kids during my absence while pursuing my studies abroad. Your patience, strength, and countless sacrifices will never be forgotten. I am deeply grateful for the love, resilience, and understanding you have shown through every challenge. Thank you for being the anchor of my journey and the heart of our family. This achievement is as much yours as it is mine.

Statement of the Supervisor

For the PhD Thesis

AN INTEGRATED GEO-HYDRO-INFORMATICS APPROACH FOR GROUNDWATER POTENTIAL ASSESSMENT IN THE HIGHLAND OF ERITREA

by Kabral Mogos Asghede.

Mr. Kabral Mogos Asghede PhD research constitutes a significant and original contribution to groundwater exploration and management in data-scarce highland environments. This reflects strong scientific maturity and an excellent ability to integrate multidisciplinary approaches to address complex hydrogeological challenges. The candidate developed and applied a comprehensive geospatial framework that combines geological mapping, groundwater potential mapping, and hydrochemical investigation into a unified research workflow. This integrated design reflects a deep understanding of groundwater systems as products of interacting geological, structural, hydrological, and geochemical controls. Importantly, this is the first study of its kind conducted in the upper Mereb catchment of the Eritrean Highlands, making it a pioneering contribution both methodologically and regionally.

In my professional opinion, this dissertation meets the standards for a PhD degree in hydrogeology and geospatial water resources research. I strongly support the public defense of this thesis and recommend that Kabral Mogos Asghede be awarded the Doctor of Philosophy (PhD) degree.

Scientific Supervisor

Dr. János Vágó

University Associate Professor, Miskolc, Hungary.

Summary

This dissertation presents the first integrated groundwater study conducted in the upper Mereb catchment, a semi-arid highland area in Eritrea facing increasing pressure from agriculture and domestic water demand. The study addressed the lack of detailed groundwater information by combining geological mapping, groundwater potential assessment, and groundwater quality analysis using remote sensing, gravity data, machine learning, field observations, and hydrochemical investigations.

The geological investigation improved the understanding of the lithology and structural framework of the area. Remote sensing analysis and field verification identified the main rock units, while gravity data and hillshade analysis revealed major faults and fracture systems that control groundwater movement and storage. These structures were found to play an important role in groundwater occurrence across the catchment. Machine learning techniques, including Artificial Neural Networks (ANN) and Support Vector Machines (SVM), helped improve lithological classification and produced more reliable geological maps. The results showed that integrating field observations with remote sensing and machine learning can effectively support geological investigations in areas with limited existing data.

Groundwater potential mapping using Analytical Hierarchy Process (AHP) and Frequency Ratio (FR) models identified favorable groundwater zones, particularly in the northwestern and northeastern parts of the catchment where fractured volcanic rocks are dominant. Validation results confirmed that both models provide reliable predictions for groundwater occurrence and can support well sitting and groundwater development planning. Groundwater quality analysis showed that most groundwater samples are suitable for drinking and irrigation. The main factors controlling groundwater chemistry are natural processes such as rock weathering and ion exchange, with some localized influence from agricultural activities. However, a few areas showed higher salinity and mineralization, indicating the need for careful groundwater management.

Overall, this study provides important baseline information for groundwater exploration, management, and protection in the upper Mereb catchment and contributes to improving groundwater knowledge in Eritrea. The integrated approach used in this research supports sustainable water resource planning and can help guide future groundwater investigations in the country.

Kabral Mogos Asghede, Miskolc, Hungary 2026

Table of Contents

List of Tables

List of Figures

1. INTRODUCTION

1.1.Background

Groundwater is one of the most vital natural resources supporting human survival, economic development, and ecosystem stability (Velis et al., 2017). Its importance is especially pronounced in arid and semi-arid regions, where surface water is scarce, rainfall is limited, and evapotranspiration rates are high (Savari et al., 2025). Under such conditions, groundwater frequently constitutes the primary and often the only reliable source of water for domestic use, agriculture, livestock production, and rural livelihoods (Ogunsanwo et al., 2024). Nevertheless, communities in these environments face persistent challenges, including spatial and temporal variability in groundwater availability, difficulties in locating productive wells, and heightened vulnerability to drought (Elsaidy et al., 2025). These challenges are further intensified by population growth, expanding irrigated agriculture, and climate variability, which collectively increase pressure on already limited water resources. Consequently, the identification and sustainable management of groundwater resources have become central concerns across arid and semi-arid regions of Africa, the Middle East, and other drought-prone areas globally (Amer et al., 2012; Zamani et al., 2022).

Eritrea, situated in the Horn of Africa, is among the countries where groundwater plays a crucial role in supporting rural communities, agriculture, and small-scale economic activities. Much of the country is characterized by low and erratic rainfall, limited surface-water storage, and a strong dependence on groundwater for drinking and irrigation. The upper Mereb catchment represents one of the most important drainage basins in the Eritrean highlands, serving as a primary water source for local communities and supporting agricultural activities that contribute significantly to regional socio-economic development (Alemngus et al., 2017; Measho et al., 2020). However, identifying suitable well locations within the region remains challenging due to complex geological conditions and the absence of systematic exploration programs. Groundwater exploration often relies on conventional approaches where frequently resulting in dry boreholes, financial losses, and inefficient use of scarce resources. Although modern geophysical methods could improve the reliability of groundwater exploration, their application remains limited due to high operational costs, logistical constraints, and limited technical capacity (Elewa et al., 2024). This situation constrains accurate assessment of groundwater resources relative to growing community demand in the region. Therefore, the application of modern methodological approaches for groundwater potential assessment, integrating key environmental conditioning factors such as geology and groundwater quality, is essential, and this forms the focus of the present study.

1.2.Aims of the PhD work

This research investigates the groundwater system of the upper Mereb catchment with the primary aim of supporting scientifically grounded decision-making for groundwater development and management in the Eritrean Highlands. The study combines a strong case-study focus on the local groundwater system with the application of an integrated methodological framework. The research therefore seeks both to improve understanding of groundwater conditions in the upper Mereb catchment and to demonstrate the value of advanced analytical methods in a data-scarce regional context.

Specifically, the research addresses the following core questions:

(i) What are the dominant lithological units and structural features that have a contribution in controlling groundwater occurrence in the upper Mereb catchment, as identified through integrated litho-structural mapping approaches?

(ii) Which areas of the catchment have the highest groundwater potential, and how reliably can these zones be delineated using complementary statistical and decision-based models?

(iii) What are the main controlling factors for groundwater quality in the upper Mereb, and to what extent is groundwater suitable for drinking and agricultural use under current hydrogeochemical conditions?

(iv) How can the integrated evaluation of groundwater occurrence, potential, and quality improve decision-making for sustainable groundwater development and resource protection at the catchment scale?

To answer these research questions, the study applies a comprehensive, multi-method framework that integrates: (1) lithological and structural mapping using remote sensing data, gravity information, hillshade-derived lineament analysis, and machine-learning techniques; (2) groundwater potential zonation through the combined application of the Analytical Hierarchy Process (AHP) and Frequency Ratio (FR) models; and (3) groundwater quality assessment based on hydrochemical parameters and multivariate statistical analyses.

The novelty of this research, therefore, lies in addressing key groundwater-related research questions through the first-time application of a fully integrated geospatial, geophysical, and data-driven framework in the upper Mereb catchment. Although the individual methods have been applied in other regions, their combined and coordinated use to explicitly

link litho-structural controls, groundwater potential, and groundwater quality represents a new contribution to the data-scarce setting of the study area. By applying this integrated approach to answer clearly defined research questions, the study generates reliable baseline information and an improved conceptual understanding of the groundwater system. These outcomes provide practical decision-support for groundwater development, resource protection, and long-term water security planning in the Eritrean Highlands.

1.3.Description of the study area

The study area is the upper Mereb catchment, located in the southern part of Eritrea (Zoba Debub), within the central highlands (Gehbrehiwot & Kozlov, 2019). The catchment covers approximately 1480 km² and includes five administrative sub-zones: Galanefhi, Debarwa, Mendefera, Dekemhare, and Mai-Ayni (Fig. 1). Geographically, the area lies at approximately 38°49′58″ E longitude and 15°02′28″ N latitude. The topography of the catchment is highly variable and consists of low-elevation flat plains, fault-bounded structural grabens, linear ridges associated with dyke swarms, and deeply dissected valleys. The Mereb river and its major tributaries drain the area, flowing predominantly from north to south. The river is seasonal (ephemeral), with flow occurring mainly during the rainy season. Elevation within the catchment ranges from approximately 1,554 to 2,450 m above mean sea level, which strongly influences local climate, runoff generation, and hydrological processes.

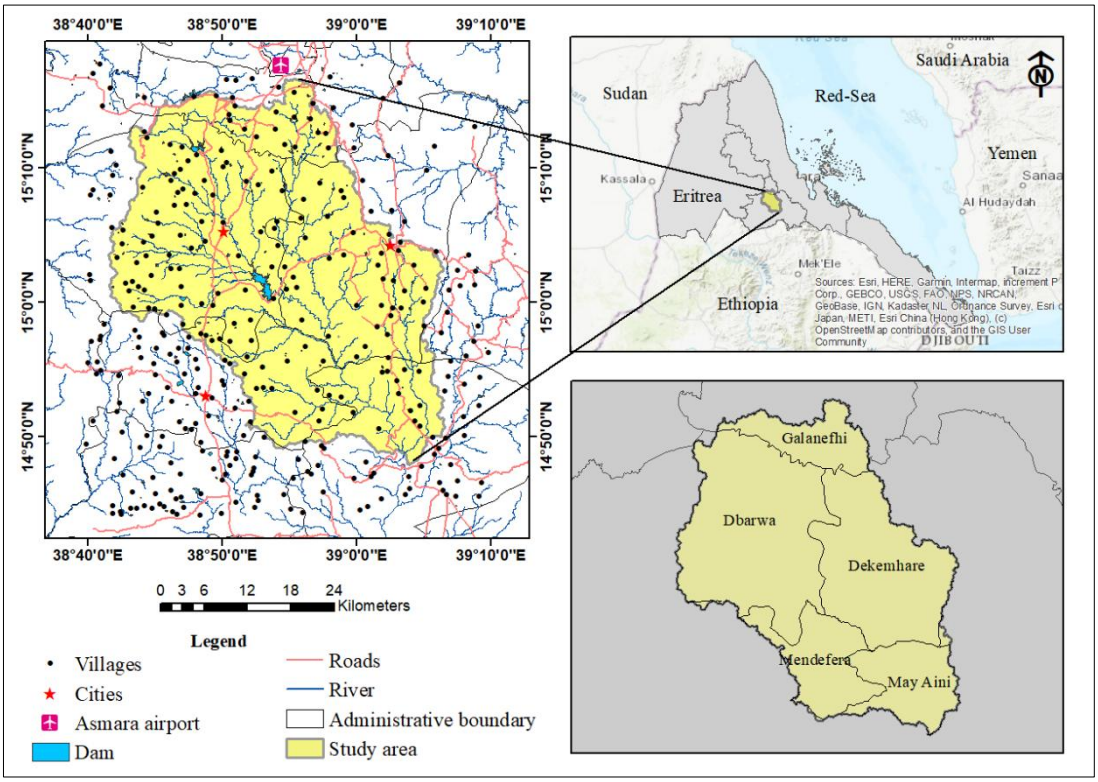

Fig. 1 Geographical location of the study area

The study area lies within the moist highland agro-climatic zone and is characterized by a generally cool climate. Relatively cold conditions prevail from mid-autumn through winter, while warmer temperatures occur from mid-spring into summer. Daily temperatures typically range from below 10 ^{0}C at the minimum to about 25 ^{0}C at the maximum. Rainfall is concentrated during the summer season, from June to September, with July and August accounting for the highest proportion of annual precipitation. The dominant source of summer rainfall is the south-westerly monsoon air masses, which originate over the Atlantic Ocean and the Gulf of Guinea and supply the bulk of the region's annual moisture. Additionally, though much lighter, rainfall occurs during the spring months (March to May), brought by moisture-bearing winds from the Indian Ocean, locally known as "Azmara," according to the study by the Water Resource Departments (WRD, 2017). The long-term mean annual rainfall in the area shows strong variability, typically ranging from less than 300 mm to more than 900mm/year (Ghebrehiwot & Kozlov, 2020). Over the past 25–30 years, however, notable changes have occurred in general climatic conditions, particularly in rainfall patterns and trends, which have become increasingly variable and unpredictable in both space and time (WRD, 2017). The inconsistency of the rainy season, coupled with this growing variability, underscores the need for careful water resource management and conservation to ensure surplus water from high-rainfall years is used during periods of low rainfall.

Geologically, the upper Mereb catchment is part of the Arabian-Nubian Shield (ANS), a significant Neoproterozoic (900–500 Ma) geological province formed by the convergence of East and West Gondwana (Ali et al., 2013; Ghebreab et al., 2009; Hamimi et al., 2022a). This shield represents a complex assemblage of igneous and metamorphic rocks that evolved through accretionary processes (Solomon & Quiel, 2006a; Teklay, 2006). The lithological framework of the study area comprises a Precambrian metamorphic basement overlain by Palaeozoic and Mesozoic sedimentary formations, as well as widespread Tertiary basaltic lava flows and granites. This complex geological history has played a crucial role in shaping the region's topography and hydrological patterns (Solomon & Ghebreab, 2006a). The catchment exhibits significant lithological diversity, with metamorphic and basaltic rocks comprising a major component of the geological units (Fig. 2). Schistose metavolcanic rocks, primarily composed of chlorite-epidote-quartz-muscovite schists, are prevalent, along with metasedimentary formations such as slates and greywackes. Granitoid intrusions vary in composition, ranging from foliated and gneissose granite to granodiorite and diorite. The volcanic succession is dominated by alkali-olivine basalt flows, underlain by a well-developed lateritic paleosol. Additionally, the presence of Mesozoic sedimentary deposits and weathered

crystalline formations further enhances the lithological complexity of the area (Solomon & Quiel, 2006a).

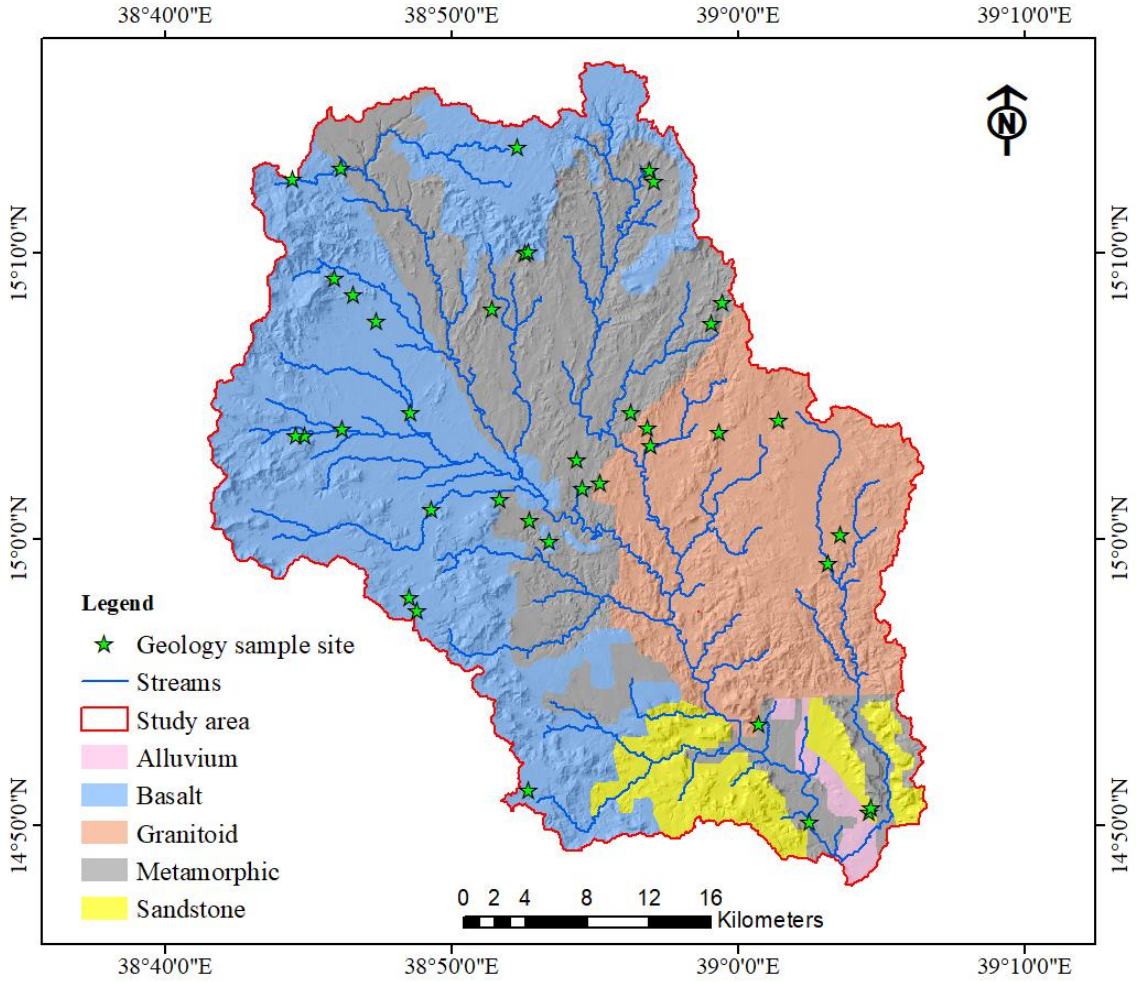

Fig. 2 Geological map of Upper Mereb area redrawn and modified after (Solomon & Quiel, 2006b).

The tectonic framework of the Eritrean Highlands is defined by an extensive network of joint systems, fault zones, and dyke swarms, which play a significant role in shaping the region's structural and geological evolution. The research area's hydrogeological characteristics and watershed have been significantly influenced by such structures (Solomon & Ghebreab, 2006b). The primary fault structures are categorized as strike-slip and normal faults, commonly exhibiting fault breccia, gouge, and well-developed slicken lines. The dominant lineament orientations NW-SE, N-S, NE-SW, and ENE-WSW reflect the strong tectonic influence of the Red Sea rift system. Sub-vertical dyke swarms, primarily composed of basaltic to dolerite intrusions, transect both granitic and basaltic formations, significantly enhancing secondary porosity and permeability (Solomon & Quiel, 2006b).

The study area is predominantly underlain by metavolcanic basement and overlying flood basalts, which in their primary state have little to no permeability and generally behave as aquicludes. Consequently, groundwater occurrence and movement are mainly controlled by secondary permeability developed through tension and shear fractures. Based on the field observations, three major courses, units are identified: (i) fractured basaltic flows, which thin eastward toward the Mereb River drainage course; (ii) fractured sub-vertical basaltic dykes that act as open subsurface conduits over several kilometers; and (iii) fractured metavolcanic basement rocks. Groundwater flow is largely concentrated along these fractured zones, particularly within the intensively jointed basaltic dykes, where closely spaced, well-connected fractures provide high secondary permeability. Permeability associated with dykes, faults, and shear zones typically extends from a few tens to several hundred meters into the surrounding host rocks, forming laterally extensive but relatively narrow groundwater flow corridors (WRD, 2017). As a result, groundwater circulation is strongly structurally controlled, with flow preferentially aligned along dyke axes, fault zones, and major fracture systems. Vegetation cover in the upper Mereb catchment reflects the semi-arid climatic conditions and varied topography of the region (Fig. 3). The area is characterized predominantly by sparse shrubland, grassland, and rangeland vegetation, with denser cover along river courses and at higher elevations where moisture availability is greater. Agricultural lands, mainly rain-fed and irrigated fields, are also present in valley bottoms and gently sloping terrains. This vegetation distribution influences surface runoff and soil protection processes across the catchment.

Fig. 3 Vegetation cover of the study area (photograph taken in summer 2024).

2. LITERATURE REVIEW

2.1.Geological Mapping

Lithological mapping forms the foundation of geological investigation, providing essential information on the spatial distribution and characteristics of rock units. Traditionally, this process relied heavily on extensive fieldwork, manual observations, and labor-intensive surveying techniques (J. Lu et al., 2023). Although these methods remain scientifically valuable, they present significant challenges, particularly in terrains that are remote, rugged, or difficult to access. Early geological mapping efforts often faced considerable logistical constraints, including limited transportation, sparse topographic information, and the high cost and time required to traverse large or environmentally harsh landscapes (Piras et al., 2017). In many regions, especially during the first attempts at lithological mapping, field-based approaches were frequently hindered by incomplete exposures, weathering effects that masked diagnostic lithological features, and the inability to cover sufficiently broad areas within practical timeframes (Z. Wang & Zuo, 2025). As a result, early maps were sometimes generalized, spatially limited, or inconsistent in detail, reflecting the inherent difficulties of manually capturing geological complexity at a regional scale.

To overcome these challenges, the scientific community gradually incorporated new tools and concepts that could enhance geological interpretation beyond what was physically observable in the field. The introduction of aerial photography provided some improvement, yet it still depended on visual interpretation and was constrained by atmospheric conditions and scale limitations (Whitmeyer et al., 2010). The subsequent advent of satellite remote sensing marked a major shift in geological mapping practices, enabling the rapid acquisition of spatially continuous data over large areas, reducing field dependency, and allowing the detection of lithological variations based on spectral properties rather than solely on physical exposure (Abdelouhed et al., 2021; A. P. Cracknell, 2018). As these capabilities expanded, remote sensing techniques evolved into an indispensable component of modern geological mapping, offering a scientifically robust means to address many of the limitations encountered in the earliest phases of lithological survey work.

The emergence of satellite remote sensing introduced a set of techniques that significantly improved geological mapping by offering broad, consistent, and objective coverage across large and inaccessible terrains (Samir et al., 2023). These methods made it possible to distinguish lithological units based on their spectral reflectance properties, providing clearer geological information than what was achievable through traditional field-only

approaches (Benaissi et al., 2022). However, spectral similarities among different rock units can still introduce ambiguities, meaning that remote sensing alone cannot always ensure accurate lithological discrimination. To reduce these uncertainties, enhanced processing techniques are applied: band ratios are used to highlight specific mineralogical signatures, while false-color composites (FCC) enhance lithological contrasts by combining spectral bands in ways that visually separate rock units more effectively (K. M. Asghede et al., 2025; Tshanga Matthieu et al., 2026). Principal Component Analysis (PCA) further improves interpretation by maximizing spectral variance and revealing subtle differences between lithologies that might otherwise remain undetected (Nagar et al., 2024). Supervised classification, especially when guided by field-derived spectral signatures, adds statistical rigor and reproducibility to lithological mapping by grouping pixels into coherent geological classes (El Fels & El Ghorfi, 2022). These remote sensing approaches have consistently proven effective in resolving complex geological patterns but applying them across large and diverse regions can be computationally demanding and may reduce generalizability; therefore, machine learning methods have emerged as a stronger alternative for improving accuracy and automation in geological mapping (W. Wang et al., 2024).

With the advancement of computational techniques, machine learning has become an increasingly important tool for enhancing lithological mapping from satellite imagery (Daoud, Shebl, Nafi, et al., 2025). Algorithms such as Artificial Neural Networks (ANN) can model nonlinear spectral relationships, while Support Vector Machines (SVM) are highly effective in high-dimensional feature spaces and often perform well even with limited training data (J. Lu et al., 2023; Zhang et al., 2025). Tree-based classifiers, including Random Forest and Random Trees, have also been explored in geological studies due to their robustness against noise and ability to handle complex spectral patterns, although their use is often influenced by data characteristics and training sample availability rather than universal superiority (Badrakh et al., 2025). Practical applications demonstrate the strength of these machine-learning approaches. For instance, El-Omairi et al. (2025) evaluated SVM, Random Trees, and ANN in the Central Anti-Atlas using Landsat-9 and Sentinel-2 imagery, reporting that SVM produced clearly defined lithological boundaries and strong classification accuracy suitable for operational geological mapping. Likewise, Ghezelbash et al. (2019) applied supervised machine-learning algorithms to exploration targeting in the Varzaghan district of NW Iran, successfully delineating mineralized zones and demonstrating the broader potential of ML-based classification in geological investigations. Together, these examples show that machine-learning techniques have become a powerful component of modern lithological

mapping, offering improved discrimination of geological units where conventional approaches may encounter limitations.

Previous remote-sensing-based geological studies in Eritrea illustrate both the value of satellite data and the need for more advanced enhancement techniques. Solomon & Quiel, (2006a) applied remote sensing for groundwater exploration and broad lithological identification in the central highlands, relying primarily on band-combination methods. While effective for reconnaissance-level mapping, such approaches provide limited spectral decorrelation and may not differentiate lithological units with subtle or overlapping spectral characteristics. Similarly, Teklay et al. (2005) used isotopic analysis to characterize basaltic units, contributing valuable insight into specific components of regional geology but not addressing the wider lithological framework across diverse rock types. These earlier efforts highlight the absence of a high-resolution, comprehensively enhanced lithological dataset that could support geological, hydrogeological, and resource-management needs. In this context, adopting integrated enhancement techniques drawing on multispectral transformations, supervised classification, and modern computational approaches offers a necessary and timely pathway for producing more accurate and operationally relevant lithological maps for Eritrea.

2.2.Structural mapping

Structural mapping is a fundamental component of geological investigation, capturing the network of linear and curvilinear features that reflect faults, fractures, shear zones, and lithological contacts (Aluko & Igwe, 2018). These structures form the primary conduits for fluid flow, influence landscape evolution, and provide essential constraints on tectonic history (Sivkov et al., 2020). Historically, lineaments were identified through extensive field mapping and visual interpretation of topographic maps or aerial photographs, relying heavily on the observer's experience and the clarity of surface expressions. Such traditional methods were inherently limited by accessibility, scale, and the difficulty of detecting subtle or deeply seated structures, particularly in areas where weathering, sediment cover, or erosion obscure geological fabrics (Mono et al., 2024). Extracting continuous structural patterns across large regions was often time-consuming and inconsistent, leading to partial or generalized representations of complex structural frameworks. These limitations highlighted the need for more systematic and objective approaches, especially in terrains where structural information plays a vital role in groundwater assessment, mineral exploration, and regional geological interpretation.

Advancements in remote-sensing and geophysical processing have significantly improved the accuracy and consistency of lineament extraction. Techniques such as hillshade visualization from digital elevation models allow the illumination of terrain from multiple directions, making subtle geomorphic lineaments more discernible than in traditional shaded relief maps (Xu et al., 2020). At the same time, gravity-based methods using Bouguer anomaly data and derivative filters, including the Total Horizontal Derivative (THD) and First Vertical Derivative (FVD), enable the detection of deeper or buried structures that lack surface expression but exert strong geological control (Alrefaee et al., 2022). Studies employing these approaches have demonstrated their effectiveness in resolving complex structural patterns. For instance, Thanh Pham et al. (2021) showed that enhanced gradient filters applied to high-resolution gravity data revealed clear subsurface lineaments in central Vietnam, offering structural insights that were not evident from surface datasets alone. (Satyakumar et al. (2022) similarly integrated DEM derivatives with gravity-derived edge detection to delineate tectonic trends in eastern India, illustrating how the combination of surface morphology and geophysical information produces a more comprehensive structural interpretation. Such examples underscore the practical value of modern lineament extraction techniques, particularly where both near-surface and deeper geological controls must be understood for hydrogeological or resource-related applications.

Structural mapping in Eritrea has primarily been conducted through optical remote-sensing and localized geophysical techniques, with early efforts mainly designed to support groundwater exploration and regional tectonic interpretation. This focus reflects the country's geological reality, where fractures and lineaments govern groundwater storage and flow. Solomon & Ghebreab, (2006b) used color composites and panchromatic Landsat TM imagery to identify major lineament trends in the central highlands, producing useful structural insights where surface expressions were sufficiently preserved. Complementing this, Drury', et al. (2001) applied ground-based geophysical profiling to detect fracture zones relevant for groundwater development; although effective for site-specific investigations, such surveys are inherently limited in spatial coverage and become increasingly resource-intensive when extended to larger terrains. These contributions form an important foundation for understanding Eritrea's structural framework, yet they also highlight a reliance on surface-visible features and localized subsurface measurements. Although such techniques are highly detailed, they are difficult to implement across large areas due to the substantial time, labor, and logistical resources they require (Abd El-Wahed et al., 2025). Therefore, the integration of satellite gravity data with DEM-derived lineament extraction offers a significant advancement to the

existing knowledge base. The combined use of these complementary datasets enhances the delineation of tectonic fabrics that influence groundwater pathways, mineral resource distribution, and broader geological evolution. In settings where regional-scale structural information remains underdeveloped, such an integrated approach provides a practical and scientifically robust means of generating comprehensive litho-structural frameworks that more reliably support a wide range of geoscientific and resource-management applications.

2.3.Groundwater Potential Mapping

Groundwater is one of the most important freshwater resources for society and ecosystems, occurring within the pore spaces and fractures of subsurface materials beneath the Earth's surface (Lentswe & Molwalefhe, 2020). It sustains domestic supply, agriculture, and industry, underpins baseflow to rivers and wetlands, and provides a strategic buffer during droughts (Aranguren-Díaz et al., 2024). Yet identifying where groundwater occurs has historically been difficult. In earlier periods, communities faced technological and logistical barriers: maps were coarse, subsurface information was scarce, and the costs of exploration surveys were high (Kpiebaya et al., 2022; Yin et al., 2018). Traditional practices for locating groundwater ranging from experiential knowledge to terrain interpretation to rudimentary dowsing with stick-offered occasional success but were inherently subjective, spatially inconsistent, and hard to validate scientifically (Berhanu & Hatiye, 2020). These constraints often led to trial-and-error siting of wells, variable success rates, and inefficient use of limited resources. To overcome these limitations, more systematic and evidence-based approaches were needed, prompting the use of geospatial methods that integrate multiple indicators of groundwater occurrence into unified decision frameworks (Suryawanshi et al., 2023).

The advent of Geographic Information Systems (GIS) and satellite Remote Sensing (RS) transformed groundwater exploration by enabling the integration of spatial datasets and the mapping of groundwater potential zones over large areas with improved consistency (Lubis et al., 2025). In these frameworks, conditioning factors such as lithology, soil type, land use/land cover (LULC), slope, drainage density, lineament density, geology, rainfall, and elevation are assembled to represent the hydrogeological controls that favor groundwater occurrence (Ahmadi et al., 2021; Shelar et al., 2023). Among the most widely used modeling approaches, the Frequency Ratio (FR) method quantifies the probabilistic association between known groundwater occurrences (e.g., wells or springs) and each class of the conditioning factors, producing data-driven weights that reduce subjectivity (Kouaied et al., 2025). The Analytical Hierarchy Process (AHP), by contrast, is an expert-based multi-criteria decision technique in which pairwise comparisons are used to derive relative weights for factors; it provides

transparent logic and internal consistency checks (Saaty & Katz, 1990; Upwanshi et al., 2023). Other approaches such as Shannon entropy for information-theoretic weighting, Fuzzy-AHP for managing uncertainty, and geophysical inputs like resistivity, gravity, and magnetics to capture subsurface conditions further expand the methodological options available (Abd El-Dayem et al., 2023; Bhadran et al., 2022; Elvis et al., 2022). FR and AHP are commonly preferred because they are simple to implement, easy to interpret, and effective even in data-limited settings (Belkendil et al., 2025). They also capture the key relationships between groundwater conditioning factors and groundwater occurrence, supporting the development of reliable groundwater potential maps (Suryawanshi et al., 2023).

Recent applications demonstrate how these methods translate into decision-ready groundwater potential maps. In Odisha, India, Sahoo et al. (2024) combined AHP with GIS to delineate groundwater potential zones, showing that carefully weighted conditioning factors can improve the prioritization of areas for exploration and recharge interventions. In the southwest of Algeria, Belkendil et al. (2025) applied the FR method with GIS to the state of Béchar and produced maps that directly informed water-scarcity management and supported sustainable agricultural planning. This illustrates how probabilistic, data-driven weighting can yield policy-relevant outputs in arid settings. Moreover, Appukuttan & Reghunath (2025) applied an integrated geospatial and machine-learning framework in the Ithikkara River Basin and obtained good predictive results, showing that such models can capture nonlinear relationships under well-controlled conditions. However, their approach relied on extensive, high-quality training datasets and rigorous calibration, which are not always feasible in data-scarce or poorly mapped regions. Collectively, these examples underscore that method selection should balance transparency, data availability, and operational goals.

In Eritrea, early groundwater assessments provided an important baseline understanding but were limited in scope and methodological integration. Solomon & Quiel (2003, 2006a) investigated groundwater occurrence in the central highlands, including the present study area, using physical surveys supported by remote-sensing indicators. Although their work contributed valuable insights into hard-rock aquifer conditions, it did not consider several key environmental conditioning factors, such as slope, soil characteristics, land-use/land-cover, drainage density, and related surface-hydrological controls, that are now widely recognized as important influences on groundwater occurrence and spatial variability. Similarly, Drury', et al. (2001) employed geophysical profiling to identify fracture zones favorable for groundwater development. While highly effective for site-specific exploration, such methods are resource-intensive, spatially restricted, and challenging to apply across broader terrains. To

cover larger areas more efficiently and to optimize the use of available resources, the adoption of a structured geospatial modeling strategy, one that systematically integrates key conditioning factors within a data-supported weighting framework, has been recommended as a necessary advancement (Islam, 2024).

As groundwater exploration efforts in Eritrea increasingly require coverage over wider and geologically diverse areas, there is a clear need for approaches that extend beyond localized surveys and site-specific investigations. In this context, integrating geospatial information and remote sensing within an AHP–FR framework provides a much-needed step toward producing reliable and scalable groundwater potential maps. This combined approach reduces subjectivity, incorporates both expert judgment and empirical evidence, and improves the representation of how key conditioning factors influence groundwater occurrence. Such a framework is particularly valuable for regions where data limitations and geological complexity have historically constrained groundwater studies, offering a more dependable basis for well siting, irrigation planning, and long-term groundwater management (Arefin, 2020; K. Asghede & Vágó, 2025).

2.4.Groundwater quality investigation

In regions where agricultural expansion, industrial activities, and population growth are rapidly increasing, assessing groundwater potential alone is no longer sufficient; groundwater quality has become equally critical for ensuring safe and sustainable use (Ram et al., 2021). Even where groundwater availability is high, its suitability for drinking, irrigation, and industrial purposes can be compromised by multiple natural and anthropogenic factors. Natural processes such as water-rock interaction, mineral dissolution, and evapotranspiration, can influence the chemical composition of groundwater, sometimes resulting in elevated salinity or hardness (Gurmessa et al., 2022). At the same time, human activities including the application of agricultural fertilizers and pesticides, industrial effluents, and improper waste disposal introduce contaminants such as nitrates, heavy metals, and organic pollutants (Alzahrani et al., 2025; Faraji & Shahryari, 2024). These changes in chemistry may pose significant health risks and reduce the suitability of groundwater for domestic and agricultural use, as demonstrated by several recent studies on the impacts of major ions and emerging contaminants (Chaudhari et al., 2024; Dheeraj et al., 2025). This growing complexity underscores the need to transition from potential-focused assessments to comprehensive evaluations of groundwater quality.

Groundwater quality has traditionally been assessed using basic physico-chemical measurements and simple comparisons with drinking water standards. While these methods provide essential baseline information, they offer only a limited understanding of the factors shaping groundwater chemistry (Karami et al., 2018). This is because aquifers often vary widely in their geological characteristics, recharge conditions, and human influences, making single-parameter evaluations inadequate for capturing the full complexity of groundwater systems. To overcome these limitations, recent research highlights the necessity of integrated, multi-method hydrochemical evaluations capable of capturing both the chemical character of groundwater and its functional suitability for different uses. For example, a multi-technique assessment conducted in the Dongjiang–Hanjiang River Basin demonstrated how combining hydrochemical analysis with statistical and spatial tools greatly strengthens interpretations and management outcomes (L. Lu et al., 2024). Similarly, in the Teboulba region of Tunisia, hydrogeochemical investigations revealed advanced mineralization processes that rendered the groundwater unsuitable for irrigation under normal conditions (Khawla & Mohamed, 2020). In the Rafsanjan Plain of Iran, the integration of GIS with hydrochemical facies enabled researchers to compare spatial variations in water quality against standard guidelines, illustrating the value of spatially referenced assessments for resource management (Hosseininia & Hassanzadeh, 2023). Together, these studies demonstrate that multi-method approaches provide a more accurate, actionable understanding of groundwater quality, and they highlight the importance of such strategies for decisionmakers in prioritizing groundwater resource management.

In Eritrea, several attempts have been made to investigate groundwater quality, although most earlier studies applied limited or single-parameter approaches. For instance, Zerai (1996) produced a national-level water quality map based solely on electrical conductivity measurements. While valuable as an early baseline, this method did not capture the full complexity of groundwater chemistry or its implications for domestic and agricultural use. In the agricultural sector, Mehari et al. (2006) assessed the salinity levels of Wadi Laba floodwaters and emphasized that improvements in water management alone cannot significantly enhance crop production without simultaneous control of soil salinity. Although informative for irrigation planning and crop monitoring, this study did not address drinking water concerns, revealing a gap in comprehensive suitability assessments. These examples indicate that while Eritrea has a history of groundwater investigation, integrated hydrochemical, statistical, and suitability-based approaches remain limited, reinforcing the need for updated methods capable of addressing the country's growing water demand and quality challenges.

To address these challenges, contemporary groundwater quality research increasingly relies on hydrochemical and multivariate analytical methods, which offer deeper insights into the sources, processes, and patterns of groundwater composition. Hydrochemical diagrams provide visual tools for identifying water types, dominant geochemical mechanisms (e.g., ion exchange, evaporation, rock dominance), and overall water suitability (Eslami et al., 2019). Complementary techniques such as ionic ratios and saturation indices help determine the origins of dissolved ions and the geochemical pathways shaping water chemistry (Mohammed et al., 2025). In addition, multivariate statistical tools, including Principal Component Analysis (PCA) and Cluster Analysis (CA), are applied to detect pollution sources, classify water types, and reveal hidden structure in complex datasets (Hagage et al., 2025). According to Kong et al. (2025), these integrated approaches not only elucidate controlling geochemical processes but also provide a scientific basis for evaluating groundwater suitability for drinking and other uses. Furthermore, agricultural suitability is commonly assessed using indices such as the Wilcox diagram and Sodium Adsorption Ratio (SAR), which evaluate the potential impact of salinity and sodicity on crop performance and soil structure (Safiur Rahman et al., 2017). When combined with spatial analysis techniques (e.g., GIS-based variability mapping), this comprehensive framework enables researchers to produce decision-support outputs that inform water supply planning, agricultural management, and long-term groundwater protection.

3. MATERIALS and METHODS

3.1.Datasets

A diverse range of datasets was utilized in this study to ensure a comprehensive and integrated assessment of groundwater potential and quality within the upper Mereb catchment. The research incorporated geological, geospatial, hydrogeological, and hydrochemical datasets, each serving a distinct analytical purpose. Geological mapping and field survey data provided the foundational understanding of lithological and structural characteristics. Multispectral Landsat imagery facilitated litho-structural delineation through advanced remote sensing techniques. Gravity data complemented this by enhancing subsurface interpretation and supporting geological validation. Furthermore, groundwater potential mapping was established using selected key environmental parameters, along with existing well locations. Finally, physicochemical datasets from groundwater samples were analyzed to evaluate water quality for domestic and agricultural suitability using statistical, graphical, and hydrochemical methods. Collectively, these datasets form an integrated framework that underpins both the spatial and qualitative dimensions of groundwater resource assessment in the study area.

3.1.1. Geological data

The geological datasets used in this research were derived from three primary sources: remote sensing data, gravity data, and field-based ground truthing. For the remote sensing component, Landsat 9 imagery (LC09_L1TP_169050_20220515_20230416_02_T1) was acquired from the U.S. Geological Survey (USGS) Earth Explorer platform (https://www.earthexplorer.usgs.gov). The dataset corresponds to path 169 and row 50, fully covering the upper Mereb catchment area. The imagery has a spatial resolution of 30 meters. It spans visible, near-infrared (NIR), and shortwave infrared (SWIR) spectral regions, which are critical for lithological discrimination and surface mineral mapping. These datasets formed the foundation for delineating major lithological units and structural features, complementing both gravity and field-based observations.

Gravity data for the study area were obtained from the GGMPlus model, which provides high-resolution gravity field data derived from satellite missions such as GRACE (Gravity Recovery and Climate Experiment) and GOCE (Gravity field and steady-state Ocean Circulation Explorer), combined with terrestrial gravity measurements, topographic data, and EGM2008 (Earth Gravitational Model 2008). The GGMPlus dataset provides global coverage at approximately 200 meters of spatial resolution, offering detailed gravity field variations. The extracted gravity data included free-air and Bouguer gravity anomalies, along with terrain

corrections. Free-air anomalies were used to study variations in the Earth's gravitational field at the geoid's surface. In contrast, Bouguer anomalies, corrected for topographic mass contributions, provided insights into subsurface density variations (Bowin, 1983). As these datasets are already fully corrected, no additional primary gravity corrections were required. Instead, further processing was undertaken in Oasis Montaj, including upward continuation, regional–residual separation, and derivative filtering, to enhance structural signals and improve the delineation of subsurface geological features relevant to structural and hydrogeological interpretation.

A field survey was conducted in and around the upper Mereb catchment area in September 2024 to provide primary geological observations and ground-truth information for subsequent remote-sensing and gravity-based analyses. A total of 38 representative rock samples were collected from accessible locations across five administrative subzones within the study area (Fig. 1 and 2). The selection of sampling sites was guided primarily by field accessibility by vehicle and on foot, as access to some areas was constrained by rugged topography, deeply incised valleys, and locally dense vegetation cover. Within these practical limitations, sampling locations were chosen to capture representative lithological units and structural settings across the catchment, which were later used to guide, validate, and refine interpretations derived from remote-sensing and geophysical datasets. The field data acquisition was conducted using essential geological tools, including a handheld GPS device, a mobile clinometer app, a rock hammer, a field notebook, and a hand lens. Field observations were carefully documented in hard-copy field notebooks and in digital formats (spreadsheets and GIS-compatible databases) for precise spatial organization and subsequent analysis. The mobile application clinometer proved invaluable for measuring few structural data, including the strike, dip, and orientation of rock units while simultaneously integrating coordinate information and capturing georeferenced images for future reference and improved spatial visualization. Geological structures such as faults, folds, joints, and bedding planes were observed to ensure a comparative representation of structural relationships with other methods, such as DEM and gravity data. Contact types and lithological boundaries were identified through detailed field mapping and visual inspection. Geomorphological features were analyzed using topographic maps and aerial imagery to enhance spatial accuracy and understanding of surface processes. Photographic documentation, cross-sections, and geological sketches complemented the data collection, providing a robust framework for interpretation.

3.1.2. Groundwater potential data

In this study, seven key environmental parameters were employed to delineate groundwater potential zones in the upper Mereb catchment: drainage density, lineament density, slope, rainfall, geology, soil, and land use/land cover (LULC). These parameters were selected based on their hydrogeological relevance, influence on groundwater occurrence and recharge processes, and, critically, their availability as spatially continuous datasets for the entire study area (K. M. Asghede & Vágó, 2025). Other hydro-geologically important parameters, such as direct groundwater recharge estimates, soil moisture, evapotranspiration, and subsurface hydraulic properties, were not included due to the absence of reliable, spatially consistent data at the catchment scale. This limitation is common in data-scarce regions and necessitates the use of surface and proxy indicators that effectively capture groundwater controls. Consequently, the selected parameters represent a practical and scientifically accepted compromise between hydrogeological relevance and data availability (Verma & Patel, 2021), and the results should be interpreted within this context. Each dataset was obtained from authoritative and reliable sources to ensure the accuracy and consistency of the analysis. Geological data were compiled from local research studies (K. M. Asghede et al., 2025), while soil data were collected from the Eritrean Ministry of Agriculture, ensuring ground-based reliability for soil classification. LULC information was derived from a Sentinel-2 imagery time series (10 m resolution), which provides detailed spatial information suitable for environmental analysis (https://www.arcgis.com/home/item.html?id=cfcb7609de5f478eb7666240902d4d3d).

Lineament data were extracted from the integration of gravity data and the Shuttle Radar Topographic Mission (SRTM) DEM, facilitating the identification of structural features influencing groundwater flow. Moreover, the slope and drainage density are also derived from the DEM. Rainfall data covering the period 1992–2022 were obtained from national meteorological records archived at the Asmara International Airport Meteorological and Ministry of Agriculture data center, which functions as a central repository for rainfall observations collected from multiple stations across the country. The well location data used in this study were obtained from the Asmara Water Resources Department and represent known groundwater abstraction points across the study area. These data indicate the spatial distribution of groundwater occurrences; however, detailed hydrogeological information associated with individual wells, such as production rates, groundwater levels and recharge conditions were not available. Based on local knowledge, most of the wells are currently active, but their performance characteristics could not be systematically evaluated. This limitation reflects the general scarcity of hydrogeological data in the region and highlights the need for more

comprehensive well documentation to support future groundwater investigations. A summary of source data is listed in Table 1. Collectively, these datasets represent a robust multi-source input base for groundwater potential modelling.

Table 1: Source of data for potential mapping

Data type	Data Source	Description
Remote Sensing Data	Satellite Imagery and Satellite gravity data	Landsat, Sentinel satellites provide multispectral images for mapping different observations. GGMPlus dataset.
Topographic data	Digital Elevation Model (DEM)	SRTM data provides elevation information for slope, drainage, and topographic analysis.
Geological data	Derived geology map and Field data	National geological surveys from Ministry of Mining and Energy, and newly developed geological map.
Soil Data	Soil Maps	National agricultural departments, FAO, USDA soil maps.
Hydrological data	Precipitation data	National metrological stations (Asmara international airport), Ministry of agriculture.
Landuse and land cover data	LULC map	Sentinel-2 10m LULC time series of the world
Well data	Asmara water resource department and mining company	Well information

3.1.3. Hydrochemical data sets

Groundwater inventory data were obtained from the Asmara Water Resource Department, collected in 2017 across the upper Mereb catchment. Its primary objective was to evaluate groundwater quality usage for domestic, agricultural, and other potential activities. A total of 48 strategically selected wells were sampled, ensuring broad spatial coverage and accessibility, while representing the principal hydrogeological settings of the study area where most villages are located nearby (Fig. 1). The sampled wells ranged in depth from 32 to 46 meters, aligning with the typical groundwater abstraction depths in the region. To maintain sample integrity, water was collected in pre-cleaned polyethene bottles and immediately preserved in ice-cooled containers during transportation to the laboratory.

Subsequently, 17 physicochemical parameters were analyzed to assess both the major and minor ionic constituents of groundwater. These parameters included pH, Electrical Conductivity (EC), Total Dissolved Solids (TDS), and Total Hardness (TH), alongside major cations such as Calcium (Ca), Magnesium (Mg), Sodium (Na), and Potassium (K), and major anions including Bicarbonate (HCO_3^-), Sulfate (SO_4^{2-}), Chloride (Cl^-), Nitrate (NO_3^-), Nitrite (NO_2^-) and additional Iron (Fe), Ammonia (NH3) and Manganese (Mn). The comprehensive analysis of these parameters provides valuable insights into the hydrochemical characteristics of groundwater and its suitability for various beneficial uses.

3.2.Methods

The methodology adopted in this study integrates remote sensing, geophysical, statistical, and machine-learning techniques. This combined approach supports a comprehensive assessment of geology, groundwater potential, and water quality in the upper Mereb catchment, offering a level of integration not previously applied in this area. Geological characterization was achieved by combining satellite remote sensing and gravity data, which were further refined using machine learning models, namely Artificial Neural Networks (ANN) and Support Vector Machines (SVM), to generate reliable and detailed lithological-structural maps. These machine learning approaches are particularly effective for lithological mapping because they can capture complex, non-linear relationships between spectral responses and rock types (El-Omairi et al., 2025). With the incorporation of field-validated observations, ANN and SVM substantially enhance classification accuracy and refine the delineation of lithological boundaries compared to conventional methods, especially in geologically complex terrains (Z. Zhang et al., 2025).

Groundwater potential mapping was carried out using a multi-criteria decision-making framework that employed the Analytical Hierarchy Process (AHP) and the Frequency Ratio model to integrate seven environmental parameters influencing groundwater occurrence. To assess groundwater quality, multivariate statistical analysis, Water Quality Index (WQI), and irrigation indices were applied to groundwater samples collected from the study area, enabling the evaluation of both domestic and agricultural suitability. The combination of these approaches provides a robust methodological framework that ensures comprehensive insights into the catchment's hydrogeological conditions.

3.2.1. Remote Sensing analysis

The workflow employed in this study, summarized in Fig. 4, outlines the sequential steps used for litho-structural mapping. Remote sensing techniques have proven highly effective for identifying and characterizing geological formations, structural features, and alteration zones across large and inaccessible terrain (Said et al., 2023). Optical satellite imagery, such as that from the Landsat series, provides a valuable spectral dataset across visible, near-infrared (NIR), and shortwave infrared (SWIR) regions, allowing for detailed discrimination of rock units and surface materials (X. Chen et al., 2007). Several image enhancement and transformation techniques, including Color Composite, Band Ratioing, Principal Component Analysis, and supervised classification, are commonly employed to maximize lithological contrast from multispectral data (Said et al., 2023; Traore et al., 2025). The analysis was supported by using field collected geological samples (Fig. 4).

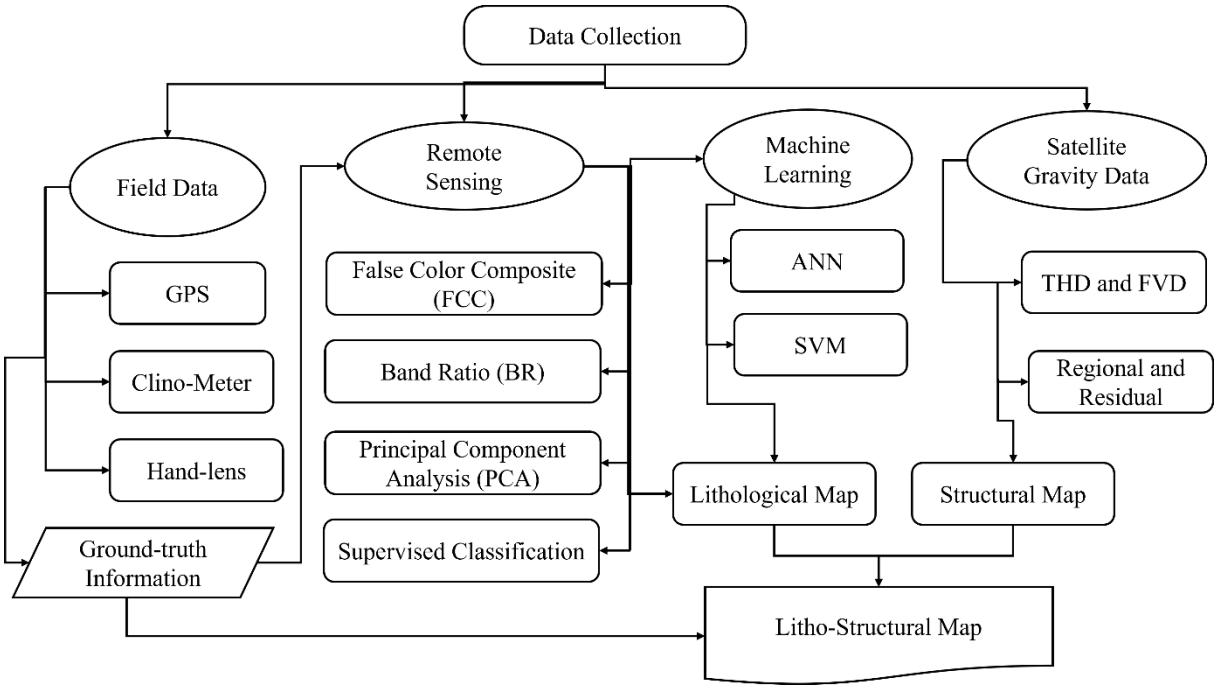

Fig. 4. The flow chart of Litho-Structural Map (THD: Total Horizontal Derivative; FVD: First Vertical Derivative; SVM: Support Vector Machine; ANN: Artificial Neural Network).

3.2.1.1.Color Composite

Color-composite techniques are fundamental in remote sensing for visualizing and interpreting multispectral satellite imagery. By assigning different spectral bands to the red, green, and blue (RGB) channels, these composites facilitate the identification of surface features, landforms, and geological structures based on their spectral and spatial characteristics (Bajwa et al., 2020). The True Color Composite (TCC) uses the visible portion of the electromagnetic spectrum, typically corresponding to blue, green, and red wavelengths, to

create a natural visual representation of the Earth's surface. This composite provides realistic imagery that effectively depicts geomorphological and land-cover features, including vegetation, water bodies, and urban areas (Akbari et al., 2003). However, its utility for lithological discrimination is limited by vegetation cover, soil moisture, and atmospheric scattering, which can mask underlying rock formations.

The False Color Composite (FCC) technique was applied to enhance the visualization of lithological and structural variations in the study area using multispectral Landsat 9 imagery. This method assigns non-visible spectral bands, particularly from the near-infrared (NIR) and shortwave infrared (SWIR) regions to the visible RGB channels, amplifying contrasts related to mineral composition, vegetation, and soil moisture (Abd El-Rahman Hegab et al., 2024). Since rocks are composed of minerals with unique spectral reflectance properties, FCC imagery provides a powerful means for distinguishing lithological units and identifying alteration zones (Ghannadpour et al., 2024).

3.2.1.2.Band Ratioing (BR)

Band ratioing was employed as a key image enhancement technique to emphasize subtle spectral variations associated with geological and lithological differences (Y. Chen et al., 2023). The method involves dividing the digital number (DN) or reflectance value of one spectral band by another, thereby minimizing the effects of illumination, topography, and albedo while highlighting diagnostic absorption or reflection characteristics of specific minerals (Du et al., 2025). By enhancing relative spectral contrast, band ratios allow effective differentiation of ferric and ferrous iron minerals, carbonates, sulfates, and hydroxyl-bearing minerals, which are often indistinguishable in raw multispectral imagery(Abrams & Yamaguchi, 2019). The technique is particularly valuable for lithological mapping, as it isolates mineral-specific spectral responses associated with alteration and weathering processes. In this study, band ratioing was systematically applied to Landsat 9 imagery to generate ratio images that enhance the detection of key mineralogical features. These ratio images were further used as inputs for composite visualization and subsequent analyses, such as Principal Component Analysis (PCA) and classification, to support litho-structural interpretation.

3.2.1.3.Supervised Classification

Supervised classification was applied to Landsat 9 imagery to map lithological units using training data derived from field observations and image interpretation. The 38 field observation points collected during the field survey were first used as reference locations to identify representative lithological classes within the imagery. Around each field observation

point, Regions of Interest (ROIs) were defined by manually delineating homogeneous areas that exhibited consistent spectral characteristics and corresponded to the same lithological unit, as confirmed by field notes and visual inspection of spectrally enhanced images (Sikakwe, 2023). Each ROI therefore consisted of multiple pixels rather than a single point, allowing the spectral variability within each lithological class to be adequately captured. In total, several hundred pixels were included across all ROIs, with pixel selection distributed among the major lithological units to ensure balanced and representative training samples. The supervised classification was then performed in ArcGIS using the Maximum Likelihood Classifier (MLC). This classifier assigns each pixel to the lithological class with the highest probability of membership based on its spectral similarity, assuming a normal statistical distribution for each class (Verbovšek & Popit, 2018). This approach allowed field-based information to be systematically translated into image-based training data for lithological classification.

3.2.2. Satellite gravity

Gravity data contain the sum of the effects of different sources, including shallow and deep bodies. These two components are the regional (deep) and residual (shallow) (Fig. 5) anomalies (Eldosouky et al., 2020). The regional field represents the long-wavelength, low-frequency variations in the potential field data, while the residual anomaly highlights the shorter-wavelength, high-frequency variations (Núñez-Demarco et al., 2023).

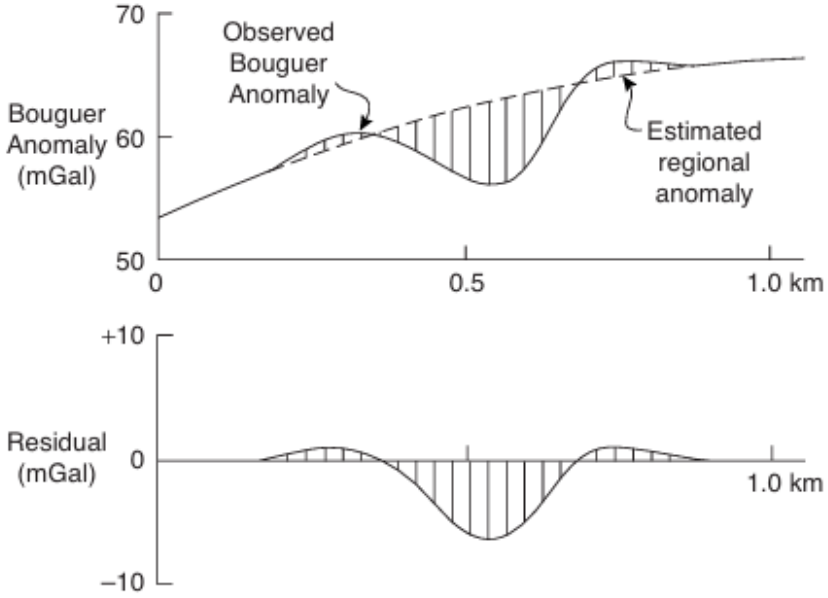

Fig. 5 Observed Bouguer anomaly, estimated regional anomaly, and residual anomaly (after Reynolds, 2011)

In this study, a Gaussian regional-residual filter with a standard deviation of 0.456 is applied to separate anomalies from gravity data during processing in Oasis Montaj software. For creating filters to distinguish regional and residual anomaly fields, the power spectrum approach was used. Using the Fast Fourier Transform (FFT), spectral analysis is performed in the wavenumber domain. FFT shifts the data from the time domain to the frequency domain, aiding in the characterization and modelling of features. FFT-based filtering is recognized as an effective approach for objective geomorphic mapping, particularly within complex terrains such as karst landscapes (González-Díez et al., 2021). When applied to DEMs and LiDAR datasets, FFT filters enhance landform boundaries, reduce positional uncertainty, and support efficient feature extraction with lower computational demands compared to conventional approaches (González-Díez et al., 2021).

Edge detection techniques, including the Total Horizontal Derivative (THD) and First Vertical Derivative (FVD), were applied to the residual gravity anomaly map to enhance and delineate structural features such as faults, fractures, and lineaments derived from gravity data processing in Oasis Montaj (Kebede et al., 2021). The total horizontal derivative (THD) or horizontal gradient of potential field data quantifies the rate of change of the strength of the gravitational and magnetic fields in the horizontal direction (Camacho & Alvarez, 2021; Grauch & Cordell, 1987). It provides information about lateral variations in the gravity and magnetic fields, with geological structures located at the highest amplitudes of the resulting anomalies (THD > 0). The magnitude of the horizontal gradients is calculated as a vector sum of horizontal derivatives of x (E-W) and y (N-S) for the gravitational field (g) (Eq. 1) as:

$$THD = \sqrt{\left(\partial g/\partial x\right)^2 + \left(\partial g/\partial y\right)^2} \quad (1)$$

Where:

g= gravity anomaly value (usually Bouguer or residual gravity anomaly), $\frac{\partial g}{\partial x}$= horizontal gradient of the gravity anomaly in the x-direction (east–west), $\frac{\partial g}{\partial y}$= horizontal gradient of the gravity anomaly in the y-direction (north–south).

The first vertical derivative (FVD) of gravity data captures the rate of change of the gravitational and magnetic field strength with respect to the vertical direction (Elrinst, 1950). It provides insight into the vertical distribution of subsurface density contrasts (Keating, 1995).

In the analysis of the FVD map, the line of zero anomaly represents the edge of the causative bodies. It is obtained by Eq. (2) as:

$$FVD = \sqrt{\left(\partial g / \partial z\right)^2} \tag{2}$$

Together, these techniques provide a clearer structural framework essential for interpreting subsurface geology and understanding groundwater flow pathways.

3.2.3. Machine Learning Models

To classify lithological units within the upper Mereb catchment, Support Vector Machine (SVM) and Artificial Neural Network (ANN) algorithms were implemented using the machine-learning modules of ENVI software. The classification was based on a remote-sensing-derived lithological map validated by field observations, ensuring its reliability as reference data. Training and testing samples were generated from this map using a point-based pixel selection approach, in which representative regions of interest (ROIs) were delineated for each lithological class to capture their spectral variability. The dataset was randomly divided into 70% for model training and 30% for independent testing. Both ANN and SVM models were trained and applied to generate lithological classification maps, and their performance was evaluated using confusion matrices from which overall accuracy and F1-score were derived. Based on these evaluation metrics, the classification result with the highest accuracy was selected as the final lithological map, supporting the reliability of remote-sensing-derived lithological mapping and demonstrating its effectiveness in reducing time and fieldwork effort, particularly in inaccessible or rugged areas (El-Omairi et al., 2025).

Support Vector Machine (SVM) is a robust, non-parametric supervised machine-learning algorithm widely applied in remote-sensing-based lithological mapping due to its strong generalization capability and effectiveness in handling complex, high-dimensional, and non-linearly separable datasets (M. J. Cracknell & Reading, 2014). In this study, SVM classification was implemented within the ENVI software environment, which provides an efficient framework for spectral data processing and model optimization. The algorithm determines an optimal separating hyperplane in a multidimensional feature space by maximizing the margin between different lithological classes, thereby minimizing classification errors (J. Lu et al., 2023). To effectively capture non-linear relationships between spectral variables and lithological units, a Radial Basis Function (RBF) kernel was employed, enhancing the discrimination of complex and heterogeneous rock assemblages (Fig. 6).

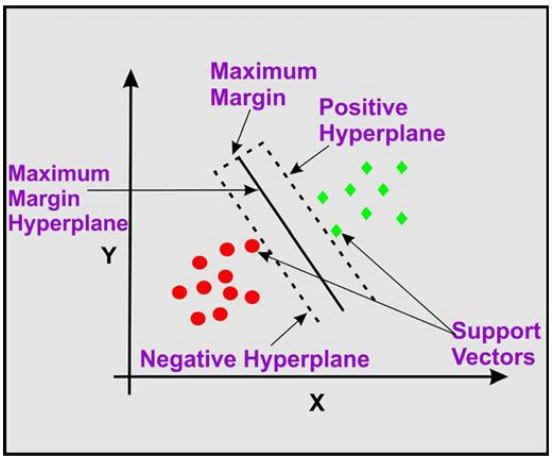

Fig. 6 Schematic diagram of support vector machine (source: Prajapati et al., 2024)).

The SVM model was configured using a penalty parameter (C) of 100 and a gamma (γ) value of 0.333, selected through iterative testing of multiple parameter combinations to ensure stable model behavior and effective lithological discrimination (K. M. Asghede et al., 2025; Ghezelbash et al., 2019). The penalty parameter controls the trade-off between margin maximization and classification error, while gamma governs the influence of individual training samples and the smoothness of the decision boundary (Xiao et al., 2026). Proper tuning of these parameters reduced both overfitting and underfitting, thereby improving classification reliability. The final SVM configuration was selected based on classification stability and accuracy assessment metrics.

Artificial Neural Networks (ANNs) were employed as an advanced machine-learning approach to classify lithological units and improve the accuracy of geological mapping. ANNs are well suited for remote-sensing-based lithological discrimination due to their ability to model complex, non-linear relationships between spectral features and geological formations (Sun et al., 2025). In this study, a feed-forward neural network architecture consisting of an input layer, one hidden layer, and an output layer was implemented in ENVI (Fig. 7), simulating the learning behavior of the human brain (Ren et al., 2019). The input layer comprised spectral bands and derived indices, including band ratios, while the hidden layer transformed these inputs into higher-level representations through weighted connections (F. X. Liu et al., 2025). Model training was performed using a learning rate of 0.200 and a momentum value of 0.9 to ensure stable convergence, with 1000 training iterations selected to balance computational efficiency and classification performance (Daoud, Shebl, Nafi, et al., 2025). Overall, the ANN approach provided a robust framework for integrating spectral information with ground-truth data, resulting in reliable lithological classification and more precise geological mapping.

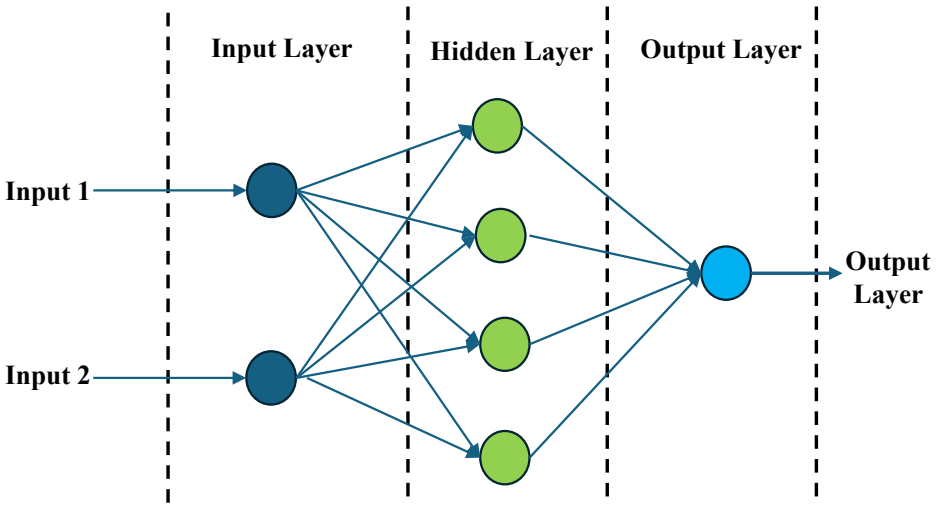

Fig. 7 Structure of ANN applied in the study

3.2.4. Analytical Hierarchy Process (AHP)

Groundwater potential mapping was undertaken to delineate areas with varying prospects for groundwater occurrence and recharge within the upper Mereb catchment. The analysis incorporated multiple environmental parameters known to influence groundwater availability and applied a set of decision-making and statistical models, including the Analytical Hierarchy Process (AHP) and the Frequency Ratio (Fig. 8). Integrating these approaches enhances both the objectivity and reliability of the mapping process, as it combines expert-driven weighting with data-driven statistical relationships. This methodological framework (Fig. 8) is essential for identifying groundwater potential zones, supporting resource planning, and guiding sustainable groundwater development in the study area.

Table 2 Saaty's scale for relative importance (Saaty & Katz, 1990)

Range of importance	Description
1	Equal importance
3	Moderate importance
5	Essential
7	Very strong importance
9	Extreme importance
2, 4, 6, 8	Intermediate values between adjacent scale values

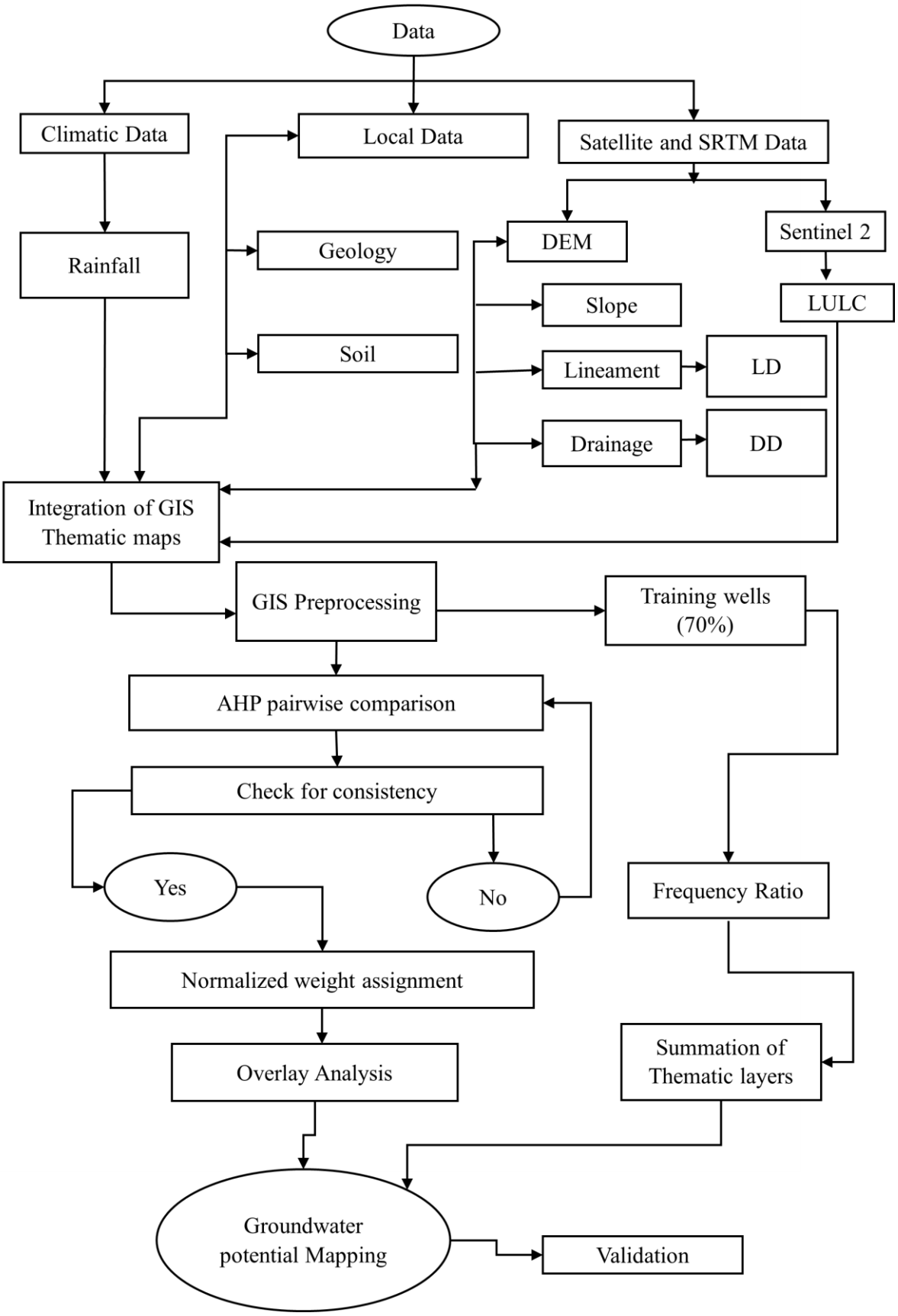

Fig. 8 Groundwater potential mapping framework using AHP and FR.

Note: DD-Drainage Density, LD-Lineament Density, LULC-Land-use/Landcover, DEM-Digital Elevation Model

The Analytic Hierarchy Process (AHP) is widely applied across diverse disciplines for decision-making (Ahmadi et al., 2021; Raja Shekar & Mathew, 2023). It enables the determination of the relative weights or priorities of criteria through systematic pairwise comparisons of the datasets (Saaty & Katz, 1990). These comparisons are made using the Saaty scale (Saaty & Katz, 1990), which ranges from 1 to 9 (Table 2), allowing for a systematic assessment of the relative importance of each parameter in the groundwater potential analysis. The AHP pairwise comparisons were derived in this study based on the expert judgment, such as, the author's and local expert hydrogeological interpretation of the study area (K. Asghede & Vágó, 2025), supported by field observations and guided by established weighting schemes reported in similar groundwater studies (Ozegin et al., 2023; Zenande et al., 2024).

In this study, the AHP models utilized seven key environmental parameters: geology, soil, rainfall, slope, land use/land cover (LULC), drainage density, and lineament density. The selection of these seven parameters was based on their well-established influence on groundwater occurrence, recharge, storage, and flow in hard-rock and semi-arid environments, as widely recognized in hydrogeological theory and previous groundwater potential studies (Adesola et al., 2023; K. M. Asghede & Vágó, 2025). The factors were selected as groundwater control parameters, with a random index value of 1.32 based on the number of factors (Table 3). Following Saaty's principle, the consistency ratio was calculated as the ratio of the consistency index to the random index (Eq. 3). The values depend on the number of selected parameters (Table 3). According to Saaty's guideline, for a parameter with seven factors, the consistency ratio should ideally be less than 0.1 to adopt the evaluated weight. The consistency index (Eq. 4) was employed to verify this criterion. Subsequently, the weight of each factor was determined, serving as a basis for prioritizing parameters in developing the groundwater potential map.

Table 3: Saaty's ratio index for different "n" values

N	3	4	5	6	7	8
RI	0.58	0.89	1.12	1.24	1.32	1.41

$$CR = \frac{CI}{RI} \tag{3}$$

$$CI = \frac{(\lambda - n)}{(n - 1)} \quad (4)$$

Where:

CI: Consistency index, CR: Consistency ratio, RI: Random index, λ: maximum principal eigenvalue, and n: number of compared elements or parameters.

Subclass ranking was assigned based on percolation rates for contributing water to underground storage, drawing on various literature reviews and expert judgments (Popalzai et al., 2023; B. Sharma & Pandey, 2023). Final weight was determined by multiplying each subclass's rank by the feature's weight. The weighted overlay tool in the ArcGIS Pro spatial analysis toolbox was used to sum all weighted features and generate the required groundwater potential map. Ensuring uniformity in cell size and projection systems across all layers is imperative to facilitate a smooth analysis process (Thanh et al., 2022). Therefore, I applied a 30m cell size and the UTM zone 37 WGS projection system.

3.2.5. Frequency Ratio (FR) Model

The Frequency Ratio (FR) model is a well-established bivariate statistical method (Fig. 8) used for assessing the spatial relationship between groundwater occurrences and conditioning factors (Pawar et al., 2024; Razandi et al., 2015). It assumes that the spatial distribution of existing groundwater features (e.g., wells) is influenced by a combination of environmental and geological parameters (Li et al., 2023). The method quantifies the degree of correlation between groundwater presence and each conditioning factor class to estimate the likelihood of groundwater occurrence in unsampled areas. The frequency ratio approach has been widely used in studies assessing groundwater potential (Belkendil et al., 2025; Das & Pardeshi, 2018). In this study, this model was applied to delineate groundwater potential zones within the upper Mereb catchment. The modelling process involved several steps: selection of influencing factors, preparation of thematic layers, spatial integration of well data, computation of frequency ratios, and generation of the final groundwater potential map (Islam, 2024). A total of seven thematic layers (Fig. 8) were selected based on their hydrogeological relevance and data availability: geology, slope, soil, land use/land cover (LULC), drainage density, lineament density, and rainfall. Each factor was derived from remote sensing data and topographic, climatic, and field survey information.

All thematic layers were processed in ArcGIS Pro and reclassified into discrete classes while maintaining a uniform spatial resolution across datasets. This step was essential because the Frequency Ratio (FR) model operates as a class-based statistical method rather than a continuous one. Reclassification allows each environmental factor to be divided into meaningful intervals, enabling the quantitative evaluation of the relationship between groundwater occurrence and the controlling parameters (Eqs. 5 and 6). A total of 190 groundwater well locations, obtained from the database of the Asmara Water Resources Department (WRD), were used as the dependent variable in the analysis. These wells were randomly split into two datasets: 70% for training the Frequency Ratio (FR) model and 30% for validation and accuracy assessment. The training dataset was spatially overlaid on each thematic layer to determine the number of wells present in each class of the conditioning factors (Elvis et al., 2022). The frequency ratio (FR) for each conditioning factor class was computed by comparing the spatial distribution of groundwater well locations with the areal distribution of that class (Eq. 5).

The FR value was calculated using the following equation:

$$FR_i = \frac{(\frac{N_{wi}}{N_w})}{(\frac{N_{pi}}{N_p})} \tag{5}$$

Where FR_i= Frequency Ratio value for class *i* of a given factor, N_{wi}= Number of groundwater well points within class *i*, N_w= Total number of groundwater well points, N_{pi}= Number of pixels (or area) within class *i*, and N_p= Total number of pixels (or total area) of the study region.

The resulting FR value represents the relative influence of each parameter class on groundwater occurrence. A value greater than one ($FR > 1$) indicates a higher probability of groundwater presence, while a value less than one ($FR < 1$) suggests an unfavorable condition for groundwater accumulation (Islam, 2024). After computing the FR values for all classes, each thematic layer was reclassified in ArcGIS according to its corresponding FR values. The reclassified layers were then integrated using a raster calculator to produce the Groundwater Potential Index (GWPI) map through the following linear summation (Eq. 6):

$$GWPI = \sum_{i=1}^{n} FR_i \tag{6}$$

where n represents the total number of conditioning factors used in the analysis.

Finally, the predictive performance of both the Analytic Hierarchy Process (AHP) and Frequency Ratio (FR) models was evaluated using Receiver Operating Characteristic (ROC) analysis. This method assesses each model's ability to correctly identify groundwater occurrence based on the distribution of observed well locations. The Area Under the Curve (AUC) was calculated for each model, providing a quantitative indicator of prediction accuracy and allowing a direct comparison of their overall discriminatory power. To complement the statistical evaluation, a spatial overlay comparison was performed to examine the spatial agreement between the AHP and FR outputs. High and very high groundwater-potential zones in both models were first reclassified into binary raster, separating high-susceptibility areas from lower-susceptibility ones. These binary layers were then combined through a cell-by-cell raster overlay operation using the Raster Calculator in ArcGIS Pro. The resulting agreement map was grouped into three categories representing non-high areas, areas of full agreement, and areas of partial agreement, enabling a structured assessment of spatial correspondence between the two modelling approaches.

3.2.6. Hydrochemical data analysis

To comprehensively assess the groundwater quality of the upper Mereb catchment, a combination of hydrochemical, graphical and statistical approaches was employed (Fig. 9). These methods were designed to interpret the chemical composition of groundwater, identify the dominant geochemical processes, and evaluate its suitability for domestic and agricultural purposes. Groundwater samples were collected and analyzed by the Asmara water resources department from representative wells for major cations (Ca^{2+}, Mg^{2+}, Na^{+}, K^{+}), anions (HCO_3^{-}, Cl^{-}, SO_4^{2-}, NO_3^{-}) and other parameters following standard procedures. The analytical results were processed using a suite of hydrochemical evaluation tools, including multivariate statistical analysis, Water Quality Index (WQI), and Irrigation Indices. To further evaluate the suitability of groundwater for irrigation, indices such as the Sodium Adsorption Ratio (SAR) and USSL were investigated. The combination of these hydrochemical methods provides a robust framework for diagnosing groundwater quality variations and supporting sustainable groundwater management in the arid and semi-arid upper Mereb catchment.

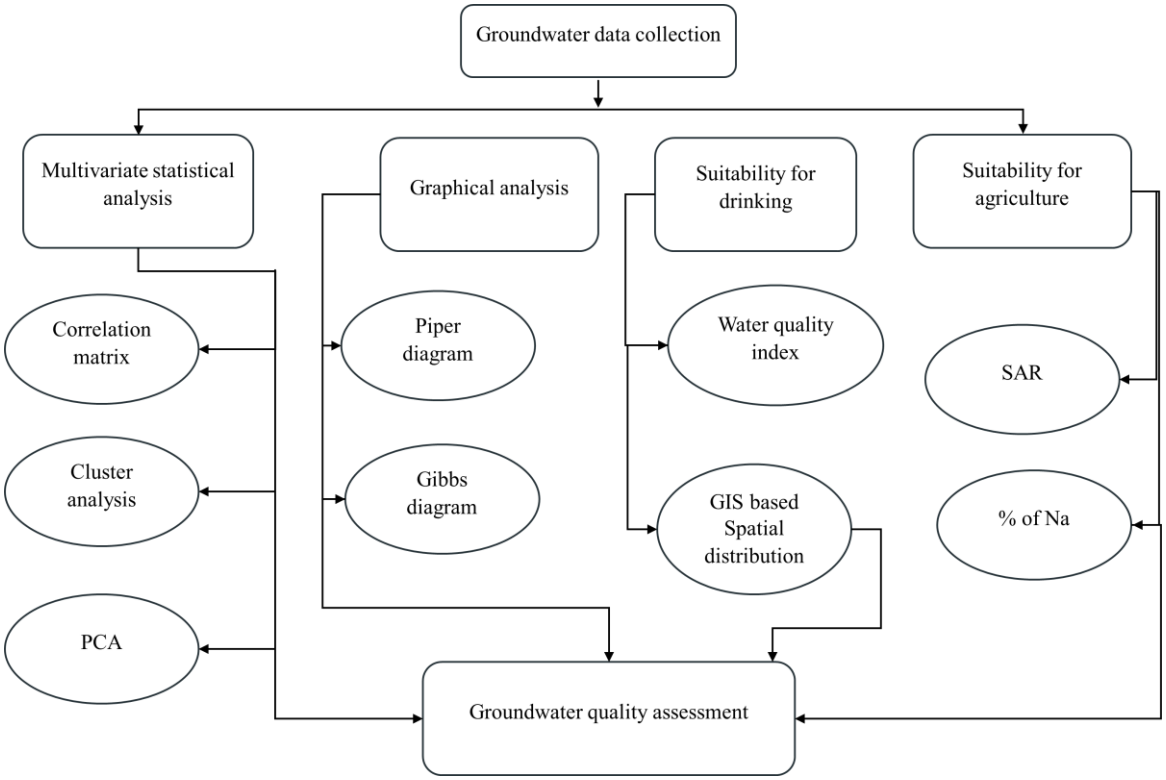

Fig. 9 Comprehensive framework of groundwater quality assessment in the upper Mereb area

3.2.6.1.Multivariate statistical analysis

Multivariate statistical methods, including Pearson's correlation, Hierarchical Cluster Analysis (HCA), and Principal Component Analysis (PCA), were applied to explore complex relationships among water quality parameters and identify underlying patterns in the dataset (P. Kumar et al., 2024). Understanding the relationships among groundwater constituents is effectively achieved through a correlation matrix, which provides insights into how other hydrochemical parameters may influence the concentration of a given hydrochemical parameter during groundwater evolution (Yan et al., 2025). In this study, the Pearson correlation coefficient was used to evaluate linear relationships among the measured hydrochemical parameters. This method was selected because the variables exhibited approximately normal distributions and linear trends, verified through basic exploratory analyses such as histograms, normal probability plots, and scatterplots. A correlation coefficient is present in every cell of the matrix that represents the associations (Gnanachandrasamy et al., 2020).

Hierarchical Cluster Analysis is a powerful numerical technique for identifying hidden patterns within datasets by grouping similar objects or variables without predefined classifications (Alitane et al., 2024). Unlike traditional classification methods, it discovers natural clusters based on internal similarities and external differences, refining groupings iteratively to achieve optimal classification (Perumal, 2025). The result of the cluster analysis

is visualized in OriginPro software using dendrograms, which reduce the complexity of the original data and provide a graphical representation of clusters and their proximity. Based on the clustering results, sampling locations belonging to the same cluster were assigned to a common group, and these grouped data were spatially interpolated within a GIS environment to generate a classification map. This process resulted in the delineation of three distinct spatial cluster maps.

Principal Component Analysis (PCA) was employed to identify the major factors controlling groundwater chemistry and to reduce redundancy among the measured physicochemical parameters. It is a multivariate statistical technique that transforms a large set of correlated variables into a smaller number of uncorrelated variables known as principal components (PCs), each representing a specific proportion of the total data variance (AL-Areeq et al., 2023; F. Liu et al., 2023). In this study, PCA was performed using OriginPro, a software package that provides robust computational and visualization tools for multivariate data analysis. Eigenvalues and eigenvectors were extracted to identify the most significant components, with components having eigenvalues greater than one (Kaiser's criterion) retained for interpretation (Bisht et al., 2025). Each component was then analyzed in relation to the hydrogeochemical and environmental context to infer the natural and anthropogenic processes influencing groundwater quality, including mineral dissolution, ion exchange, and agricultural inputs. Overall, PCA facilitated a more efficient and objective interpretation of complex groundwater chemistry data, serving as a diagnostic tool for identifying key controlling mechanisms and spatial patterns (Ghimire et al., 2025).

3.2.6.2. Water quality index

It is a mathematical tool used to assess water quality. It converts extensive water-quality data into a single numerical value, enabling the representation of water-quality levels (Horton, 1965). These indices are designed to provide a concise summary, facilitate easy comprehension and comparison, and reduce the amount of information in the raw data. To evaluate the suitability of the water samples for human consumption, the physicochemical parameters analyzed were compared with the World Health Organization (WHO, 2011) recommended drinking water quality standards. These standards, which serve as reference values for calculating the Water Quality Index (WQI), are presented in Table 4.

Table 4: Weights and relative weights for each parameter used for calculating WQI

Parameter (mg/L)	Weight (Wi)	Relative weight (Wi)	WHO Guideline (2011)
pH*	4	0.071	8.5
EC#	2	0.036	1500
TDS	5	0.089	500
ALKA	2	0.036	300
TH	2	0.036	500
Ca	3	0.054	75
Mg	3	0.054	150
Na	4	0.071	200
K	2	0.036	12
Fe	4	0.071	0.7
Mn	3	0.054	0.1
HCO_3	2	0.036	350
SO_4	4	0.071	200
Cl	4	0.071	250
NO_3	5	0.089	45
NO_2	5	0.089	3
NH_3	2	0.036	0.5

In computing WQI, three steps are followed. In the first step, each of the 17 parameters collected from the Asmara Water Resources Department has been assigned a weight (wi) based on its relative importance to the overall quality of drinking water. The maximum weight of 5 has been assigned to parameters such as TDS, NO2, and NO3- owing to their significant role in water quality assessment (Mohammed, Eltijani, et al., 2023; Shaibur et al., 2024). Other parameters were assigned weights (Wi) ranging from 1 to 5 based on their importance in determining water quality (Table 4).

In the second step, the relative weight (Wi) is computed from Eq. 7 as

$$Wi = \frac{wi}{\sum_{i=1}^{n} wi} \tag{7}$$

Where the Wi is the relative weight, wi is the weight of each parameter, and n is the number of parameters. Calculated relative weight (wi) values for each parameter are given in Table 4.

*: No unit, #: µS/cm

In the third step, a quality rating scale (q_i) for each parameter was computed by dividing its concentration in each water sample by its respective standard concentration as (Eq. 8)

$$q_i = \frac{C_i}{S_i} \times 100 \quad (8)$$

where qi is the quality rating scale, Ci is the concentration of each chemical parameter in each water sample, in mg/L, and Si is the standard water quality for each chemical parameter, in mg/L, according to the WHO (2011) guidelines. For computing the WQI, the SI_i is first determined for each chemical parameter (Eq. 9), which is then used to determine the WQI (Eq. 10) as:

$$SI_i = w_i \times q_i \quad (9)$$

$$WQI = \sum_{i=1}^{n} \mathrm{SI}_i \quad (10)$$

where the SI_i is the sub-index of the i^{th} parameter, q_i is the rating based on the concentration of the i^{th} parameter, and n is the number of parameters. The calculated water quality index was classified into five classes: excellent (0–50), good (51–100), poor (101–200), very poor (201–300), and not suitable for drinking (>300) (Amit Hasan et al., 2026). Finally, based on the measured water quality parameters, a spatial distribution map was developed using the Inverse Distance Weighting (IDW) interpolation technique within a GIS environment to assess the spatial variability of groundwater quality across the study area.

3.2.6.3. Irrigation indices

Groundwater suitability is crucial for sustaining agricultural productivity, especially in regions with limited surface water. It ensures crops receive adequate, good-quality water for healthy growth and yields (Mohammed, Kaya, et al., 2023). Assessing groundwater quality helps prevent soil degradation and salinity issues over time (Jarray et al., 2023; Mohamed et al., 2023). Ultimately, understanding suitability supports sustainable agricultural practices and long-term food security. The suitability of groundwater for irrigation is evaluated using the Sodium Adsorption Ratio (SAR) and Sodium percentage (Na%).

The Sodium Adsorption Ratio is a key indicator used to evaluate the suitability of water for irrigation, specifically assessing the potential for soil sodium hazard (Richards, 1954). It reflects the relative concentrations of Na^+, Ca^{2+}, and Mg^{2+} ions in water. High values can lead to soil dispersion, reduced permeability, and poor soil structure, negatively affecting crop productivity (Mohammed, Kaya, et al., 2023; Shemsanga, 2024). Therefore, measuring SAR is

essential for managing irrigation water quality and maintaining long-term soil health and is calculated using Eq. 11.

$$SAR = \frac{Na^{+}}{\sqrt{\frac{\sqrt{(Ca^{2+} + Mg^{2+})}}{2}}} \tag{11}$$

where Na, Ca and Mg are expressed in meq/L. The SAR range for irrigation water is categorized into four classes: SAR<10, suitable for most crops and soil types; SAR between 10 and 18, is classified as moderate use for soils; SAR between 18 and 26, is considered doubtful; and SAR > 26, is considered unsuitable (Faraji & Shahryari, 2024). Based on the United States Salinity Laboratory (USSL) diagram, the water was classified as "low sodium and medium salinity" (S1–C2) and "low sodium and high salinity" (S1–C3).

Sodium percentage is another important parameter used to assess the suitability of water for irrigation, indicating the proportion of Na^{+} ions relative to the total cations (calcium, magnesium, sodium, and potassium) present in the water (Wilcox, 1948). High sodium levels can reduce soil permeability, impair drainage, and lower soil fertility, ultimately harming crop growth (Demo et al., 2025). Evaluating sodium percentage helps farmers and water managers determine potential risks and take appropriate measures to protect soil health and agricultural productivity.

The Na% can be calculated using Eq. 12 as:

$$Na\% = \frac{Na^{+}}{(Ca^{2+} + Mg^{2+} + Na^{+} + K^{+})} \tag{12}$$

where all the parameter concentrations are expressed in meq/L, according to the percentage of sodium water, which is classified as excellent (< 20%), good (20 – 40 %), permissible (40 – 60 %), doubtful (60 – 80 %), and unsuitable (>80 %) (Singh et al., 2024) in this study, different physicochemical parameters of groundwater were analyzed using data collected by the Water Resources Department in Asmara in 2017.

4. RESULT and DISCUSSION

This section presents the major findings of the study, beginning with the lithological and structural characterization of the upper Mereb catchment derived from remote sensing, field observations, satellite gravity data, and machine-learning enhancements. These geological results form the basis for developing the GIS and remote sensing-based groundwater potential model, where key environmental conditioning factors are evaluated and integrated to delineate potential groundwater zones. The section further examines groundwater quality using physicochemical analyses of collected groundwater samples, hydrochemical diagrams, and multivariate statistical techniques to assess the suitability of groundwater for drinking and agricultural use. Together, these results provide a comprehensive understanding of the groundwater system, integrating geological controls, resource potential, and water quality conditions within the catchment.

4.1.Geological mapping

4.1.1. Lithological identification

The lithological discrimination results derived from mineral-sensitive band ratios and supervised classification show a clear spatial differentiation of the major rock units in the study area. The application of band ratios targeting ferrous minerals, hydroxyl-bearing minerals, and ferric iron oxides significantly enhanced spectral contrast among lithologies (Fig. 10). The Maximum Likelihood supervised classification (Fig. 10a) delineates the dominant lithological units with good spatial consistency, while the 5/6 band ratio highlights metasedimentary and metamorphic units concentrated in the eastern sector of the area (Fig. 10b). Basaltic rocks are distinctly emphasized by the 6/7 band ratio, appearing prominently in the western sector (Fig. 10c), reflecting their mafic mineral composition. Ferric oxide band combinations (4/3) clearly identify lateritic surfaces, which extend along a north–south trend through the central part of the study area (Fig. 10d).

In Fig. 10, the high and low legend values represent relative index values derived from mineral-specific band ratios. It indicates the strength of spectral responses associated with the corresponding mineral constituents, where higher values reflect stronger mineral signatures and lower values indicate weaker or absent mineral expression. These lithological units are hydro-geologically significant because fractured basalts and lateritic covers commonly favor higher infiltration and groundwater storage, whereas groundwater occurrence in crystalline metamorphic and metasedimentary rocks is largely controlled by secondary porosity associated with fractures and weathering (Sikakwe, 2023).

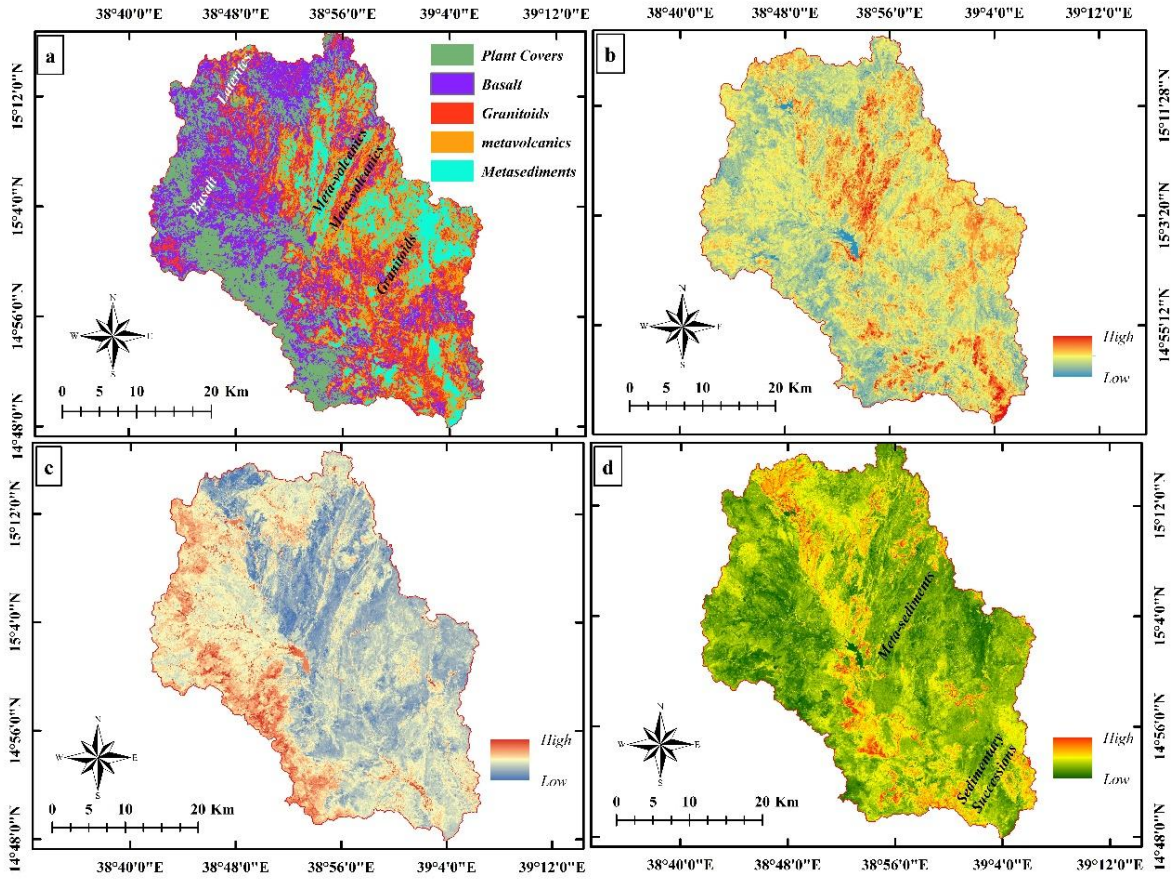

Fig.10 Supervised and mineral sensitive lithological classification (a) Maximum likelihood supervised classification; (b) band 5/6; (c) bands 6/7; (d) ferric oxide bands 4/3.

The evaluation of false-color composites (FCCs) and spectral transformation techniques demonstrates the strong capability of Landsat-9 imagery for lithological discrimination in the upper Mereb catchment. Comparative analysis of several FCC combinations (R6G3B1, R7G5B3, R5G4B3, and R6G5B4; Fig. 11a–d) shows notable differences in their effectiveness for highlighting geological units based on spectral contrast and spatial expression. Among these, the R6G3B1 composite produced the clearest separation of major lithological units, allowing basaltic flows, metavolcanic and metasedimentary sequences, granitic bodies, and lateritic deposits to be distinguished by distinct color tones and patterns (Fig. 11a). It highlights the advantage of combining shortwave infrared and visible bands to enhance lithological contrasts in areas with sparse vegetation and cloud cover where bedrock signatures dominate (Ghrefat et al., 2021).

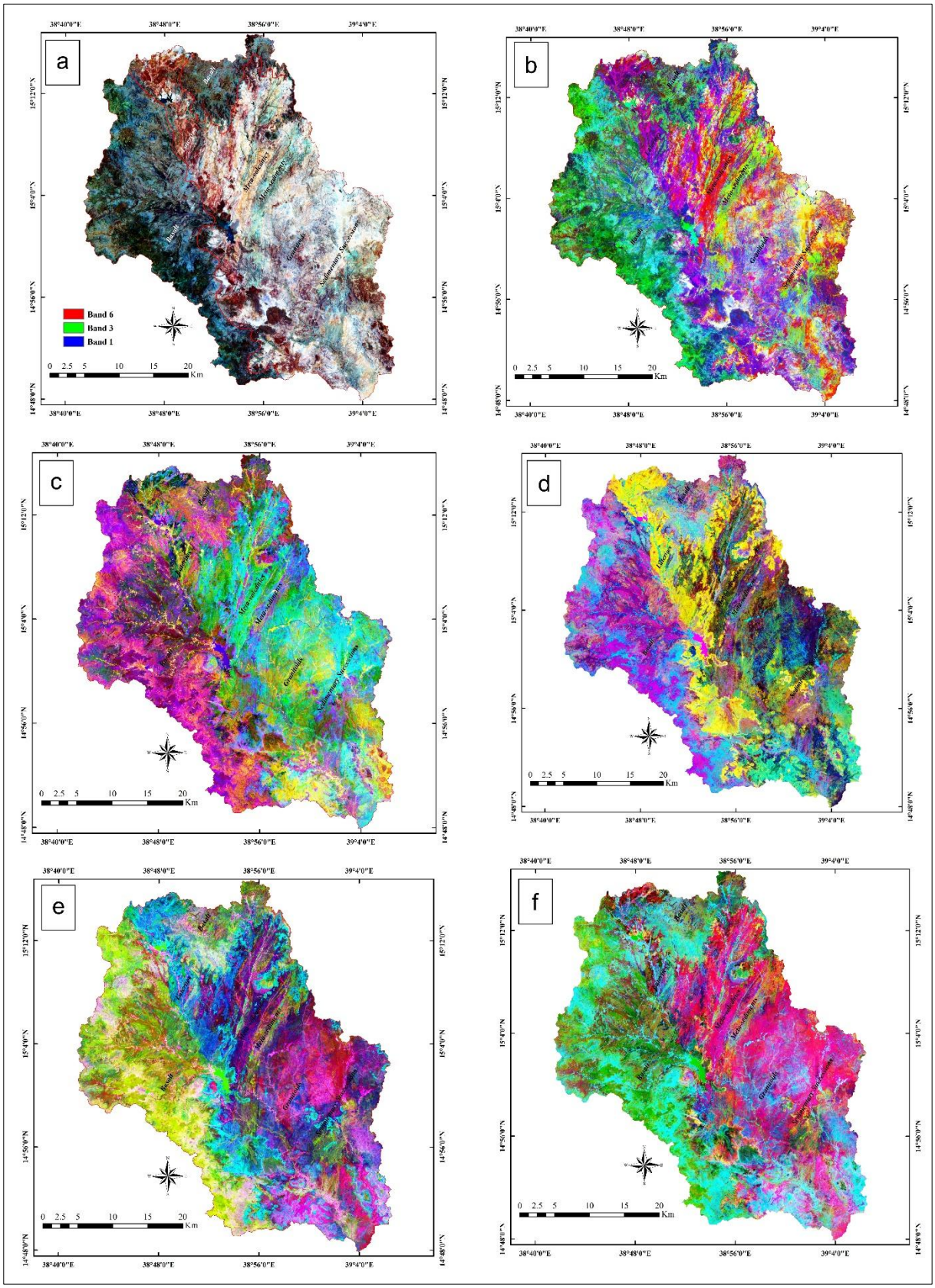

Fig. 11 L9 based band combination; (a) 631 in RGB; (b) 753 in RGB, (c) 543 in RGB; (d) 654 in RGB; (e) PC of bands 5/4,5/7,3/1in RGB; (f) 2/1–5/4, 5/6, 6/7 in RGB.

Principal Component Analysis (PCA) and selected band-ratio images further enhanced lithological boundary definition by emphasizing relative spectral variations rather than

categorical classes, where pixel values represent processed spectral responses displayed through RGB compositing (Fig. 11e, f). These enhanced images clearly emphasize major lithological units, with basaltic rocks distinctly expressed in the western sector, granitic bodies more prominent toward the east, and sedimentary to metasedimentary units differentiated by tonal variations in their respective zones. Because FCCs, PCA outputs, and band-ratio images depict relative spectral responses through color combinations, a conventional legend is not applicable. Therefore, lithological unit names are indicated directly within the figure panels to ensure the maps remain interpretable when viewed independently (Fig. 11). Compared to individual approaches, the combined use of FCCs, PCA, band ratios, and supervised classification provided more coherent and reliable lithological mapping.

The lithological framework derived from the integrated analysis of Landsat-9 imagery provides a valuable basis for understanding groundwater occurrence and hydrogeological variability in the highlands of Eritrea. The clear spatial delineation of basaltic rocks, lateritic covers, metavolcanic sequences, and crystalline units highlights zones with contrasting infiltration capacity, storage potential, and groundwater flow behavior. Basaltic and lateritic terrains are particularly important due to their tendency to develop permeable weathered and fractured zones, whereas groundwater in metamorphic and granitic units is mainly confined to structurally controlled pathways (Paswan et al., 2025). Consequently, the detailed lithological characterization presented here constitutes a critical environmental parameter for subsequent groundwater potential modeling and for interpreting spatial patterns of groundwater quality. Moreover, the results demonstrate that tailoring spectral indices and false-color composites to the mineralogical characteristics of the terrain significantly improves lithological discrimination, thereby strengthening geological understanding for groundwater-related decision-making in arid and semi-arid regions (Daoud, Shebl, Abdelkader, et al., 2025).

4.1.2. Lineament extraction

The development of the lineament map in the study area was based on the integration of multiple gravity-derived products and topographic analysis. The complete Bouguer anomaly map (Fig. 12a) was obtained directly from GGMPlus, which provides pre-corrected gravity data including standard Bouguer and terrain corrections. The anomaly values range from approximately −165 mGal to −121 mGal, reflecting subsurface density variations. Gravity highs are interpreted as zones of dense lithologies such as mafic intrusions or crystalline basement, whereas gravity lows are associated with less dense materials, including sedimentary cover or fractured zones (Haughton et al., 2009; Senosy et al., 2013). To improve the interpretation of deeper structures, the Bouguer anomaly was upward continued to 100 m (Fig.

12b), which suppresses high-frequency signals and enhances regional trends (Bezák et al., 2023). Subsequent anomaly separation produced the regional anomaly (Fig. 12c), highlighting deep-seated tectonic features, and the residual anomaly (Fig. 12d), which emphasizes shallow structures such as faults and lithological boundaries. These structural features are critical for hydrogeological interpretation, as zones associated with gravity lows and residual anomalies are likely to represent areas of increased porosity and permeability.

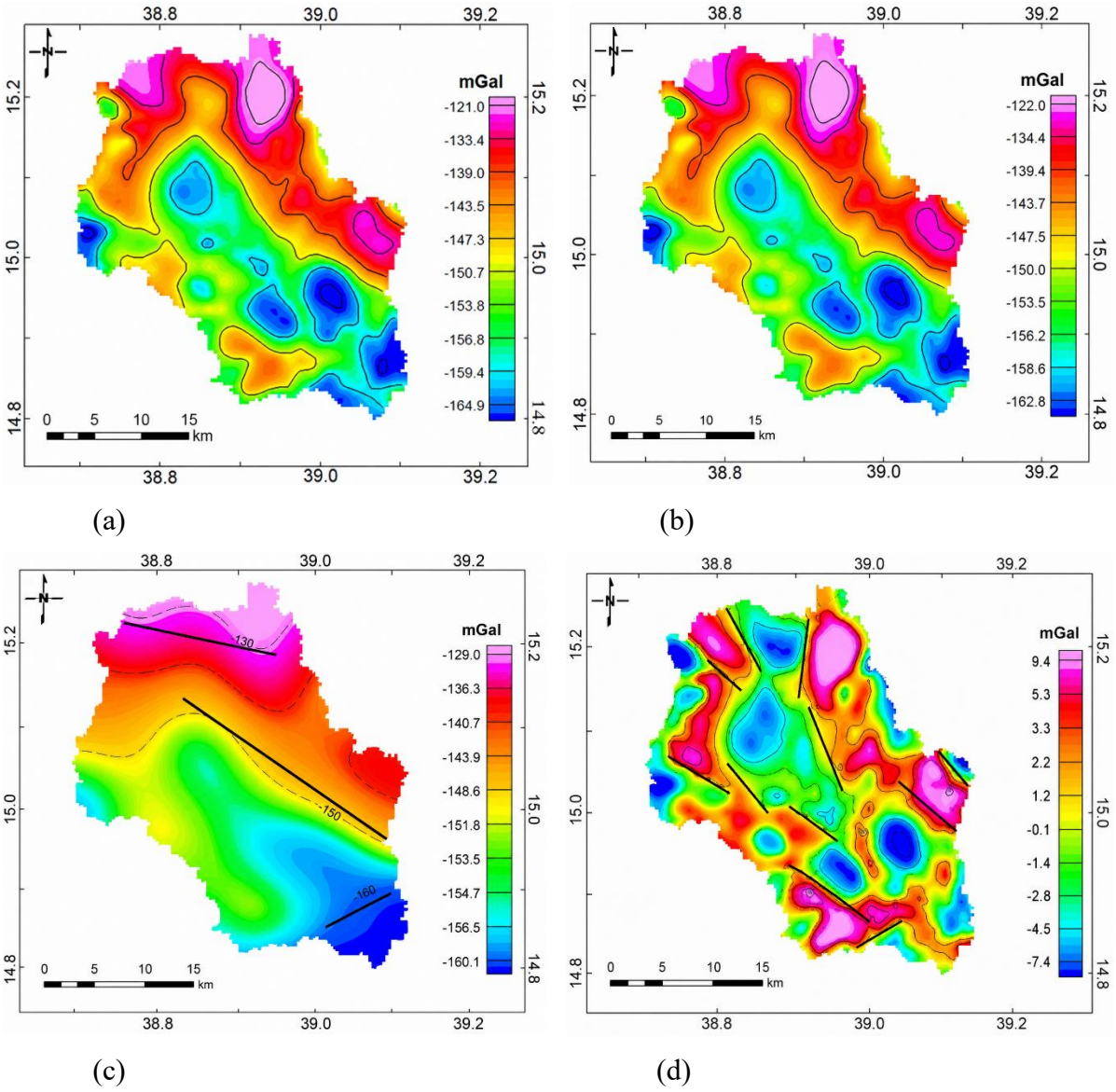

Fig. 12 Satellite gravity based structural identification; (a) Bouguer anomaly map; (b) Upward continued Bouguer anomalies to 100 m; (c) Regional anomaly map; (d) Residual anomaly map of upper Mereb area.

Further structural enhancement was achieved using derivative techniques. The total horizontal derivative (THD) map (Fig. 13a) enhances lateral density contrasts and effectively delineates structural boundaries (Lghoul et al., 2023), while the first vertical derivative (FVD)

map (Fig. 13b) emphasizes near-surface discontinuities. Lineaments extracted from these maps show dominant NE–SW and NW–SE orientations, consistent with the regional tectonic framework of the Arabian-Nubian Shield (Hamimi et al., 2022b). The NE–SW trends are interpreted as extensional features related to Red Sea rifting, whereas NW–SE trends may reflect strike-slip or oblique tectonic stresses associated with plate interactions. Importantly, the distinction between regional and residual lineaments has hydrogeological significance: deep-seated regional structures may act as major conduits controlling large-scale groundwater flow, while shallow residual lineaments represent fracture zones that enhance local permeability, groundwater recharge, and storage (Epuh et al., 2020). Thus, the integration of these gravity-derived lineaments provides insight not only into tectonic evolution but also into structural controls on groundwater occurrence.

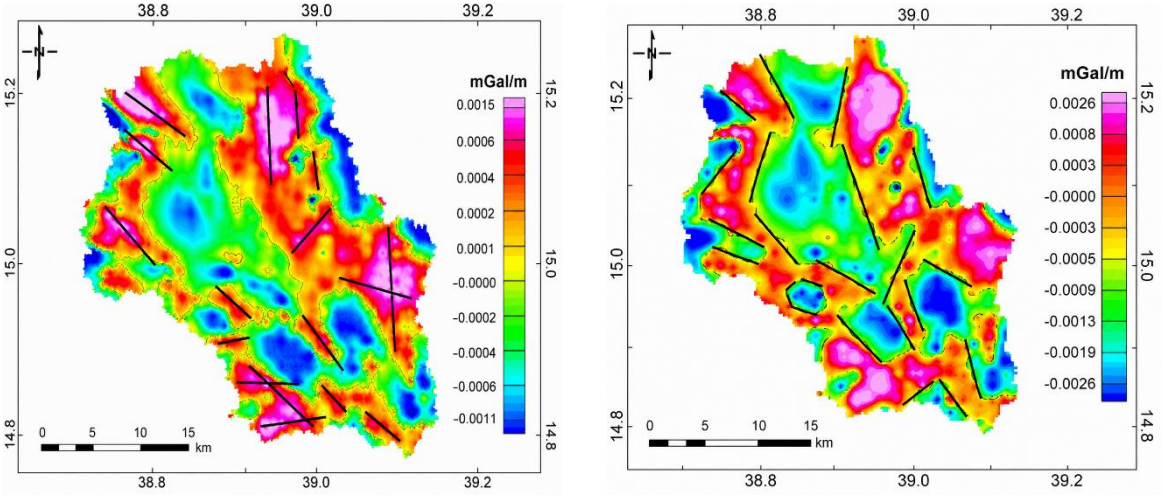

(a) (b)

Fig. 13 Identification of edges and shallow litho-features; (a) The total horizontal derivative map showing fault zones and lithological boundaries; (b) The first vertical derivative map showing near-surface features and density contrast

To complement subsurface analysis, surface lineaments were extracted from DEM data using four hillshade images with varying illumination angles (315–45, 90–50, 100–60, and 200–50). Lineaments were manually digitized by visually tracing linear features, ensuring consistency through comparison across hillshade views (Sadiq et al., 2022). The composite lineament map (Fig. 14a) integrates all extracted features from gravity derivatives and DEM analysis, showing good spatial agreement between surface and subsurface structures. However, to address redundancy and noise, a filtering and generalization step was applied to produce the final lineament network (Fig. 14b). This refinement was carried out manually, guided by geological knowledge, spatial continuity, and structural relevance. Less distinct and repetitive features were removed, while consistent and well-defined lineaments were retained,

particularly those supported by multiple datasets. The resulting map highlights the principal structural trends, which are relevant for groundwater interpretation as they may influence fracture distribution and groundwater movement.

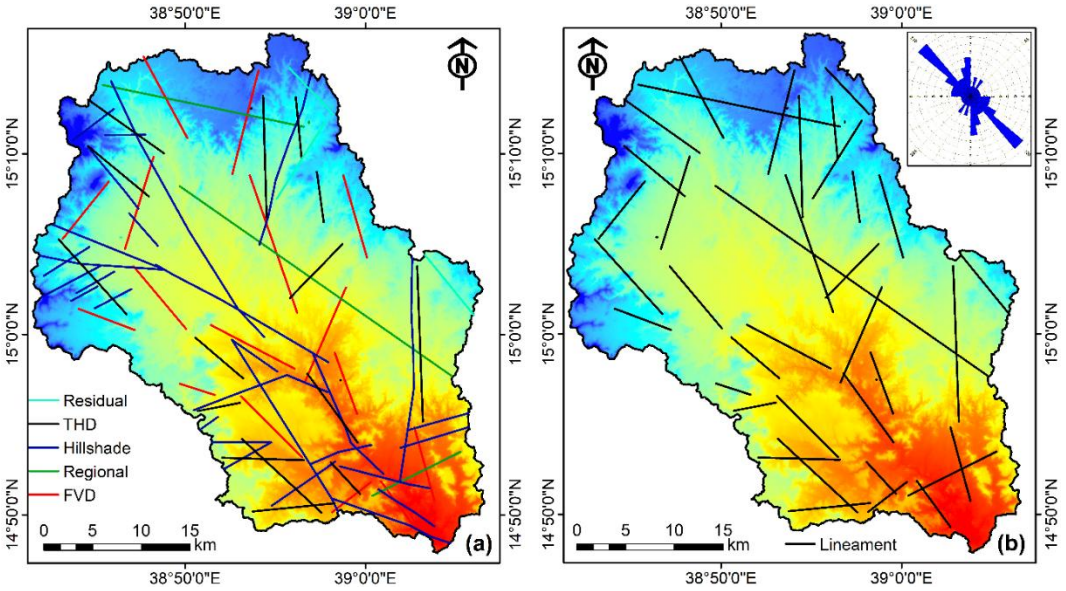

Fig. 14 Integration of lineaments obtained from (a) gravity and hillshade map, (b) final filtered structural map.

4.1.3. Litho-structural map

The litho-structural map of the study area (Fig. 15) was produced by integrating remote sensing data and gravity-derived structural information, providing a comprehensive representation of both the lithological distribution and the structural framework. The lithological units were delineated by correlating satellite imagery spectral signatures with field-based ground-truth observations. Six major lithological units were identified, including basalt, granite, laterites, sedimentary rocks, meta-sedimentary rocks, and meta-volcanic rocks. Basaltic units dominate the western part of the study area, covering 39.5% (584.6 km²) and forming extensive, relatively continuous outcrops. Lateritic deposits are prominently developed in the central sector, accounting for 14.5% (214.5 km²), and extend predominantly north–south. Granite bodies account for 22.8% (337.2 km²) of the area and, together with metavolcanic units (9.6%, 141.5 km²) and metasedimentary units (5.7%, 84.8 km²), are mainly exposed in the eastern and southeastern parts, reflecting marked lithological heterogeneity and a complex geological evolution.

Sedimentary units occupy about 8% (118.8 km²) and are primarily distributed in the southern and southeastern downstream portions of the upper Mereb catchment. The superimposed lineament network reveals well-developed structural features that cut across

multiple lithological units, indicating strong structural control on the regional geological framework. The associated rose diagram highlights a dominant NW–SE lineament orientation, suggesting a principal tectonic trend that has influenced both lithological emplacement and subsequent deformation (Fig. 14b). Overall, the litho-structural map highlights the value of integrating diverse datasets to accurately delineate lithological boundaries and structural patterns (Bosino et al., 2019; Fagbohun et al., 2017). The combined interpretation of remote sensing data, field observations, and gravity information provides a more complete understanding of both surface and subsurface geological conditions, representing the first comprehensive litho-structural characterization of the upper Mereb area.

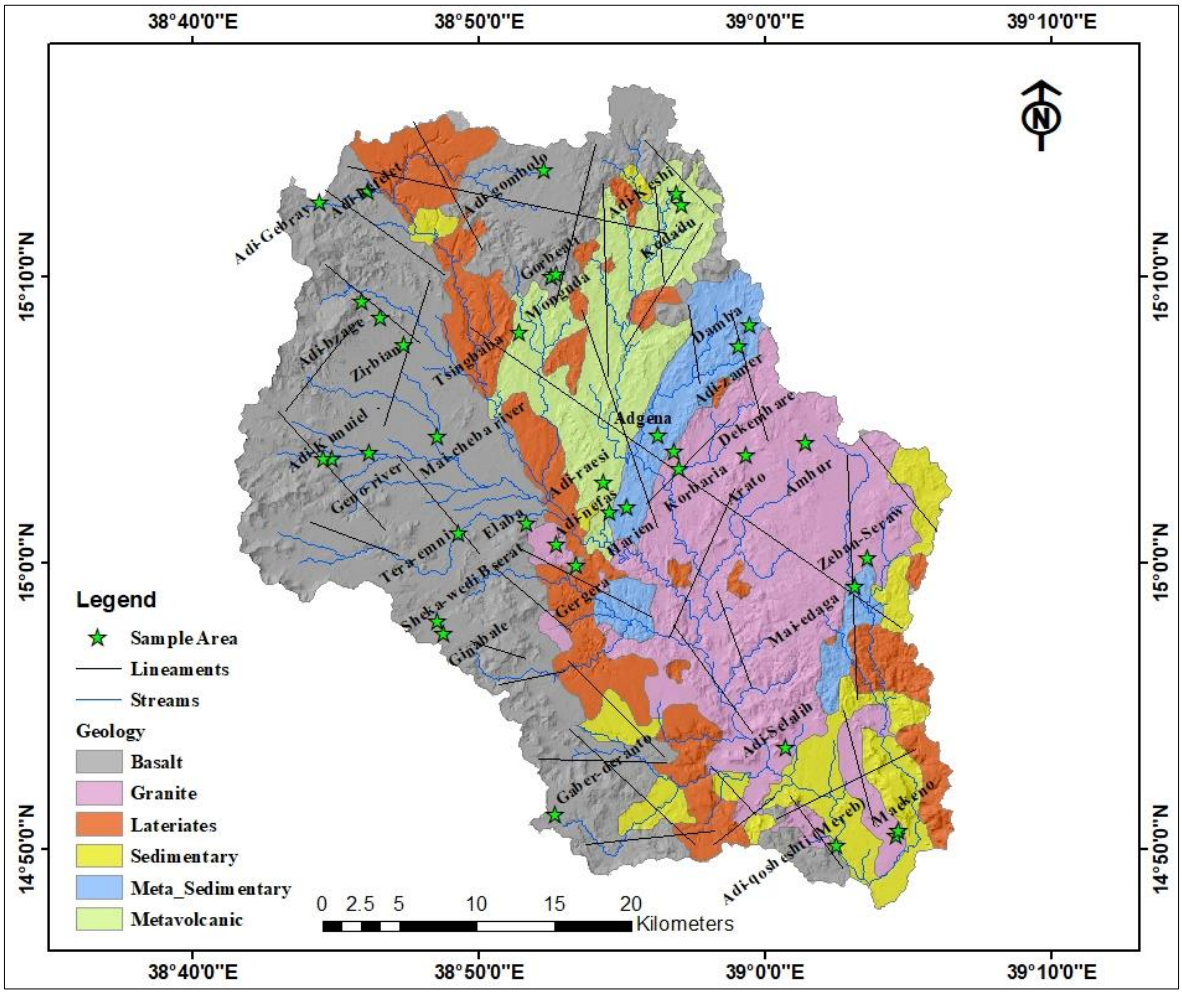

Fig. 15 Geological map of upper Mereb obtained from the analysis of remote sensing and gravity data and confirmed by detailed field observations.

Field observations covered most accessible sectors of the area and provided reliable ground-truth information that confirms the presence, distribution, and characteristics of the major lithological and structural units identified through remote sensing and geophysical analyses. The study area comprises different lithological units during the field observation:

intermediate metavolcanic rocks, sedimentary rocks, granitic intrusions, and basaltic lava flows, with extensive lateritic deposits developed in the northern and southern parts (Fig.16). These investigations confirm that the metavolcanic rocks are predominantly felsic to intermediate in composition and locally display greenschist-type mineral assemblages, as observed at Dekemhare near Adi Nefas (Fig. 16i).

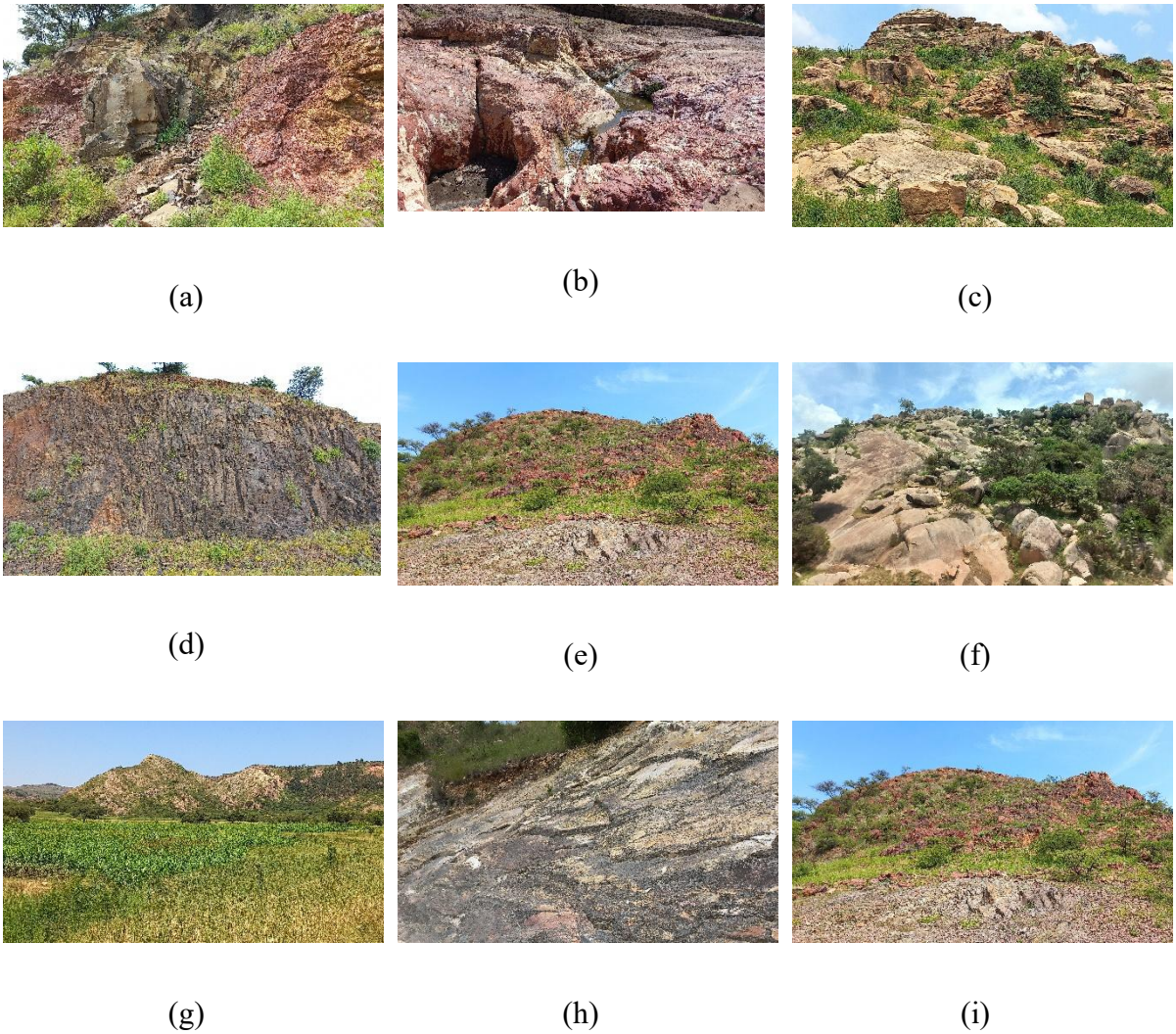

(a) (b) (c)

(d) (e) (f)

(g) (h) (i)

Fig. 16 Geological sample sites, photograph taken in summer 2024 showing:

(a) Mafic dyke (Monguda area), (b) Metavolcanic (Adi-Kefelet, at Endagabir Maichelot), (c) Sedimentary rock (at Maekeno, Mai-Ayni), (d) Basalt (at Sheka-wedi Bserat), (e) Laterite (near Adi-Zamer), (f) Granitoid (near Dekemhare), (g) Meta-sediment (near Adi-Keshi), (h) Rhyolite lateralized (near Gorbeati), (i) Metavolcanics with rhyolite laterite (near Dekemhare Adi_nefas).

At Gorbeati, rhyolitic and lateritized rocks are classified as low- to medium-grade metamorphic rocks of greenschist facies. They are well foliated, striking 043° and dipping 68° toward the west (dip direction 313°) (Fig. 16h). Similar units are also observed at Adi-Kefelet near Endagabir Maichelot, where the upper portions are strongly lateritized, forming red laterite and white bauxite horizons that are occasionally interlayered, producing distinctive red-and-

white banding (Fig.16b). The sedimentary sequence, unconformably overlying the metamorphic in the southern part of the area (Maekeno near Mai-Ayni), extends E–W and comprises arkose sandstone, mudstone with shale intercalations, and quartz-rich sandstone (Fig.16c). Crossbedding in these units indicates paleocurrents trending predominantly southward. Granitic intrusions, particularly around Dekemhare and Elaba (Fig. 16f), consist mainly of quartz, sodium-rich plagioclase, and K-feldspar; the Elaba granite is quartz-phyric, with exceptionally large crystals, but is weakly resistant to weathering, contributing to extensive soil cover.

Basaltic lava flows dominate the western third of the study area, unconformably overlying the lateritized basement, and are composed of multiple eruptive episodes with massive lower units and amygdaloidal upper parts. The basalt, fine- to medium-grained and olivine-phyric, typically exhibits spheroidal weathering around Monguda (Fig. 16a) and columnar jointing south of Dubarwa at Sheka Wedi Bisrat (Figure 16d). The laterite unit (Fig. 16e), up to 10 m thick, occurs between the basalt and overlying sediments; its low permeability creates spring horizons at its upper contacts. Structurally, mafic dykes trending N–S (000/90 or 180/90) crosscut almost all units and are especially prominent in Monguda, while a dense swarm of basaltic dykes striking between 210° and 300° dips steeply westward (85–90°). Quartz veins, fractures, and joints of variable orientation are also widespread.

Overall, the litho-structural map, supported by targeted field observations and photographic documentation of key outcrops (Fig. 16), provides a reliable representation of the major lithological and structural units of the study area, despite unavoidable limitations related to accessibility and spatial coverage. Field observations confirmed the presence and surface expression of the six dominant lithological units: basalt, granite, laterite, sedimentary, metasedimentary, and metavolcanic rocks. These strengthening interpretations derived from remote sensing, gravity analysis, and DEM-based structural mapping. From a groundwater perspective, this litho-structural framework defines the primary controls on infiltration, storage, and subsurface flow in the hard-rock terrain. Where, weathered sedimentary and lateritic units favor recharge and shallow storage, and fractured basalts, granites, and metavolcanics provide secondary porosity and preferential flow paths along structural discontinuities. Although field validation was constrained to accessible areas, the integrated litho-structural interpretation provides a sound basis for groundwater-focused analyses and offers a reference framework for future investigations in the study area. In this context, exploring machine-learning applications becomes increasingly important in geological mapping, as training algorithms on representative

spectral signatures can reduce extensive fieldwork demands, save time and resources, and improve the consistency of lithological discrimination across difficult-to-access terrains.

4.1.4. Machine learning analysis (MLA)

Based on results from the L9 satellite imagery (FCC, band ratios, and principal components), supported by field observations presented in the previous sections, training and testing datasets for the machine learning algorithms were generated in ENVI. A point-based sampling approach (Fig. 17) was adopted to capture the complexity of lithological units within the study area, with 70% of the samples used for training and 30% reserved for testing and validation (Table 5). The classification results of the ANN and SVM models are presented in Table 6, focusing on overall accuracy and F1-score. The ANN model achieved an overall accuracy of 79.89%, which is comparable to that of the SVM (79.22%). Similarly, the F1-score of ANN (0.85) was slightly higher than that of SVM (0.84), indicating a comparable level of agreement between predicted and actual classes.

Table 5: Training and testing data used to map the lithological units using machine learning models

Lithology	Training data	Testing data	Percentage %
Basalt	875	227	25.943
Laterites	834	273	32.734
Metasediments	849	212	24.97
Metavolcanics	928	245	26.40
Granitic rocks	889	264	29.70
Sedimentary sequences	816	243	29.79
Water body	786	177	22.52

The confusion matrix (Table 7 and 8) reveals several notable misclassifications that highlight underlying spectral similarities and geological interrelations among the lithological units. Table 7 shows a considerable number of basalt samples (26 pixels) were misclassified as granite, likely due to overlapping spectral features, particularly in altered zones or at the margins of intrusive bodies where compositional gradients occur. Similarly, granitoids (particularly quartz-phyric granite) were misclassified as basalts (26 pixels), possibly due to mafic intrusions within granitoid bodies that exhibit basalt-like spectral characteristics. The most prominent misclassification occurred between laterites and metavolcanic rocks, with 72

lateritic pixels having a similar mineral composition and 115 metavolcanic pixels misclassified as laterites. This confusion stems from the compositional relationship between these units: laterites often form from the intense weathering of volcanic rocks, resulting in similar iron-rich, oxidized surfaces with nearly indistinguishable spectral signatures (Voll et al., 2020).

Table 6 Comparison of ANN and SVM Classification Results

Metric	SVM Classification	ANN Classification
Overall Accuracy	79.22% (1300/1641)	79.89% (1311/1641)
F1-Score	0.84	0.85

Table 7: Confusion Matrix of ANN classifier

Class	Basalt	Laterites	Metasediment	Meta-volcanic	Sedimentary	Granite	Water Body	Total
Basalt	197	0	8	3	0	26	0	234
Laterites	2	157	0	72	0	1	0	232
Meta-sediment	2	0	179	1	8	6	0	196
Meta-volcanic	0	115	1	211	18	5	0	350
Sedimentary	0	0	18	3	210	7	0	238
Granite	26	1	6	4	7	180	0	224
Water Body	0	0	0	0	0	0	177	177
Total	227	273	212	245	243	264	177	1641

Additionally in table 7, metamorphic units such as metasediments and metavolcanics exhibited notable confusion with sedimentary rocks. For instance, 8 pixels of metasediments and 18 of metavolcanics were classified as sedimentary rocks, due to the preservation of sedimentary rocks in low-grade metamorphosed rocks and surface weathering effects that obscure diagnostic spectral features. Granites also contributed to this misclassification trend, with 7 pixels confused with sedimentary rocks, possibly where granite surfaces are heavily weathered and fractured. These patterns emphasize the limitations of the current classification

approach in distinguishing lithologies with overlapping spectral responses, particularly in transitional zones and areas affected by weathering and alteration.

Table 8: Confusion Matrix of the SVM model

Class	Basalt	Laterites	Meta-sediment	Meta-volcanic	Sedimentary	Granite	Water Body	Total
Basalt	205	0	8	0	0	8	0	221
Laterites	0	161	0	3	0	2	0	259
Meta-sediment	14	0	178	0	3	9	0	196
Meta-volcanic	0	110	2	197	3	4	0	315
Sedimentary	0	0	15	41	228	9	0	287
Granite	8	2	9	4	9	154	0	186
Water Body	0	0	0	0	0	0	177	177
Total	227	273	212	245	243	264	177	1641

The SVM classification results (Table 8) reveal several persistent and significant misclassifications, particularly among lithological units with similar spectral characteristics or overlapping geological contexts. One of the most prominent patterns is confusion between metavolcanic rocks and laterites, with 110 metavolcanic pixels misclassified as laterites, a pattern similar to that of the ANN classifier. Additionally, metasediments showed significant confusion with both sedimentary and granitic rocks; specifically, 14 metasediment pixels were misclassified as basalts, 3 as sedimentary rocks, and 9 as granitoids. These errors can be attributed to spectral overlaps caused by compositional similarities, especially in low-grade metamorphic rocks that retain sedimentary features or exhibit weathered surfaces. Basalts were largely well-classified, though a small number of pixels were confused with metasediments (8) and granitoids (8), again suggesting challenges in boundary zones or areas with altered mafic rocks. Figure 17 illustrates the spatial distribution and class composition of the training data used for lithological prediction.

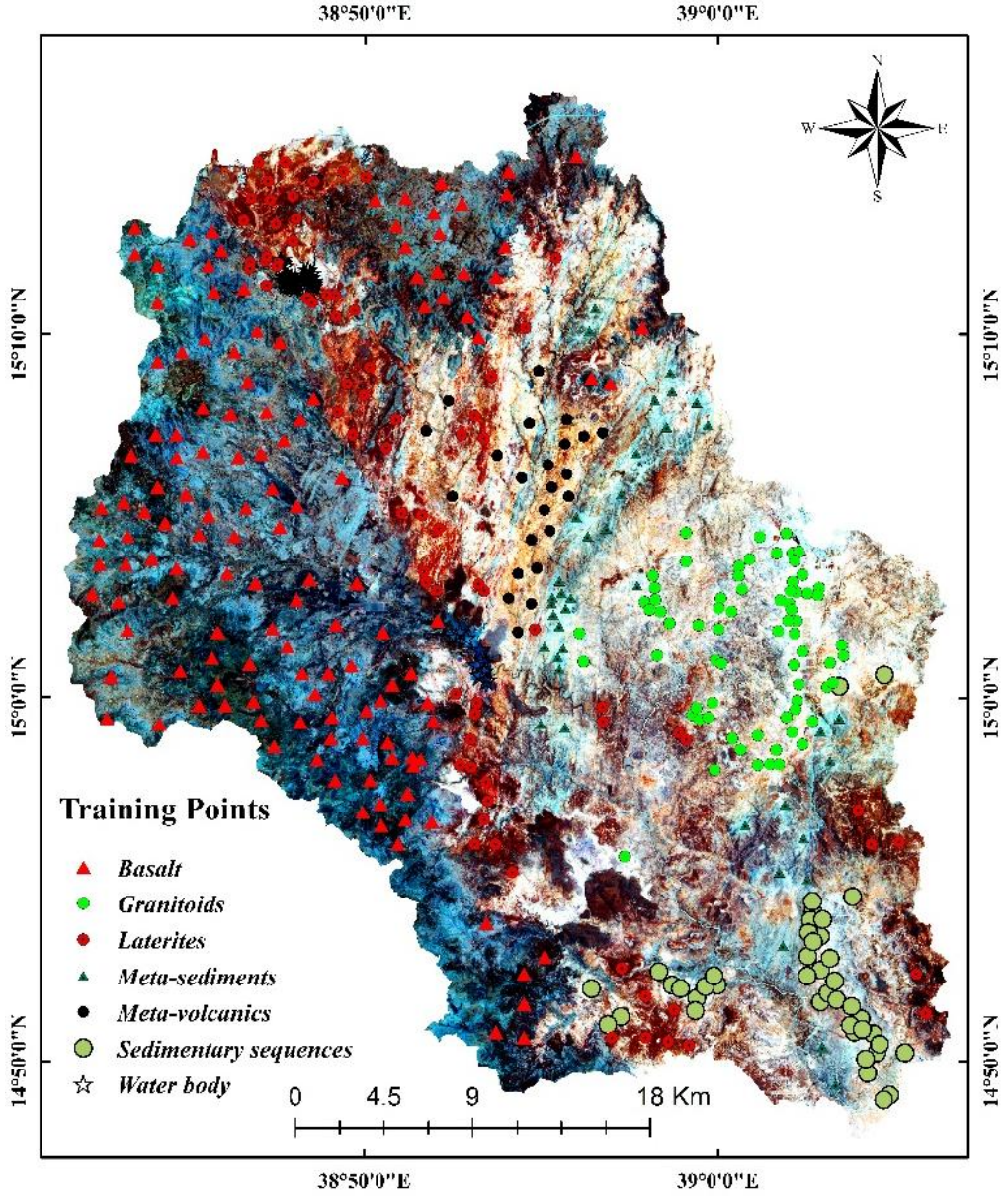

Fig. 17 The distribution of the training data used for lithological prediction

Finally, an ANN-based lithological map of the study area was produced based on the overall accuracy and F1-score results (Fig. 18). The resulting map reveals a generally good classification performance, although some misclassification was observed in laterites, metavolcanics, and granitic rocks, likely due to complex spectral signatures and spectral similarities with adjacent lithological units. Overall, the application of machine-learning techniques to lithological mapping demonstrates strong performance in supporting and validating remote-sensing-based geological interpretations. The classification results indicate that data-driven models are capable of effectively distinguishing major lithological units using spectral information, with consistent accuracy and balanced performance across classes. Beyond classification accuracy, the approach offers clear practical advantages by reducing the need for extensive fieldwork, particularly in areas with limited accessibility, thereby saving

time, effort, and resources. Consequently, machine-learning-assisted mapping is especially valuable in data-scarce and rugged terrains, such as the upper Mereb area. From a groundwater perspective, improved lithological discrimination enhances understanding of aquifer-hosting units and their spatial continuity, which is essential for groundwater potential assessment and resource planning. Importantly, the machine-learning framework adds value by providing a flexible and repeatable approach that can be readily updated as higher-resolution data or additional training information become available, offering future researchers an effective pathway to refine geological and groundwater-related interpretations.

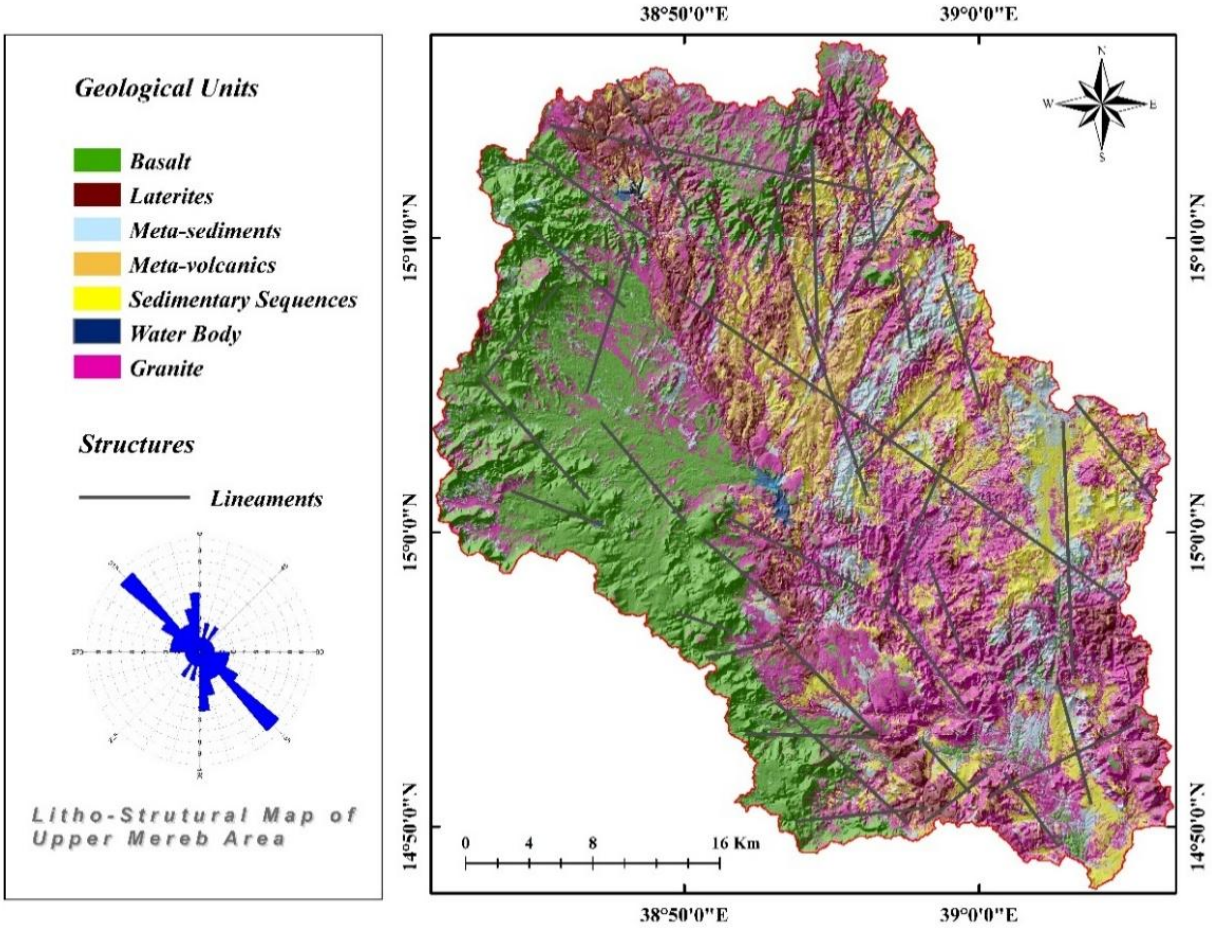

Fig. 18 Litho-structural map of upper Mereb area generated from integration of remote sensing, gravity data and machine learning algorithms (ANN)

4.2.Groundwater potential mapping

This study employed a geospatial approach integrating GIS and remote sensing techniques to delineate groundwater potential zones in the upper Mereb catchment, Eritrea. Two methodological frameworks, the Analytical Hierarchy Process (AHP) and Frequency Ratio (FR), were applied to assess and compare groundwater potential across the region. The novelty of this study lies in the first application of an integrated AHP–FR geospatial framework

in the upper Mereb catchment, enabling cross-validation of expert- and data-driven groundwater potential assessments in a data-limited, structurally complex environment.

4.2.1. Conditional factors

To identify groundwater potential zones, it is crucial to examine the primary environmental and hydrogeological factors that control groundwater occurrence, recharge, and movement (Díaz-Alcaide & Martínez-Santos, 2019). Groundwater availability is shaped by the interaction of surface processes, subsurface properties, and climatic influences, each affecting infiltration, storage capacity, and flow pathways in distinct ways (Davamani et al., 2024). In line with established hydrogeological principles, seven conditioning parameters known to significantly influence groundwater distribution were selected to construct a comprehensive and spatially integrated groundwater potential model as discussed in the following sections.

Table 9: AHP-based pairwise comparison matrix and weights of conditioning factors

Parameter	Geology	Soil	Lineament Density	Rainfall	LU/LC	Slope	Drainage density	Criteria weights
Geology	1	2	2	3	3	4	4	29.40%
Soil	0.5	1	2	2	3	3	4	21.70%
Lineament density	0.5	0.5	1	2	3	3	4	17.80%
Rainfall	0.33	0.5	0.5	1	2	3	3	12.40%
LULC	0.33	0.3	0.33	0.5	1	2	2	8.10%
Slope	0.25	0.3	0.33	0.33	0.5	1	2	6.10%
Drainage density	0.25	0.25	0.25	0.33	0.5	0.5	1	4.60%

The relative importance of the selected conditioning factors was quantified using an AHP-based pairwise comparison matrix (Table 9) with the reference of expertise judgement, which reflects their comparative influence on groundwater occurrence in the study area. The results indicate that geology (29.4%) and soil (21.7%) exert the strongest control, highlighting the dominant role of lithological permeability and soil infiltration capacity in groundwater recharge. Lineament density (17.8%) and rainfall (12.4%) also make significant contributions, underscoring the importance of structural pathways and climatic inputs, whereas LULC (8.1%), slope (6.1%), and drainage density (4.6%) play secondary but supportive roles in regulating runoff and infiltration processes. Based on these weights, each thematic layer was reclassified and assigned ranks, and normalized weights were applied (Table 9) to standardize their influence prior to integration. These weighted layers were subsequently combined using a GIS-based weighted overlay technique to generate the final groundwater potential zonation map.

Table 10: Normalized weights of conditioning factors for Groundwater Potential Mapping

Factor	Normalized weight	Weight based on Saaty's scale
Geology	29.4	
Lateriates		4
Basalt		5
Granit		2
Meta-Sedimentary		3
Meta-Volcanic		3
Sedimentary		5
Soil	21.7	
Vertic Cambisol		2
Luvisol		3
Cambisol		4
Lineament Density (km/km2)	17.8	
0 - 0.015		1
0.015 - 0.045		2
0.045 - 0.086		3
0.086 - 0.135		4
0.135 - 0.19		5
Rainfall (mm)	12.4	
45.36 - 49.35		5
42.65 - 45.36		4
40.45 - 42.65		3
38.8 - 40.45		2
36.3 - 38.8		1
Landuse/Landcover	8.1	
Water		7
Trees		5
Flooded Vegetation		6
Crops		5
Built Area		1
Bare Grounds		1
Rangeland		5
Slope (Degree)	6.1	
0 - 4.69		5
4.69 - 10.55		4
10.55 - 17.82		3
17.82 - 26.97		2
26.97 - 59.81		1
Drainage Density (km/km2)	4.6	
0 - 0.15		5
0.15 - 0.39		4
0.39 - 0.63		3
0.63 - 0.91		2
0.91 - 1.62		1

4.2.1.1.Drainage density

The drainage density map of the upper Mereb catchment (Fig. 19) ranges from 0 to 1.62 km/km^2, reflecting substantial spatial variation in surface drainage development across the basin. Higher weights were assigned to low-drainage-density zones, as sparse drainage networks favor greater infiltration and groundwater recharge. In contrast, high-drainage-density areas were assigned lower weights due to dominant surface runoff and reduced groundwater accumulation potential (Gidafie et al., 2024).

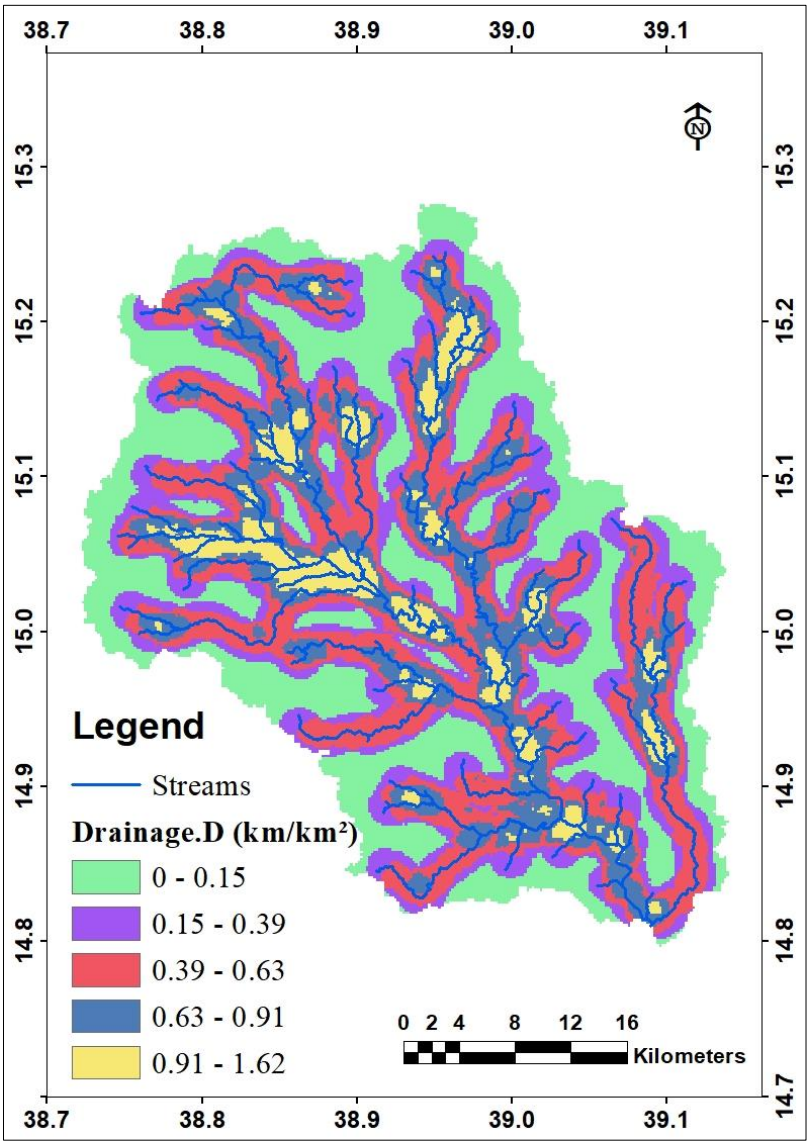

Fig. 19 Spatial Classification of Drainage Density in the Upper Mereb Catchment

Areas with low drainage density (0 - 0.15 km/km^2) are mainly located in the central and lower parts of the catchment, where gentle topography, relatively permeable lithological units, and mature soil profiles promote higher infiltration and reduced surface runoff (Fig. 19). These conditions enhance groundwater recharge, consistent with previous studies highlighting the

hydrological significance of low drainage density in favorable recharge environments (Shelar et al., 2023). In contrast, zones with high drainage density (0.91-1.62 km/km^2) are concentrated in the upper and peripheral areas of the watershed, where steep slopes, shallow weathering profiles, and less permeable geological formations accelerate runoff and restrict subsurface percolation. Intermediate density classes (0.15 - 0.91 km/km^2) represent transitional conditions influenced by moderate slopes and mixed lithological assemblages that allow limited infiltration. As such, drainage density serves as a key geomorphological indicator in the multi-criteria groundwater potential mapping framework, complementing structural, lithological, and climatic parameters to improve the accuracy and reliability of groundwater prospectivity assessment in the upper Mereb catchment.

4.2.1.2.Lineament Density

The lineament density map of the upper Mereb catchment (Fig. 20), derived from integrated satellite gravity data and DEM-based hillshade analysis presented in the previous section, exhibits values ranging from 0 to 0.19 km/km², indicating considerable spatial variation in structural intensity across the basin (K. M. Asghede et al., 2025). High lineament density zones, ranging from 0.135 to 0.19 km/km^2, are primarily concentrated in the central and northeastern parts of the catchment. These areas correspond to regions subjected to significant tectonic activity, resulting in dense networks of fractures and faults. Such structural discontinuities substantially enhance secondary porosity and permeability, enabling greater groundwater infiltration and facilitating subsurface flow along fracture-controlled pathways (Epuh et al., 2020). In contrast, low lineament density regions, ranging from 0 to 0.015 km/km², are predominantly observed in the western and southern portions of the catchment. These zones represent relatively massive, unfractured lithological units, where limited fracture connectivity restricts groundwater movement and reduces recharge potential.

The spatial distribution of lineament density also highlights the strong structural control exerted on groundwater dynamics within the catchment. Intermediate density zones (0.015–0.135 km/km^2) exhibit moderate structural influence, forming transitional areas where groundwater pathways are locally enhanced but less extensive than in high-density zones. The alignment of high-density lineament clusters with major regional structural trends, as interpreted from both gravity anomalies and SRTM-derived hillshade, further validates the mapped features and their geological significance. Zones with dense and well-connected lineaments were assigned higher weights because fractures greatly enhance groundwater recharge and storage (K. Asghede & Vágó, 2025; Sahoo et al., 2024). In contrast, areas with few or poorly developed lineaments received lower weights since limited fracturing restricts

infiltration and reduces groundwater potential. Overall, the lineament density parameter serves as a critical structural indicator within the multi-criteria groundwater potential assessment, complementing lithological and geomorphological controls in delineating viable aquifer zones across the upper Mereb catchment.

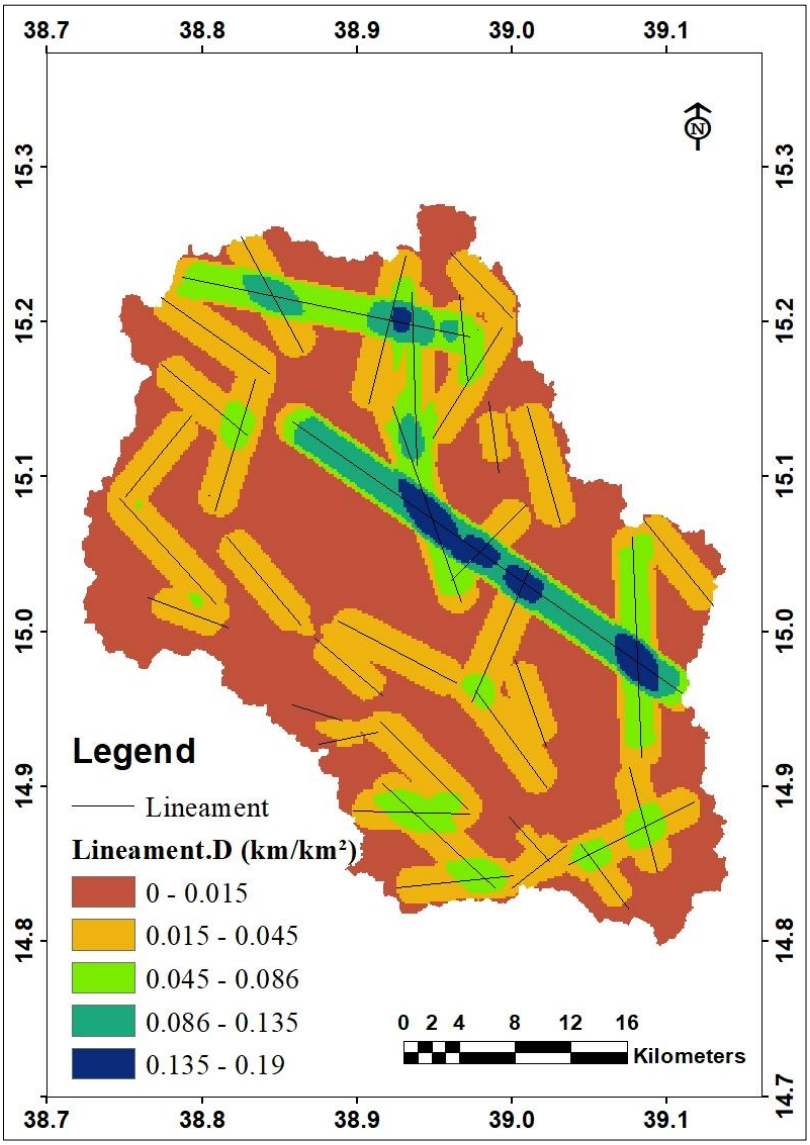

Fig. 20 Lineament Density Distribution Map of the Upper Mereb Catchment Slope

4.2.1.3.Slope

The slope map of the upper Mereb catchment (Fig. 21) reveals marked spatial variability, with gradients ranging from 0^0 to 59.81^0, reflecting a highly heterogeneous topographic setting. Gentle slopes (0 - 4.69°), which dominate the western and central parts of the catchment, form broad, low-gradient surfaces that slow runoff, increase water residence time, and facilitate deeper infiltration. Because these terrains strongly enhance recharge, they were assigned higher weights in the AHP framework. Moderate slopes (4.69 -17.82^0) occur

mainly in transitional areas between valley floors and uplands, where infiltration and runoff processes operate at intermediate levels. In contrast, steep to very steep slopes (17.82 - 59.81^0), concentrated along the escarpments and high-relief eastern and northern margins, were assigned the lowest weights because they promote rapid surface runoff and limit infiltration, thereby reducing groundwater recharge potential. These spatial patterns reaffirm well-established hydrological principles that flatter terrains favor infiltration, while steeper slopes enhance erosion and fast flow routing (Belkendil et al., 2025).

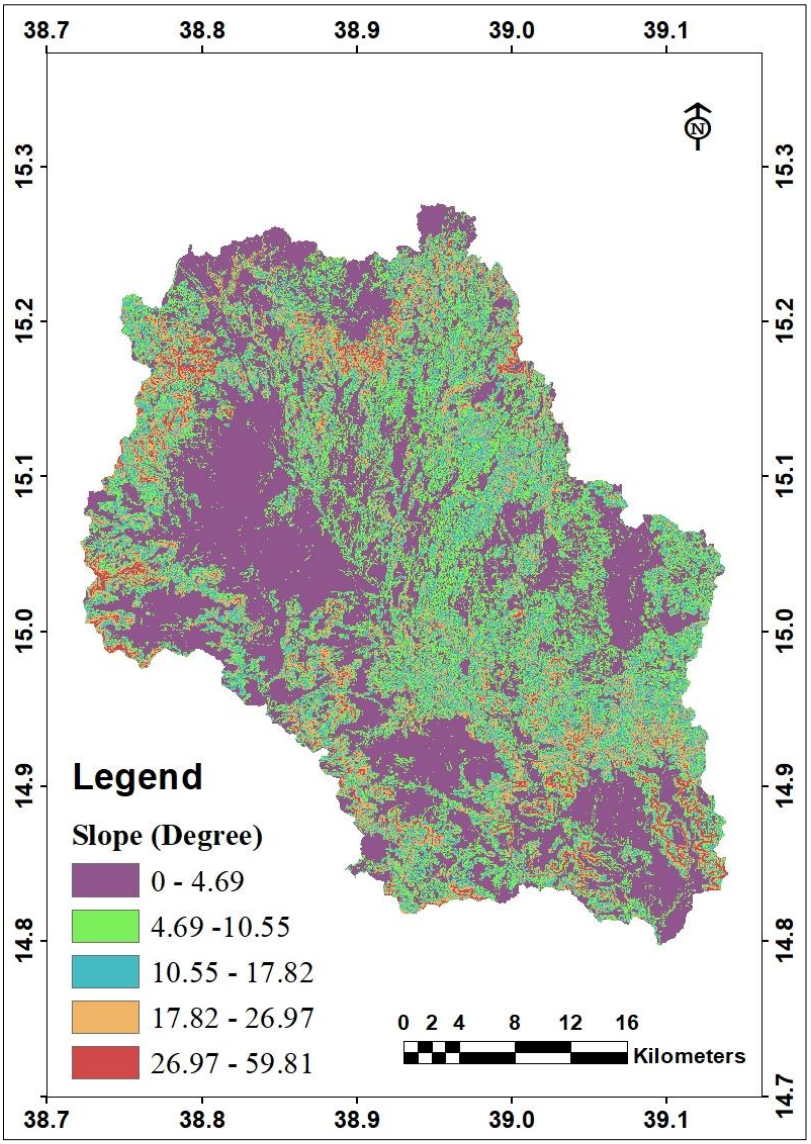

Fig. 21 Slope Gradient Classification Map of the Upper Mereb Catchment

To properly integrate topographic influence into the groundwater potential assessment, the slope layer was classified into five categories flat, gentle, moderate, steep, and very steep. Lower slope classes received higher weights in the multi-criteria analysis due to their greater capacity to support recharge, whereas higher slope classes were assigned lower weights because they tend to generate accelerated runoff (Ben Brahim et al., 2024) . This classification captures

the hydrological significance of terrain variability and ensures that slope characteristics are accurately represented within the groundwater potential model. Overall, the spatial distribution indicates that low-lying, gently sloping zones constitute the most favorable areas for groundwater accumulation, complementing other controlling factors such as lithology, drainage density, and lineament density.

4.2.1.4.Rainfall

To incorporate the influence of rainfall in groundwater potential mapping, long-term rainfall records from ten meteorological stations were processed to generate a spatially continuous rainfall surface. Thirty-year monthly rainfall data (1992–2022) were averaged to derive mean annual rainfall values for each station, ensuring temporal consistency and minimizing the influence of interannual climatic variability. The station-based rainfall averages were interpolated using the Inverse Distance Weighting (IDW) method in ArcGIS to produce a rainfall raster representing the spatial distribution of precipitation across the study area. The rainfall values were then classified into five categories: very low, low, moderate, high, and very high, based on their relative contribution to groundwater recharge. Higher rainfall classes were assigned greater weights in the AHP analysis because increased precipitation generally enhances infiltration and aquifer replenishment.

The spatial distribution of rainfall across the upper Mereb catchment (Fig. 22) shows a clear south-to-north gradient, with mean annual rainfall ranging from approximately 36.3 mm to 49.35 mm. The southern and southwestern parts of the catchment receive relatively higher rainfall amounts (45.36–49.35 mm), mainly due to elevated topography and orographic uplift that enhance precipitation, whereas the northern and northeastern areas experience lower rainfall values (36.3–38.8 mm) because of reduced elevation and weaker orographic influence. This spatial variability highlights the important role of topography in controlling rainfall distribution and groundwater recharge potential within the basin. Areas receiving higher rainfall generally favor greater infiltration and aquifer replenishment and were therefore assigned higher weights in the groundwater potential assessment (Verma & Patel, 2021), while low-rainfall zones, which experience limited recharge, received lower ranks in the weighting scheme (Hamdan et al., 2025). The resulting rainfall layer, therefore, plays a critical role in the multi-criteria evaluation, ensuring that precipitation spatial variability is accurately represented in the groundwater potential model.

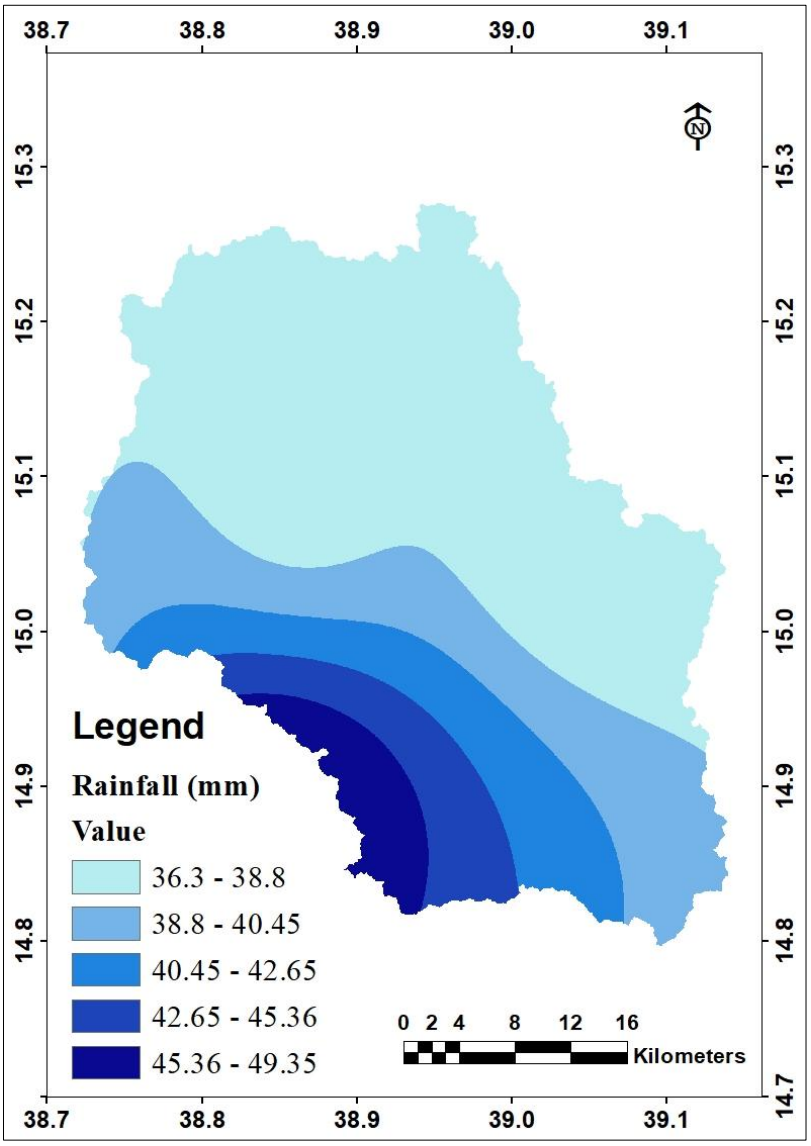

Fig. 22 Rainfall Distribution Map of the Upper Mereb Catchment

4.2.1.5.Geology

Geology plays a fundamental role in controlling groundwater occurrence, as lithological and structural characteristics dictate aquifer properties such as porosity, permeability, and fracture connectivity (Ozegin et al., 2023). In this study, a high-resolution geological map of the upper Mereb catchment was prepared by integrating field surveys and advanced remote sensing techniques (K. M. Asghede et al., 2025). This geological dataset served as a critical input for groundwater potential mapping, providing spatially explicit information on lithology and structural controls that influence recharge and storage dynamics. The geological formation of the upper Mereb catchment (Fig. 23) comprises diverse lithological units, including basalt, granitoids, laterites, metasedimentary, metavolcanic, and sedimentary rocks. Among these, basalt (584.6 km^2) and granite (337.2 km^2) occupy the largest portions of the catchment, primarily in the western and southeastern regions, respectively. Based on groundwater

contribution, higher weights were assigned to basalt and sedimentary rocks, and the lowest weight was assigned to granite. It is because basalt and sedimentary formations generally exhibit higher primary and secondary porosity, such as fractures, vesicles, and permeable bedding planes, which enhance infiltration and storage capacity compared to the low-porosity crystalline structure of granite (Bjørlykke, 2014; Navarre-Sitchler et al., 2009).

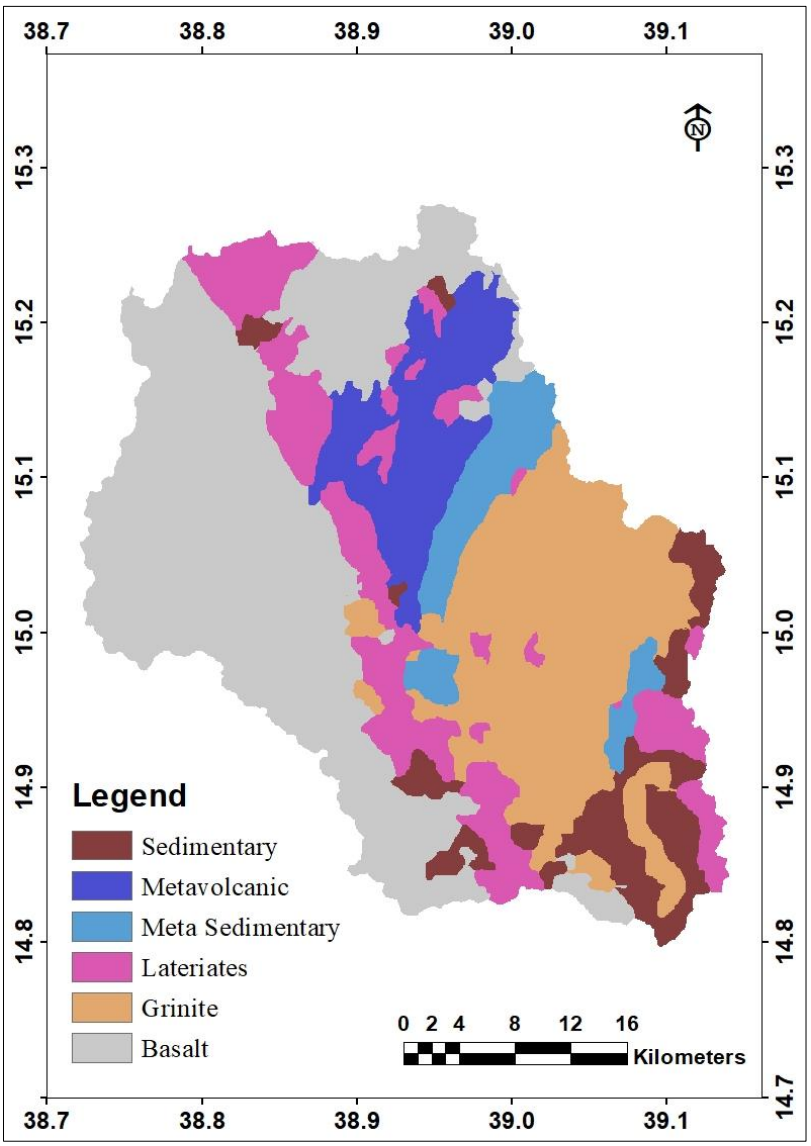

Fig. 23 Lithological Classification Map of the Upper Mereb Catchment, Eritrea

4.2.1.6.Soil

Soil characteristics play a crucial role in determining infiltration capacity, groundwater recharge potential, and overall subsurface hydrodynamics (T. Wang et al., 2015). Coarse-textured soils such as sandy or loamy types generally facilitate higher infiltration and percolation rates, whereas fine-textured, clayey soils impede water movement and promote surface runoff (Schoonover & Crim, 2015). The soil distribution within the upper Mereb

catchment, as illustrated in Fig. 24, reveals three dominant soil types: Cambisol, Vertic Cambisol, and Luvisol. Cambisols occupy the largest portion of the catchment, extending across the central, eastern, and northern regions. These soils are generally loamy to sandy-loam in texture, with moderate structure development, allowing relatively good infiltration (Table 10) and water-holding capacity (Świtoniak et al., 2016). The soil dataset, originally at 30 m spatial resolution, was used in a GIS framework together with other conditioning factors (DEM and remote sensing layers), all standardized to the same spatial resolution to ensure consistency in the groundwater potential analysis.

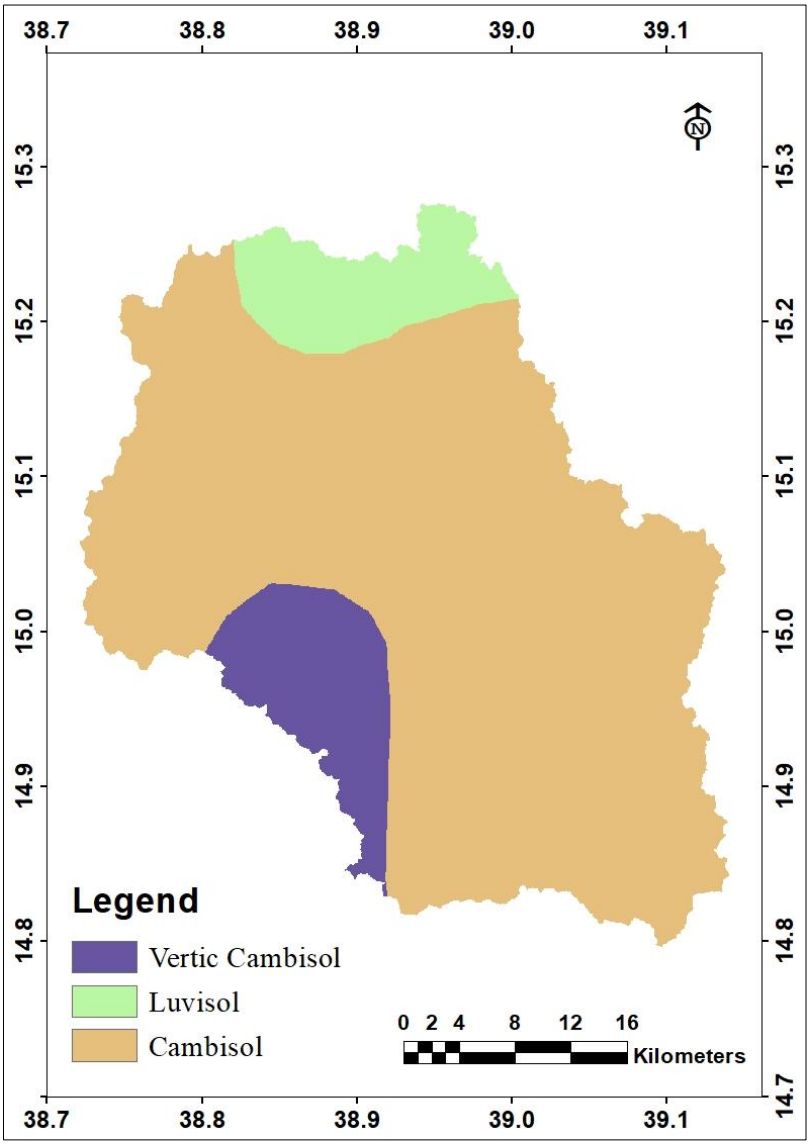

Fig. 24 Soil Type Classification Map of the Upper Mereb Catchment

Vertic Cambisols are concentrated in the southwestern part, characterized by a clay-rich texture with shrink–swell properties due to the presence of expansive clay minerals, which can influence surface cracking and seasonal water movement (Papini et al., 2011). Luvisols occur

in a relatively small area in the north and typically exhibit a clay-enriched subsurface horizon, with surface layers ranging from loam to clay loam, reflecting significant clay translocation and moderate permeability (Świtoniak et al., 2016). The interplay between soil type and lithology strongly influences groundwater occurrence in the study area.

4.2.1.7.Land Use/Land Cover (LULC)

Land use and land cover significantly influence hydrological processes, including surface runoff, infiltration, and evapotranspiration (Shadmehri Toosi et al., 2025). In this study, Sentinel-2 imagery with a 10 m spatial resolution was used to classify the upper Mereb catchment into major LULC categories: water bodies, tree cover, vegetation, cropland, built-up areas, bare ground, and rangeland.

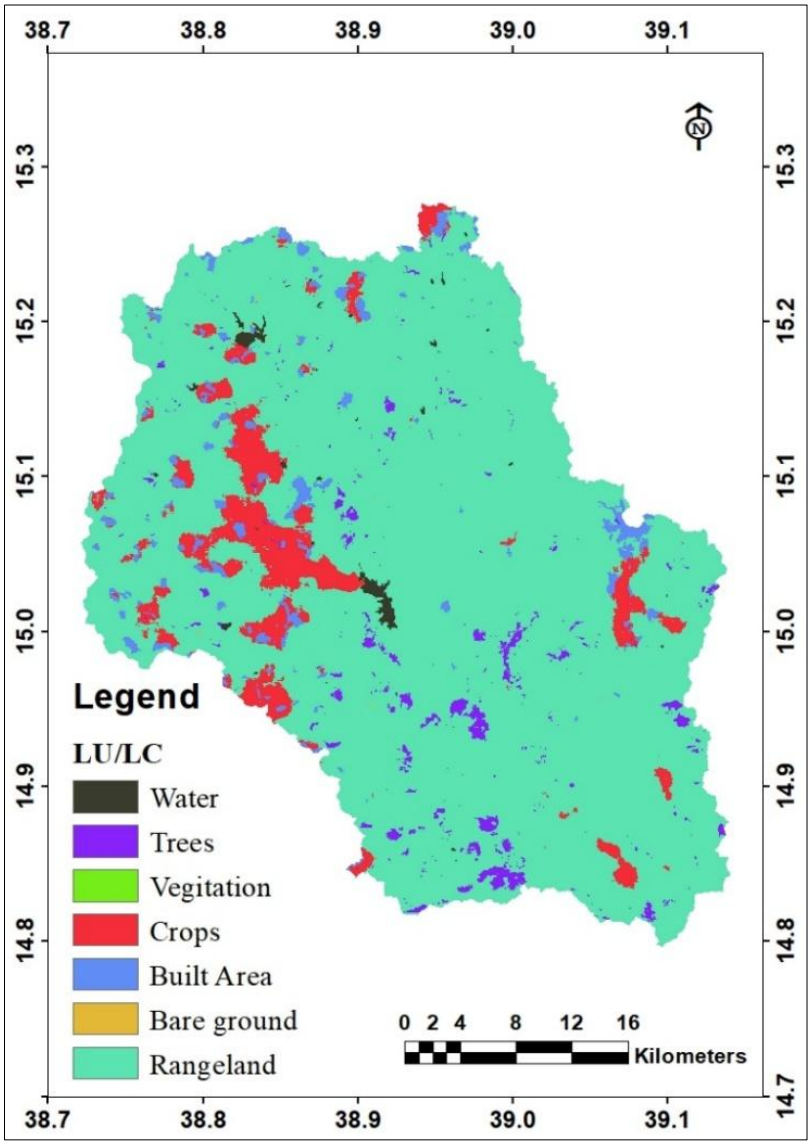

Fig. 25 Land Use/Land Cover Classification Map of the Upper Mereb Catchment

Each land-use/land-cover (LULC) class was assigned a groundwater potential weight based on its hydrological behavior and influence on infiltration and surface runoff. Vegetated and agricultural areas were assigned relatively higher weights due to their greater infiltration capacity and reduced runoff, thereby promoting groundwater recharge, whereas built-up areas and barren surfaces were assigned lower weights because of their impervious nature, which restricts infiltration and enhances rapid runoff. The LULC analysis of the upper Mereb catchment derived from Sentinel-2 imagery (Fig. 25) reveals that the area is largely dominated by non-forested and sparsely vegetated surfaces. Rangeland constitutes approximately 88.01% of the total area, followed by cropped land (6.83%), tree-covered areas (2.01%), and built-up land (2.58%), while exposed bare ground (0.026%), dense vegetation (0.0018%), and surface water bodies (0.52%) occupy only minor proportions. This dominance of rangeland and sparsely vegetated surfaces indicates widespread soil and rock exposure, which has important implications for surface runoff, infiltration behavior, and groundwater recharge dynamics. Consequently, the systematic weighting of LULC classes ensures that their spatial distribution and hydrological significance are appropriately reflected in the groundwater potential mapping process, while also supporting reliable lithological and structural interpretation from remote-sensing data.

4.2.2. Delineation of potential mapping using AHP

All environmental parameters analyzed and processed in the GIS environment were used as inputs for delineating the groundwater potential map. The application of AHP in this study provides a robust framework for assessing the spatial variability of groundwater potential, particularly under data-limited conditions. The following sections present the spatial distribution, area coverage, and interpretation of the AHP-based groundwater potential maps.

The resulting AHP-based groundwater potential map delineated five distinct zones: very low, low, moderate, and very high potential (Fig. 26). The spatial distribution pattern from Table 11 revealed that moderate potential zones cover the largest area (50.04%), primarily concentrated in the central and northeastern parts of the catchment. The low-potential areas account for 35.61%, mostly distributed in the southern and southeastern regions characterized by hilly and mountainous terrain with steep slopes and shallow soils. High potential zones constitute 10.51% of the total area, while very high potential zones occupy only 3.32%, mainly in flat lands and areas under intensive agriculture where recharge conditions are favorable, which is clearly seen in the northwest of the study area (Fig. 26). The very low potential zones (0.52%) are confined to areas where granite is abundant and with steep gradients, indicating limited infiltration capacity. The model results show high groundwater potential in areas with

high drainage density. This inconsistency could be due to various factors, such as the influence of flat slopes and the nature of lithology, which affect the amount of water recharge and thus the potential (K. M. Asghede & Vágó, 2025). Comparable results were also reported in the Barda Rash District in northern Iraq (Hamamin, 2024). This area shares many of the same physical and environmental landscape characteristics as the present study site.

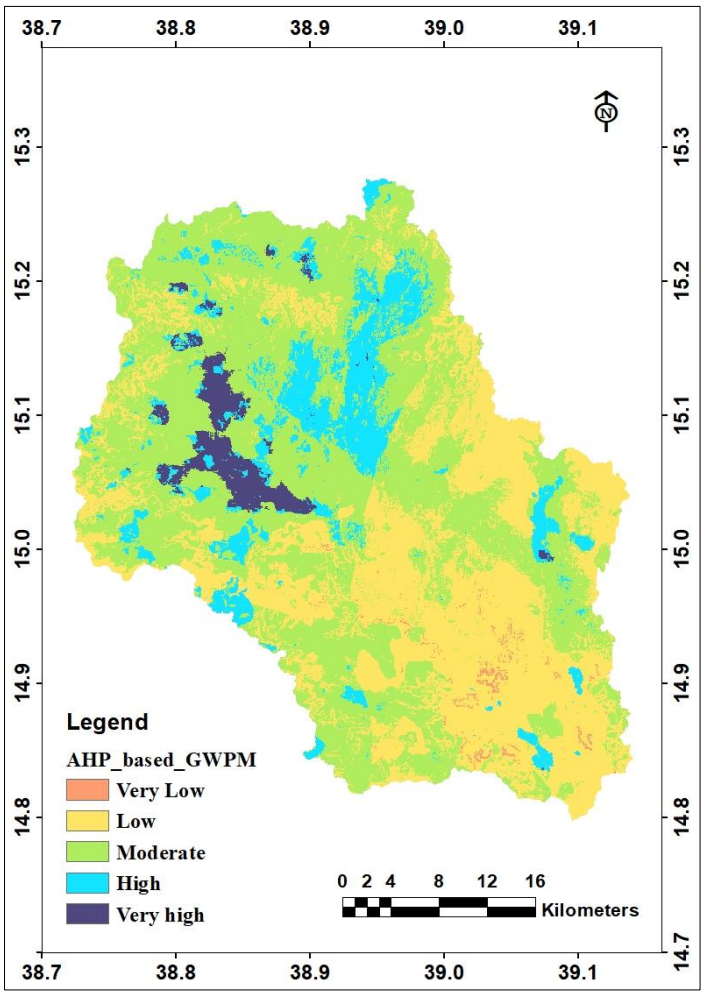

Fig. 26 Groundwater Potential Map of the upper Mereb area derived using the AHP method.

Table 11: AHP-FR based groundwater potential aerial coverage

S.No.	Potential zones	AHP coverage area (%)	FR coverage area (%)
1	Very low	0.52	17.26
2	Low	35.61	30.23
3	Moderate	50.04	30.98
4	High	10.51	15.31
5	Very high	3.32	6.22

The results demonstrate that integrating expert knowledge with GIS-derived environmental parameters provides an effective framework for groundwater potential mapping in data-scarce arid and semi-arid regions. Notably, this work represents the first application of an AHP-based groundwater assessment in the upper Mereb catchment, offering new insights into the spatial distribution of groundwater resources. The spatial classification of groundwater potential zones (Fig. 26), together with their quantified area coverage, provides valuable decision-support information for local communities and water resource management authorities. This classification helps identify priority areas for groundwater exploration, well sitting, and sustainable land and agricultural planning. The dominance of moderate to low potential zones across much of the upper Mereb catchment underscores the need for careful groundwater development strategies, while the limited extent of high- and very-high-potential zones underscores the importance of targeted resource allocation. In the present work, the use of AHP for groundwater potential mapping in an arid and semi-arid environment is supported by previous research, as similar AHP-based assessments have proven effective in guiding groundwater management and planning by providing transparent and easily interpretable outputs for decision-makers (Adesola et al., 2023; Belkendil et al., 2025). However, despite its advantages, the AHP approach is inherently dependent on expert judgment and subjective weighting, which may lead to inconsistencies, such as the occurrence of high groundwater potential in areas with high drainage density observed in this work. These limitations highlight the need to complement knowledge-driven methods with data-driven approaches, thereby providing a rationale for applying the Frequency Ratio model in the subsequent analysis to enhance objectivity and improve the reliability of groundwater potential delineation (Belkendil et al., 2025).

4.2.3. Frequency ratio

The Frequency Ratio (FR) analysis provides a quantitative measure of the relationship between groundwater occurrence and contributing environmental parameters, with values greater than 1 indicating a positive association and values less than 1 indicating a negative association (M. Kumar et al., 2022). The spatial results of the analysis are shown on Fig 27. Before interpreting the spatial results, Table 12 summarizes the statistical procedure used to derive the Frequency Ratios (FR) for each conditioning factor and its subclasses. For every thematic layer, the map was divided into subclasses, and the number of groundwater wells falling within each subclass was counted and compared with the total number of pixels representing that subclass in the study area (Pawar et al., 2024). The percentage of wells expresses the proportion of groundwater occurrences within a given subclass, while the

percentage of pixels represents the areal extent of that subclass. The FR value was then calculated as the ratio of the well percentage to the pixel percentage, providing a quantitative measure of the strength of association between each subclass and groundwater occurrence. This table therefore provides the statistical foundation for identifying favorable and unfavorable conditions for groundwater potential.

Table 12: Weight is given to each thematic layer and its subclasses by frequency ratio method

S.No	Class	Sub-Class	Frequency Ratio (FR)				
			No. of Wells	No. of Pixels	% of wells	% of pixels	FR
1	Lithology	Lateriates	9	236618	0.0682	0.1447	0.4711
		Basalt	56	648267	0.4242	0.3965	1.0700
		Granite	30	372764	0.2273	0.2280	0.9968
		Meta-Sedimentary	7	93215	0.0530	0.0570	0.9301
		Metavolcanic	18	154728	0.1364	0.0946	1.4409
		Sedimentary	12	129366	0.0909	0.0791	1.1489
2	Lineament	0 - 0.015	23	342704	0.1742	0.2091	0.8334
		0.015 - 0.045	42	397410	0.3182	0.2424	1.3124
		0.045 - 0.086	33	474192	0.2500	0.2893	0.8642
		0.086 - 0.135	23	284039	0.1742	0.1733	1.0056
		0.135 - 0.19	11	140880	0.0833	0.0859	0.9696
3	Rainfall	36.3 - 38.8	82	873648	0.6212	0.5330	1.1656
		38.8 - 40.45	29	360349	0.2197	0.2198	0.9994
		40.45 - 42.65	10	199802	0.0758	0.1219	0.6215
		42.65 - 45.36	4	123166	0.0303	0.0751	0.4033
		45.36 - 49.35	7	82260	0.0530	0.0502	1.0568
4	Landuse/Landcover	Water	0	431	0.0000	0.0003	0.0000
		Trees	5	42327	0.0379	0.0258	1.4669
		Vegitation	31	111997	0.2348	0.0683	3.4373
		Crops	93	1442787	0.7045	0.8802	0.8005
		Built area	2	33054	0.0152	0.0202	0.7514
		Bare ground	0	30	0.0000	0.0000	0.0000
		Rangeland	1	8576	0.0076	0.0052	1.4480
5	Slope	0 - 4.69	91	753957	0.6894	0.4619	1.4924
		4.69 - 10.55	28	404823	0.2121	0.2480	0.8552
		10.55 - 17.82	9	248972	0.0682	0.1525	0.4470
		17.82 - 26.97	3	162443	0.0227	0.0995	0.2284
		26.97 - 59.81	1	61999	0.0076	0.0380	0.1994
6	Drainage density	0 - 0.15	41	524148	0.3106	0.3198	0.9712
		0.15 - 0.39	32	316518	0.2424	0.1931	1.2552
		0.39 - 0.63	28	403704	0.2121	0.2463	0.8611
		0.63 - 0.91	28	273252	0.2121	0.1667	1.2722
		0.91 - 1.62	3	121249	0.0227	0.0740	0.3072
7	Soil	Vertic cambisol	13	155252	0.0985	0.0947	1.0398
		Luvisol	12	133021	0.0909	0.0811	1.1203
		Cambisol	107	1350950	0.8106	0.8241	0.9836

Among the parameters, geology exhibited FR values ranging from 0.47 to 1.44, with the highest ratios associated with basaltic and metavolcanic formations (Table 12). These

volcanic units possess well-developed secondary porosity due to fracturing and weathering, which enhances groundwater storage and movement (Khan et al., 2024). In contrast, the sedimentary and crystalline rock units exhibited lower FR values, reflecting their limited permeability and reduced recharge potential. This is primarily because these formations lack sufficient secondary porosity, such as interconnected fractures or dissolution features that would facilitate effective groundwater movement through the rock matrix (Wadi et al., 2022). Structural and geomorphological parameters also demonstrated clear relationships with groundwater occurrence. Lineament density showed FR values ranging from 0.83 to 1.31, underscoring the importance of faults and fractures as preferential pathways for subsurface flow. Drainage density exhibited FR values ranging from 0.31 to 1.27. Higher FR values were generally associated with low-to-moderate drainage density zones, which represent areas where the balance between runoff and infiltration favor groundwater recharge (Razandi et al., 2015). Slope contributed to a FR range of 0.20 to 1.49, with high ratios occurring consistently in low-slope areas. Gentle, flat terrain facilitates infiltration and reduces runoff, reinforcing the well-established inverse relationship between slope and groundwater potential reported in FR-based studies (Thanh et al., 2022).

Land use/land cover, rainfall, and soil characteristics further supported the spatial patterns of groundwater potential. LULC exhibited the widest FR range (0-3.43; Table 12), with agricultural areas showing the highest value due to enhanced infiltration promoted by cultivation practices and the presence of permeable alluvial soils. Rainfall also exerted a strong positive influence, with high FR ratios in the relatively wetter northern and southwestern parts of the catchment, reflecting precipitation's dominant role as the primary source of recharge. Soil type contributed more to FR, with vertic cambisol and luvisol showing higher FR values due to their higher infiltration capacity, compared to cambisol (Table 12). Together, these results underscore the FR model's capacity to delineate recharge-favorable zones by capturing the combined effects of geological structure, surface conditions, and climatic inputs on groundwater occurrence, as demonstrated by other researchers' studies (Guru et al., 2017).

The FR model delineated five groundwater potential zones (GWPZ) within the upper Mereb catchment, as shown on Fig. 27. The spatial distribution indicates that moderate potential zones dominate the catchment, covering 30.98% of the total area, followed closely by low potential zones (30.23%) as listed in Table 11. These zones are widely distributed across the central and eastern parts of the catchment, where lithology, slope, and soil conditions provide moderate infiltration capacity. High-potential zones (15.31%) and very high-potential zones (6.22%) are concentrated mainly in the northwestern and northeastern regions, coinciding with

areas of dense lineaments, fractured basaltic formations, and gentle slopes that favor groundwater recharge. The clustering of high and very-high-potential zones in structurally controlled regions underscores the critical role of secondary porosity and lineament density in groundwater availability (Akinluyi et al., 2018). Conversely, very low potential zones (17.26%) occur predominantly in the southern and southeastern mountainous areas, where steep slopes and compact lithologies limit infiltration and groundwater storage. The strong correlation between geomorphological settings and groundwater occurrence has been emphasized in several regional studies (Githinji et al., 2022; Hamdan et al., 2025; Oyda et al., 2025). These findings highlight the importance of prioritizing groundwater development in the northwestern and northeastern sectors while adopting soil and water conservation measures in low-potential areas to enhance recharge and reduce runoff.

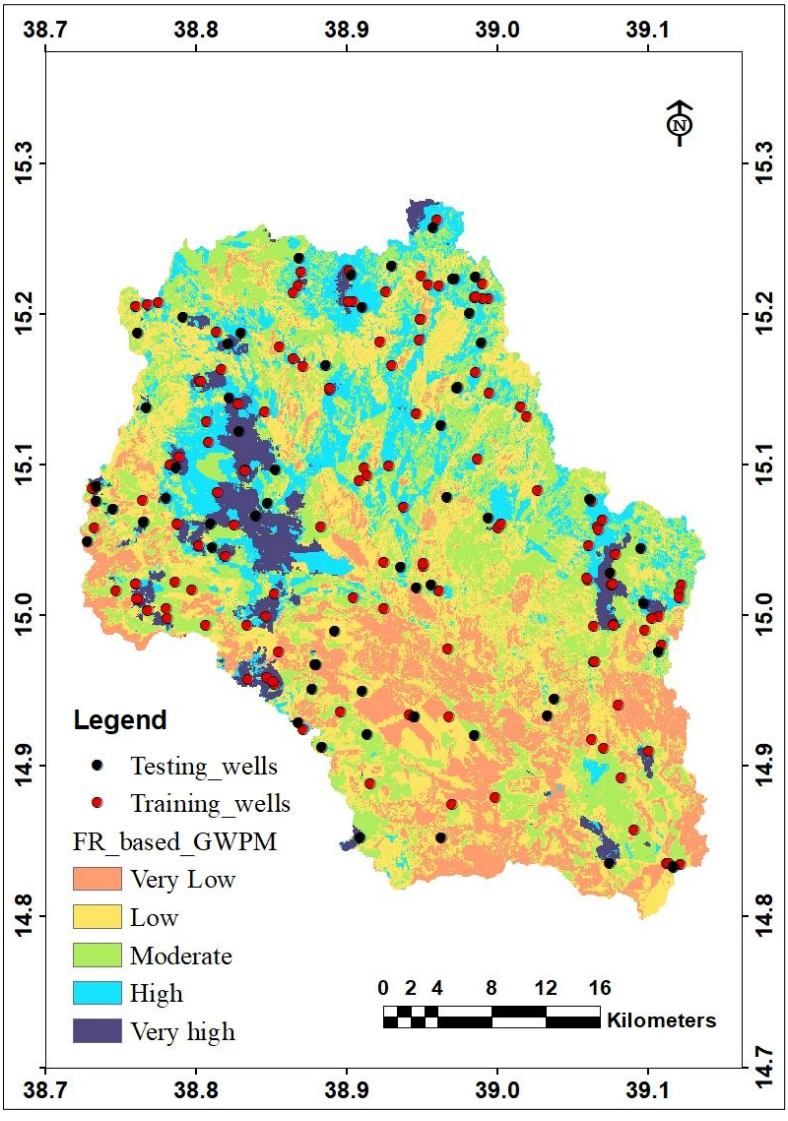

Fig. 27 Frequency Ratio–based groundwater potential map of the upper Mereb catchment

It is important to note that the Frequency Ratio model in this study is based on the spatial distribution of existing wells as indicators of groundwater occurrence. While this approach provides useful insights into groundwater potential, the distribution of wells may partly reflect accessibility and water demand rather than purely hydrogeological conditions. As such, the resulting groundwater potential zones should be interpreted as indicative rather than definitive representations of groundwater availability. Nevertheless, the spatial patterns identified in this study show strong agreement with controlling factors such as lineament density, lithology, and slope, supporting the overall reliability of the model. Future studies incorporating detailed productivity well data and hydrogeological measurements would further improve the accuracy and validation of the groundwater potential assessment.

4.2.4. Validation and Comparison

The predictive performance of the groundwater potential mapping models was evaluated using Receiver Operating Characteristic (ROC) curves and their corresponding Area Under the Curve (AUC) values (Fig. 28). A total of 190 groundwater well locations were used for the assessment, of which 132 wells (70%) were allocated for training the model and 58 wells (30%) were reserved for independent validation. The ROC curves were generated by comparing model-derived groundwater potential values with this testing dataset, allowing an objective evaluation of the models' predictive capability (Dongare et al., 2024). The ROC-AUC values obtained for the models are 0.704 for AHP and 0.748 for FR, indicating varying levels of predictive accuracy in delineating groundwater potential zones within the upper Mereb catchment.

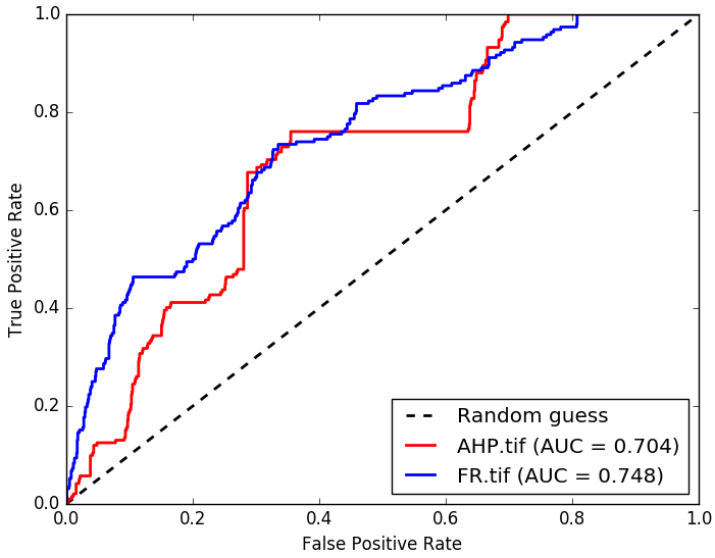

Fig. 28 ROC/AUC model validation for AHP and FR methods for the use of groundwater potential mapping

Among the models, the FR approach achieved the highest predictive accuracy (AUC = 0.748), indicating a slightly stronger capability to distinguish between groundwater-bearing and non-groundwater-bearing locations. This performance reflects the strength of its data-driven formulation, which more effectively captures the statistical relationships between groundwater occurrences and the environmental conditioning factors considered in the analysis. The AHP model, with an AUC of 0.704, also performed reasonably well, providing a structured framework for integrating expert knowledge on geological, geomorphological, hydrological, and remote-sensing parameters. While the resulting groundwater-potential outputs constitute a valuable tool for sustainable water-resource management, continuous monitoring and field validation remain essential to ensure their long-term reliability (Belkendil et al., 2025).

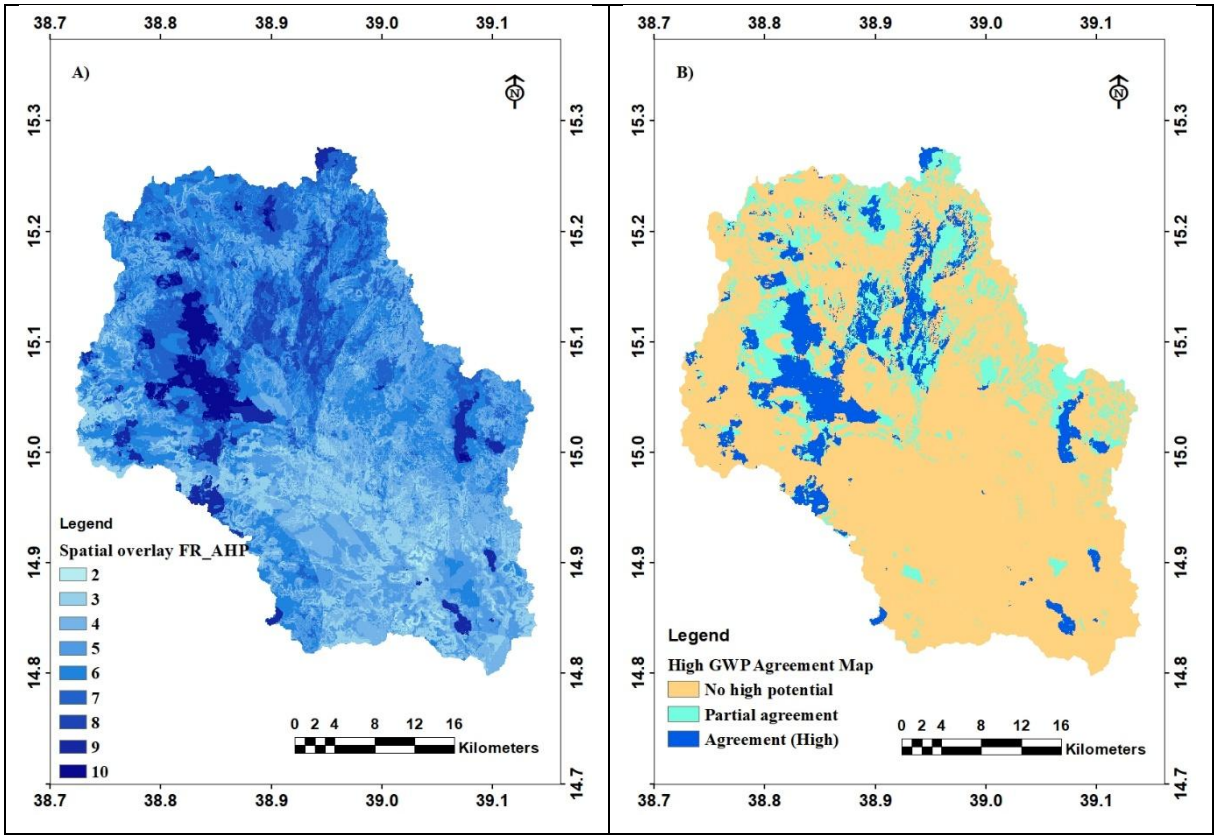

Fig. 29 Comparison of spatial agreement between FR and AHP models: (A) Spatial overlay output illustrating the distribution of combined class values; and (B) Three-category agreement map showing the level of correspondence between the two models.

The spatial overlay output was generated by combining the binary AHP and FR rasters through a cell-by-cell raster calculation, resulting in a map that displays all possible combinations of class values derived from the two models (Fig. 29a). However, the large number of resulting class combinations makes this output difficult to interpret and less suitable

for decision-making, thereby highlighting the need to simplify the results into three agreement categories to provide a clearer and more meaningful comparison between the models (Fig. 29b). The spatial overlay comparison of high and very high groundwater-potential zones predicted by both AHP and FR indicates that 75.06% of the study area falls within the non-high-potential category (moderate to low), 14.5% is identified as high potential by only one of the models, and 10.4% represents areas of agreement where both models simultaneously predict high potential (Fig. 29b). This comparison shows that AHP and FR exhibit strong spatial consistency in mapping high and very high potential zones in the northwestern and northeastern parts of the catchment, where relatively flat terrain and favorable geological conditions enhance groundwater percolation. Likewise, both models consistently delineate low-potential zones in the southern hilly and mountainous regions where, steep slopes and shallow soils limit infiltration. Overall, the overlay approach quantifies the spatial agreement between the two modeling techniques and provides valuable insight into the robustness of high-potential zone delineation across the catchment.

In summary, the validation of both AHP and Frequency Ratio models using ROC analysis, combined with their spatial comparison through overlay methods, demonstrates consistent performance in delineating groundwater potential zones in the upper Mereb catchment. This integrated approach provides useful outputs to support decision-making in Eritrea, offering scientifically grounded information for groundwater planning and resource management. Importantly, this study represents the first application of such a methodology in the country, helping to address a critical gap in groundwater potential assessment. However, the results should be interpreted with consideration of certain limitations, particularly the reliance on well location data without detailed productivity information and the inherent assumptions within the applied models. Despite these constraints, the findings establish a baseline for future work, where the incorporation of more comprehensive hydrogeological data and advanced approaches, such as machine learning techniques, could further improve the reliability and predictive capability of groundwater potential mapping.

4.3.Groundwater quality assessment

Groundwater quality in the upper Mereb catchment was evaluated from both hydrogeochemical and suitability perspectives to understand its overall suitability for human consumption and agricultural use. The assessment focuses on identifying the dominant processes controlling groundwater chemistry and how these processes influence water quality variations across the study area. In addition, the spatial and chemical characteristics of

groundwater were analyzed to determine its suitability for drinking and irrigation purposes under the prevailing environmental conditions.

4.3.1. Ionic balance

Ionic balance analysis was conducted to evaluate the reliability of groundwater chemical data (Fig. 30). Major cations (such as Na^+, K^+, Ca^{2+}, and Mg^{2+}) and anions (including Cl^-, SO_4^{2-}, HCO_3^-, and NO_3^-) were measured and converted from mg/L to milliequivalents per liter (meq/L) to assess the electrical neutrality of the water samples (Subba Rao et al., 2022). The ionic balance error was calculated using the standard formula, and the results were compared against the acceptable threshold of ±10% (Fig. 30). Most samples exhibited ionic balance errors within this range, confirming the accuracy of the analytical procedures and the suitability of the data for further hydrochemical interpretation. However, samples that exceed the threshold may indicate potential issues, such as analytical inaccuracies, missing ionic species, or external influences, such anthropogenic contamination (Jarray et al., 2023; P. Kumar et al., 2024). These deviations highlight the importance of ionic balance analysis not only as a quality control measure but also as a diagnostic tool for identifying possible environmental or geochemical anomalies in the groundwater system.

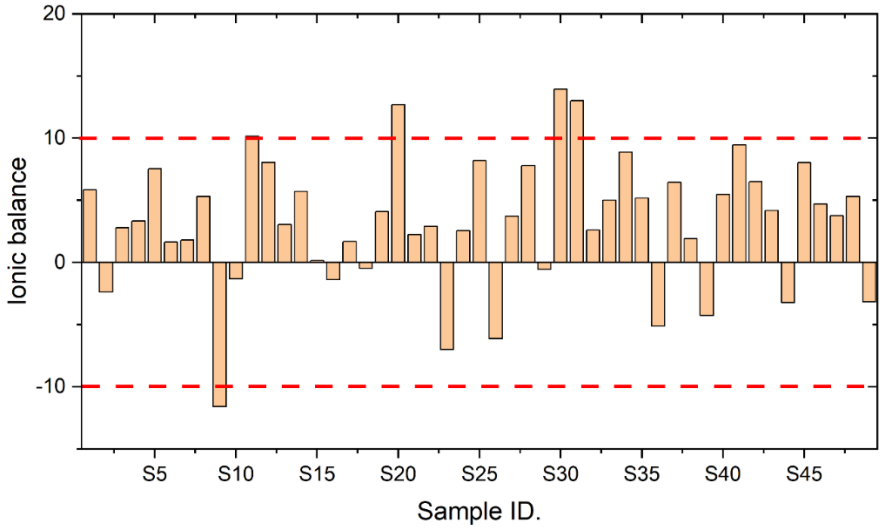

Fig. 30 Bar plot showing the electrical balance of the samples analyzed

4.3.2. Descriptive statistics

The physiochemical characterization of groundwater samples revealed considerable spatial and statistical variability (Table 13) across the study area, influenced by both natural geochemical processes and anthropogenic activities. The pH values ranged from 5.61 to 8.68, with a mean of 7.44 and a standard deviation of 0.51, indicating that the groundwater is generally neutral to slightly alkaline. Spatially, higher pH values were observed in the western

and northern zones (Fig. 31a), while lower values were concentrated in the eastern part of the study area. This distribution may reflect differences in lithology, recharge conditions, or localized acidification from agricultural runoff (Alzahrani et al., 2025). Electrical conductivity (EC) ranged from 135 to 1649 µS/cm, with a mean of 755.82 µS/cm, indicating moderate to high mineralization. EC is an important indicator of the total dissolved ions in groundwater and is widely used to assess salinity levels and overall water suitability for domestic and agricultural use (Mkilima, 2023). The highest EC concentrations were found in both the eastern and western parts of the study area (Fig. 31b), while the northern and southern zones exhibited lower values. This pattern may be attributed to increased ion dissolution from soil-rock interactions in the east and west, possibly exacerbated by irrigation return flow and fertilizer application. Similarly, total dissolved solids (TDS) ranged from 90.45 to 1104.83 mg/L (Fig. 31c), with elevated concentrations in the eastern and western zones, reinforcing the spatial correlation with EC and indicating potential salinity concerns. Alkalinity values ranged from 40 to 488 mg/L, with a mean of 242.01 mg/L. High alkalinity was predominantly observed in the northern, western, and central parts of the study area (Fig. 31d), suggesting the influence of carbonate-rich formations and buffering capacity against pH fluctuations. Total hardness (TH) ranged from 22 to 560 mg/L, with a mean of 285.53 mg/L. Spatially, TH was highest in the eastern and southwestern zones. At the same time, the central and southern regions showed lower concentrations (Fig. 31e). This distribution aligns with the presence of calcium and magnesium ions, which are primary contributors to hardness.

Calcium concentrations varied between 7.2 and 160 mg/L (mean: 69.47 mg/L), with elevated levels in the northeastern and southwestern zones, and lower concentrations in the southern part (Fig. 31f). Magnesium ranged from 0.96 to 72 mg/L (mean: 27.61 mg/L), with high concentrations in the eastern and western zones, and lower values in the north and south (Fig. 31g), suggesting it may contribute to variations in water hardness (Ingin et al., 2024). Sodium concentrations ranged from 2.3 to 165 mg/L (mean: 42.86 mg/L), with the highest concentrated values in the eastern zone (Fig. 31h). This could possibly be due to ion exchange processes or anthropogenic inputs such as wastewater and fertilizers (Hagage et al., 2025). Potassium levels were generally low (mean: 1.44 mg/L), with localized high concentrations in the western, northern, and southern zones (Fig. 31i), potentially linked to agricultural activities. Iron and manganese showed mean concentrations of 0.77 mg/L and 0.18 mg/L, respectively. Iron was elevated in the eastern and western zones (Fig. 31j), while manganese was concentrated in the northern part (Fig. 31k). The elevated iron and manganese concentrations may also result from the weathering of Fe-Mn-rich lithologies and agricultural activities with

important implications for groundwater quality and irrigation suitability (Amit Hasan et al., 2026).

Table 13: Descriptive statistics of the analyzed parameters

Physiochemical Parameter	Mean	Standard Deviation	Minimum	Maximum
pH	7.44	0.51	5.61	8.68
EC	755.82	320.15	135	1649
TDS	513.35	217.7	90.45	1104.83
ALKA	242.01	99.25	40	488
TH	285.53	124.59	22	560
Ca	69.47	30.09	7.2	160
Mg	27.61	15.97	0.96	72
Na	42.86	30.43	2.3	165
K	1.44	1.78	0	9.32
Fe	0.77	1.35	0	5.5
Mn	0.18	0.21	0	0.9
HCO3	302.58	105.78	48.8	595.36
SO4	44.45	41.91	3	288
Cl	44.22	41.84	0.07	200
NO3	25.98	31.81	0.32	165.63
NO2	0.29	0.62	0	2.93
NH3	0.32	0.41	0	2.19

Among the anions, bicarbonate (HCO_3^-) was dominant, with a mean of 302.58 mg/L and high concentrations in the western and parts of the northern zones (Fig. 31l). Sulfate (SO_4^{2-}) ranged from 3 to 288 mg/L (mean: 44.45 mg/L), with elevated levels in the central part of the study area (Fig. 31m), possibly due to gypsum dissolution or anthropogenic inputs which can cause test of water and illness (M. K. Sharma & Kumar, 2020; Sultana et al., 2025). Chloride (Cl^-) concentrations ranged from 0.07 to 200 mg/L (mean: 44.22 mg/L), with high values restricted to the eastern zone (Fig. 31n), indicating potential contamination from domestic or agricultural sources. Nitrate (NO_3^-) and nitrite (NO_2^-) showed similar spatial patterns, with high concentrations in the southern and northeastern zones (Fig. 31o and Fig. 31p). Nitrate levels reached up to 165.63 mg/L (mean: 25.98 mg/L), suggesting significant agricultural influence (Sanad et al., 2024). Ammonia (NH_3) concentrations were highest in the central and northern zones (Fig. 31q), possibly indicating organic pollution or microbial activity (X. kun Li et al., 2013). Overall, the spatial distribution of physiochemical parameters, as revealed through IDW interpolation in ArcGIS, highlights the heterogeneous nature of groundwater quality in the study area, which was practiced in other similar arid areas (Dandge & Patil, 2022). These variations underscore the combined effects of geological formations, land use practices, and anthropogenic pressures. The integration of statistical and spatial analyses provides a

comprehensive understanding of groundwater chemistry, essential for effective resource management and pollution mitigation strategies (Tunio et al., 2025).

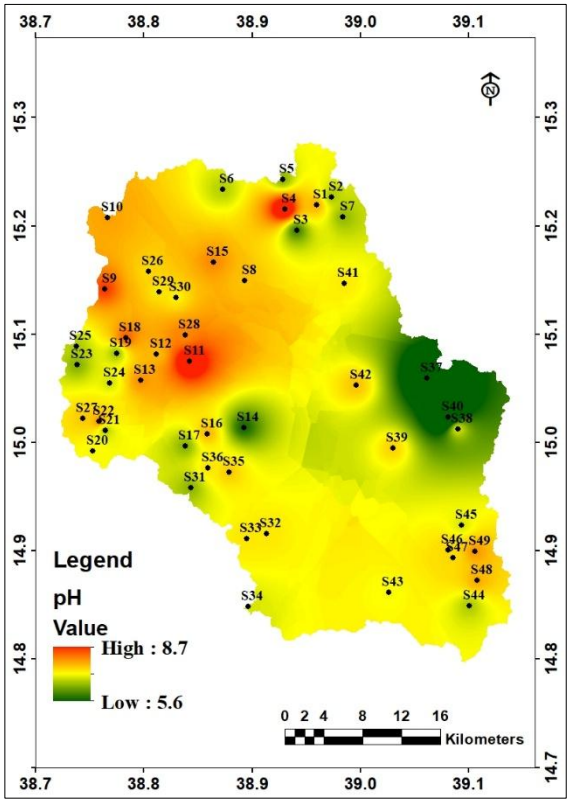

(a)

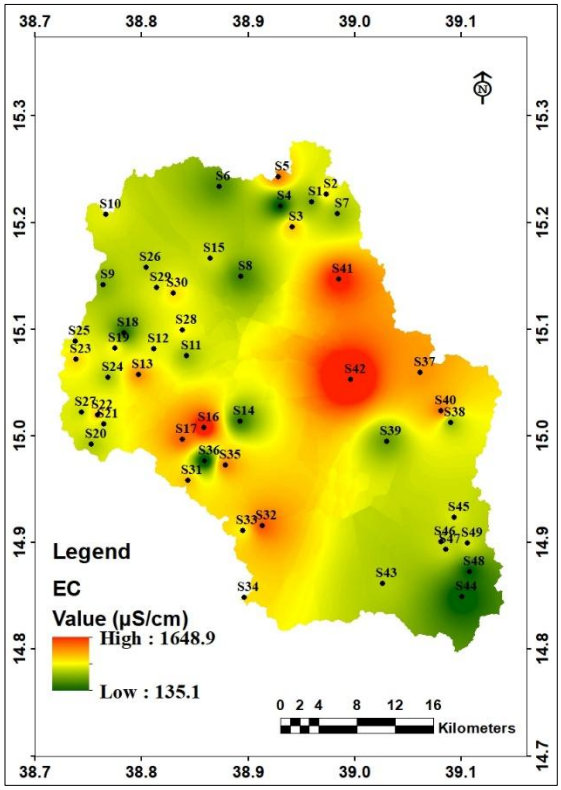

(b)

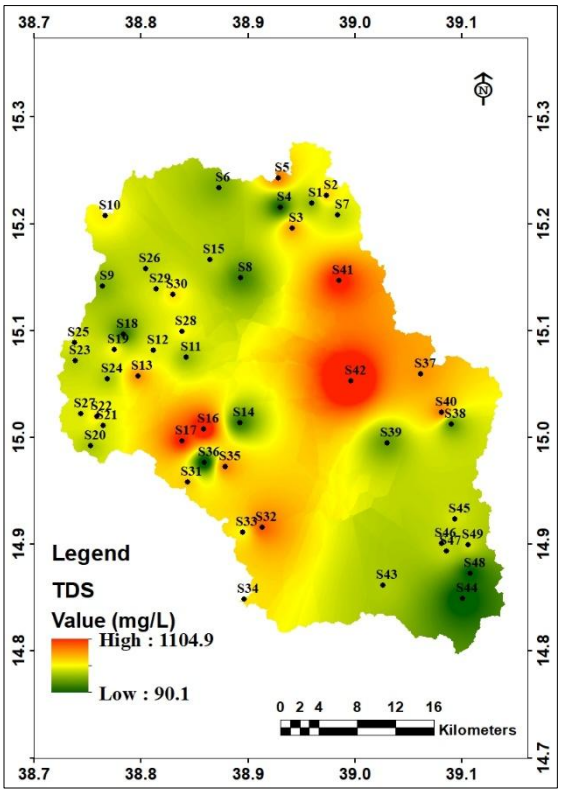

(c)

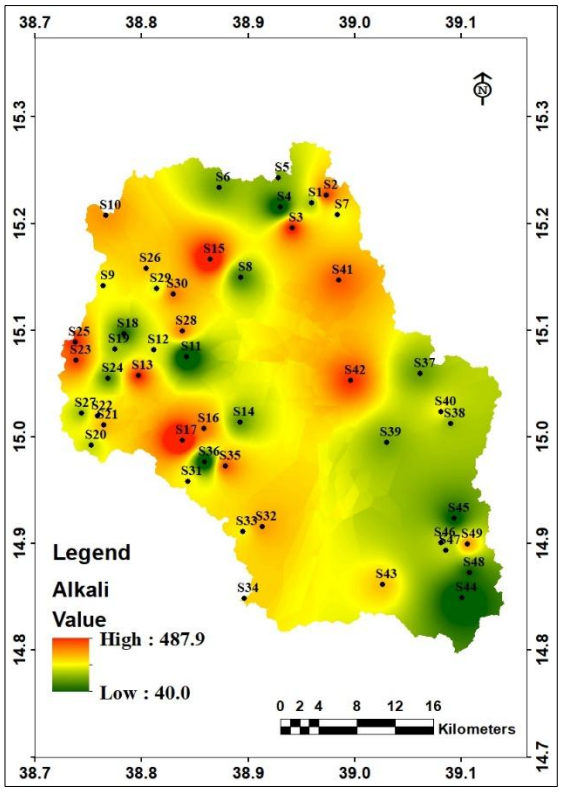

(d)

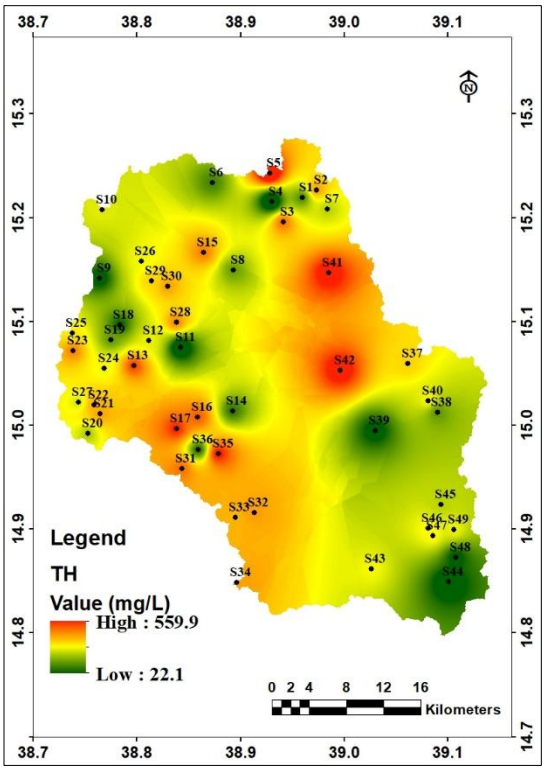
Legend
TH
Value (mg/L)
High : 559.9
Low : 22.1
0 2 4 8 12 16
Kilometers

(e)

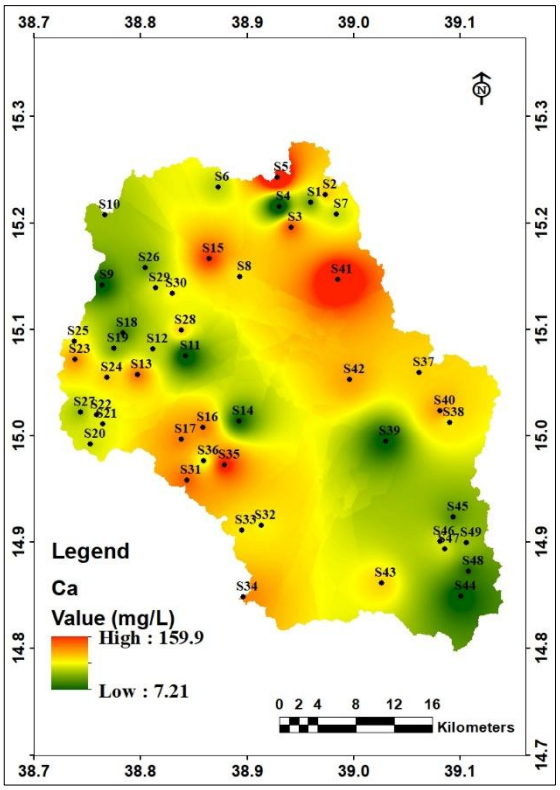
Legend
Ca
Value (mg/L)
High : 159.9
Low : 7.21
0 2 4 8 12 16
Kilometers

(f)

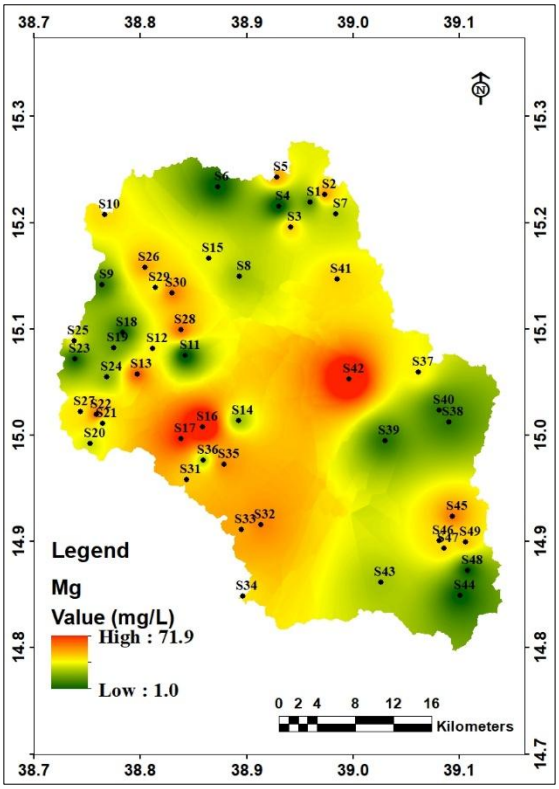
Legend
Mg
Value (mg/L)
High : 71.9
Low : 1.0
0 2 4 8 12 16
Kilometers

(g)

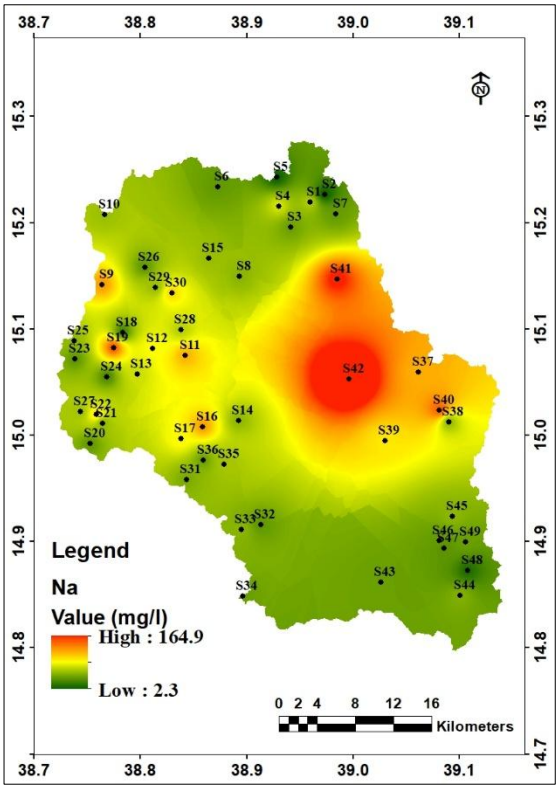
Legend
Na
Value (mg/l)
High : 164.9
Low : 2.3
0 2 4 8 12 16
Kilometers

(h)

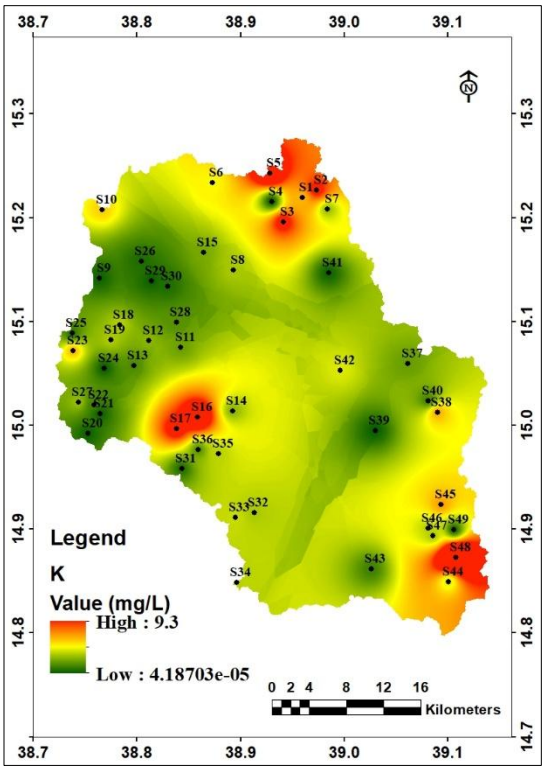
Legend
K
Value (mg/L)
High : 9.3
Low : 4.18703e-05
0 2 4 8 12 16
Kilometers

(i)

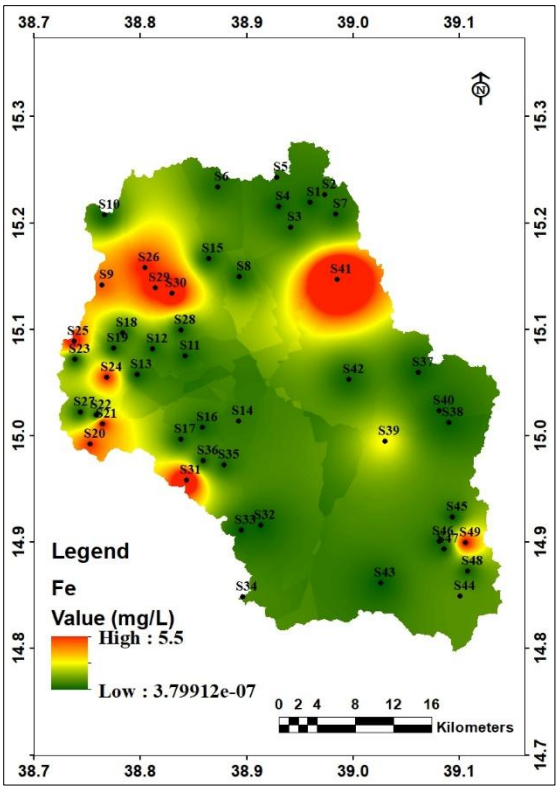
Legend
Fe
Value (mg/L)
High : 5.5
Low : 3.79912e-07
0 2 4 8 12 16
Kilometers

(j)

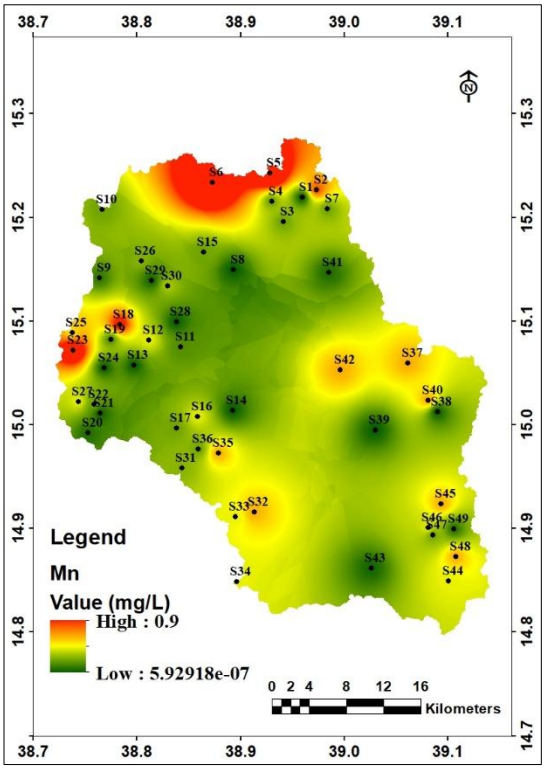
Legend
Mn
Value (mg/L)
High : 0.9
Low : 5.92918e-07
0 2 4 8 12 16
Kilometers

(k)

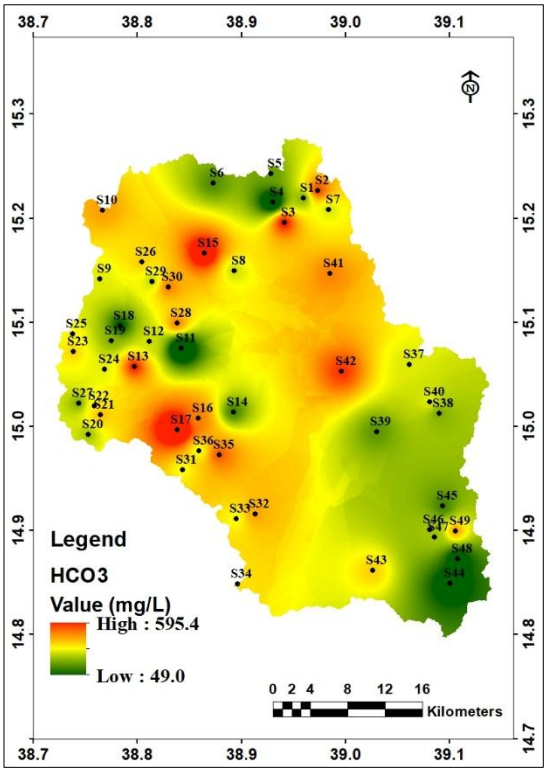
Legend
HCO3
Value (mg/L)
High : 595.4
Low : 49.0
0 2 4 8 12 16
Kilometers

(l)

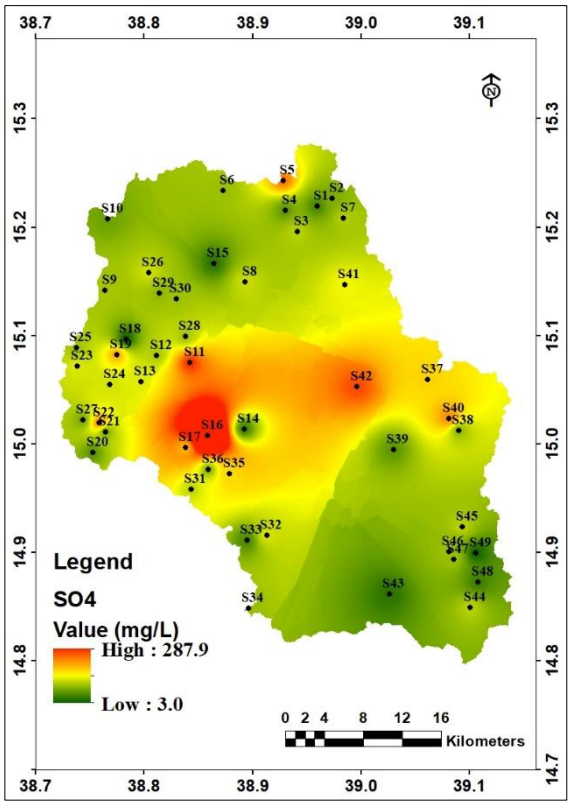
Legend
SO4
Value (mg/L)
High : 287.9
Low : 3.0
0 2 4 8 12 16
Kilometers

(m)

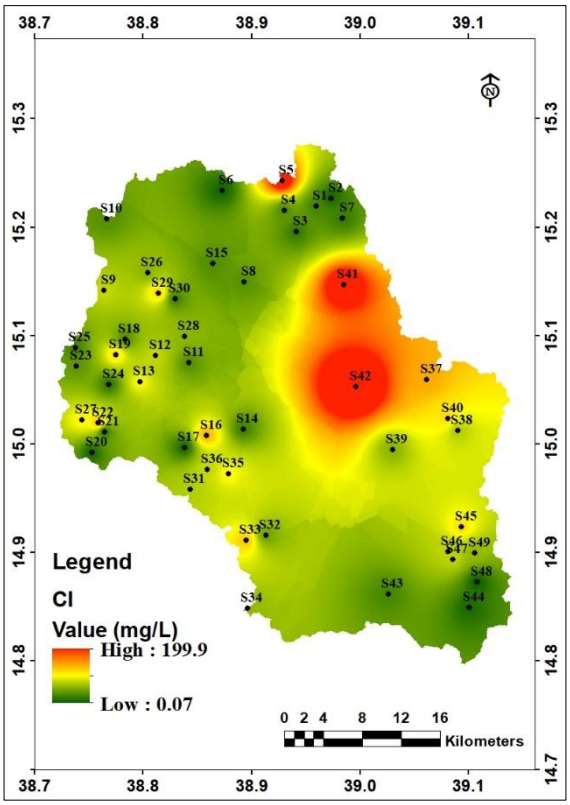
Legend
Cl
Value (mg/L)
High : 199.9
Low : 0.07
0 2 4 8 12 16
Kilometers

(n)

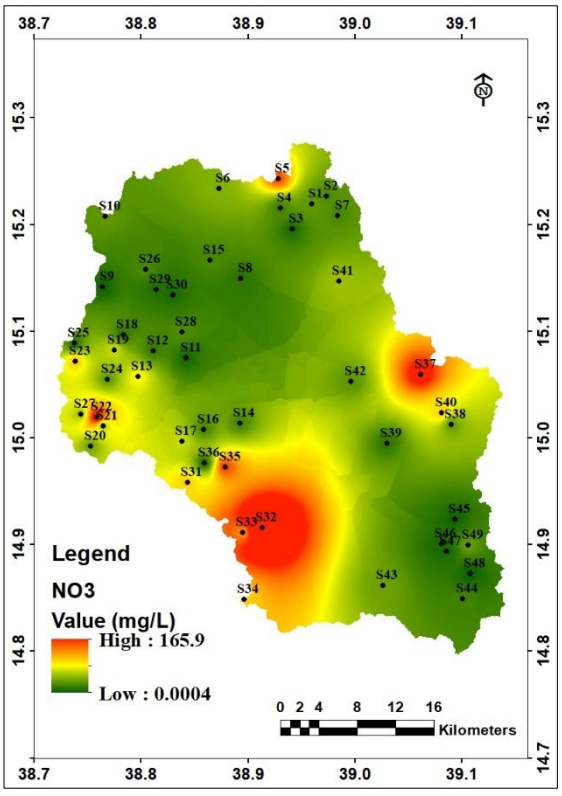
Legend
NO3
Value (mg/L)
High : 165.9
Low : 0.0004
0 2 4 8 12 16
Kilometers

(o)

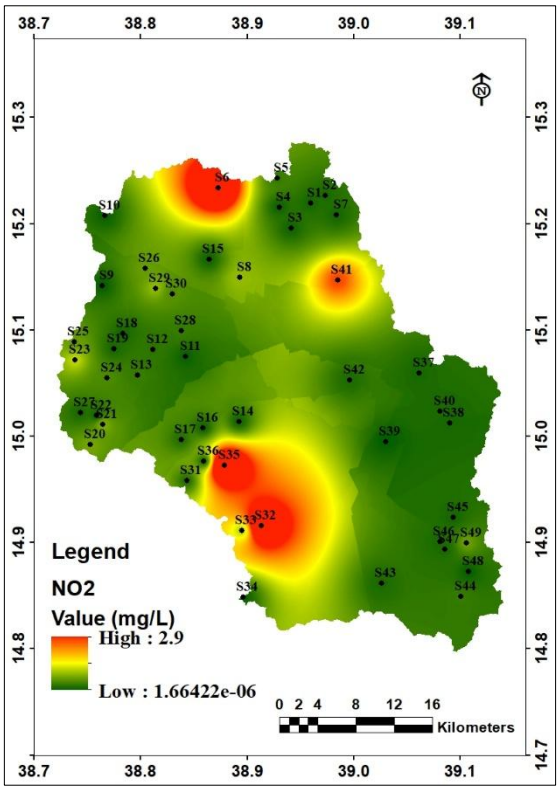
Legend
NO2
Value (mg/L)
High : 2.9
Low : 1.66422e-06
0 2 4 8 12 16
Kilometers

(p)

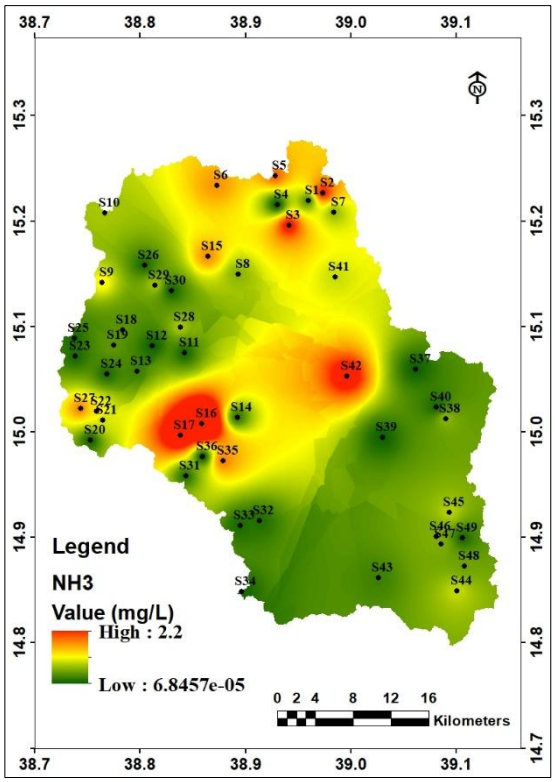

(q)

Fig. 31 Spatial distribution of quality parameters a) pH, b) EC, c) TDS, d) Alkal, e) TH, f) Ca, g) Mg, h) Na, i) K, j) Fe, k) Mn, l) HCO_3, m) SO_4, n) Cl, o) NO_3, p) NO_2, q) NH_3

4.3.3. Groundwater facies and geochemical processes

To better understand the hydrochemical evolution of the groundwater system, a suite of geochemical evaluation tools was applied to identify dominant hydrochemical facies and the processes governing water chemistry. These approaches provide complementary insights into ion sources, mineral stability, water-rock interactions, evaporation–crystallization effects, and possible anthropogenic influences. To date, no comprehensive hydrochemical investigation of this kind has been conducted in Eritrea, making this study the first to apply an integrated methodological framework to characterize groundwater evolution in upper Mereb area. By combining facies classification, process-based diagrams, mineral saturation modelling, and ionic–statistical relationships, the study establishes a foundational basis for interpreting groundwater quality and guiding future exploration.

4.3.3.1.Piper diagrams

The Piper diagram provided the basis for various significant insights into the hydrogeochemical data (Karmegam et al., 2011). The diagram reveals that the groundwater of the study area is predominantly characterized by Ca-Mg-HCO_3 type, indicating waters influenced by rock-water interaction or evaporitic inputs (Fig. 32). The dominance of Ca^{2+} and

Mg^{2+} in the cation triangle suggests significant interaction with carbonate-bearing lithologies, such as limestone and dolomite (Moubchir et al., 2024). This pattern is consistent with groundwater systems hosted in volcanic and metamorphic terrains where secondary porosity and fracture networks allow rapid infiltration and increased water-rock interaction (Mohammed et al., 2022).

The anion ternary plot displayed a clearer pattern, with most samples concentrated toward the HCO_3^- corner, indicating that bicarbonate is the predominant anion in the system. In areas underlain by basaltic and metavolcanic rocks, groundwater commonly develops bicarbonate-rich compositions due to the weathering of silicate minerals, which releases Ca^{2+}, Mg^{2+}, and HCO_3^- into solution (Ghimire et al., 2025). This geochemical signature supports the interpretation that recharge zones within the catchment, particularly within fractured highland terrains, promote active water-rock interaction and ongoing hydrochemical evolution. Overall, the Piper diagram clearly reflects the hydrogeological characteristics of the upper Mereb catchment, where recharge-driven Ca-Mg-HCO_3 waters dominate regions underlain by volcanic and metamorphic lithologies (K. M. Asghede et al., 2026). These findings are consistent with groundwater geochemical patterns observed in studies from India and Hungary (Krishnamoorthy & Lakshmanan, 2024; Mohammed et al., 2025).

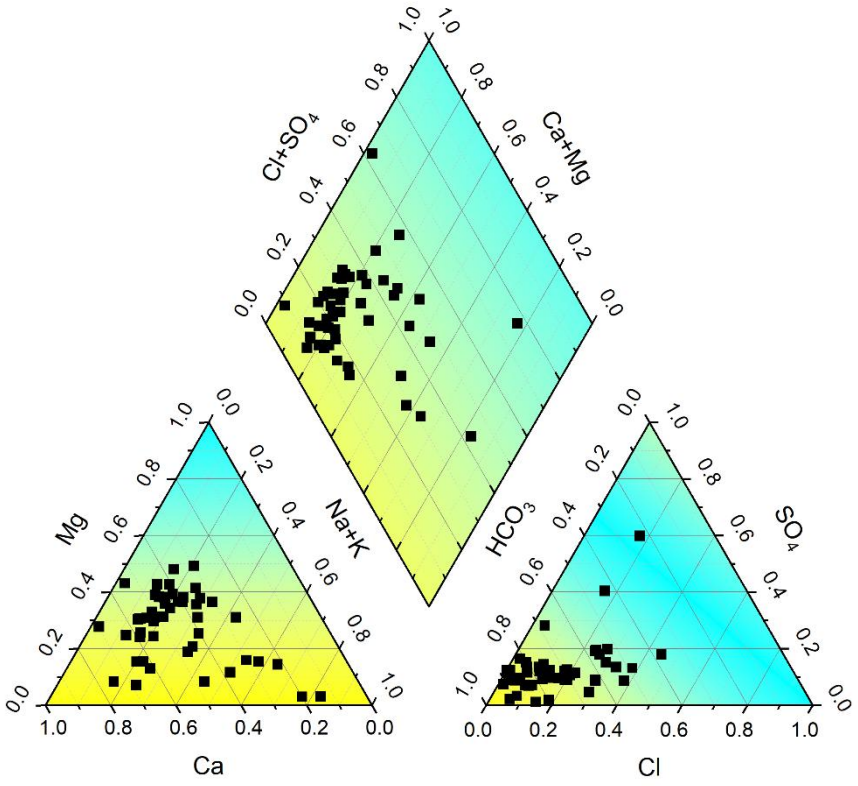

Fig. 32 Piper diagram showing the major water facies in the study area

4.3.3.2.Gibbs diagram

The controlling mechanisms of groundwater chemistry are illustrated in the Gibbs diagrams presented in Figure 33, where cation ratios (Fig. 33a) and anion ratios (Fig. 33b) are plotted against TDS. The spatial positioning of the groundwater samples within these diagrams helps clarify the dominant geochemical processes shaping the water composition. In both the cation and anion fields, most samples are situated within the rock–water interaction dominance zone, clearly demonstrating that groundwater chemistry is primarily governed by the interaction between flowing water and the surrounding geological materials. This dominance highlights the substantial role of mineral weathering processes in influencing the chemical characteristics of the groundwater (Sun et al., 2025).

A slight extension of data points toward the evaporation-dominance field is visible in the cation plot. Although limited in extent, this shift may reflect localized evaporative concentration, potentially occurring in shallow aquifers or regions experiencing high evapotranspiration. Under such conditions, sodium may become relatively enriched compared to calcium, subtly steering the water chemistry toward the evaporation endmember (Bourmada et al., 2024; Kong et al., 2025). Nevertheless, this evaporative influence remains secondary and does not outweigh the overarching control exerted by rock-water interactions across the dataset.

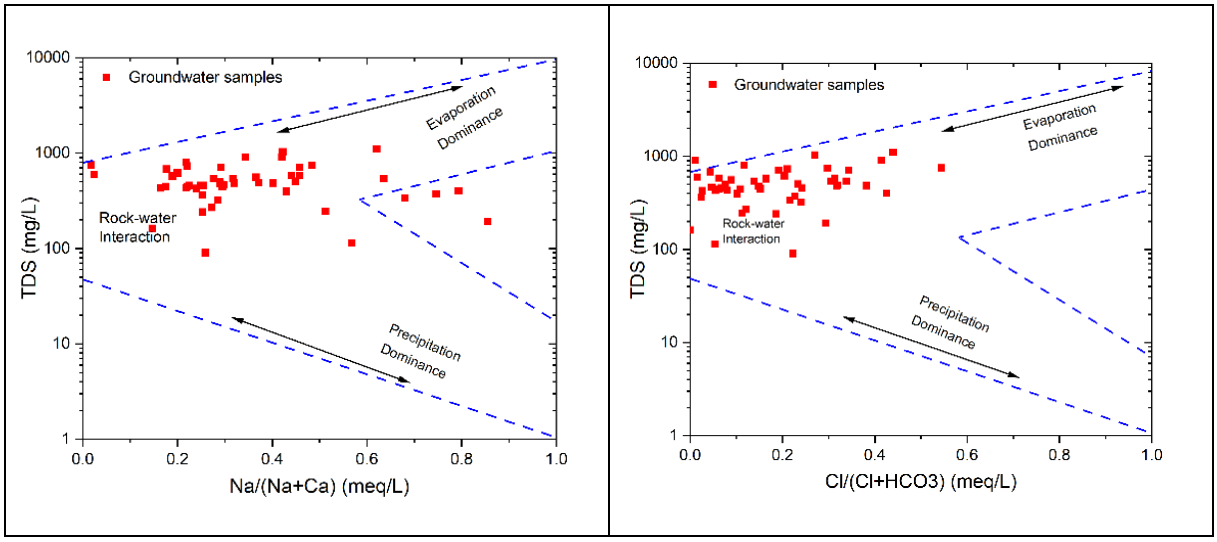

(a) (b)

Fig. 33 A Gibbs diagram showing the major geochemical processes in the groundwater system

4.3.3.3.Saturation Index

Figure 34 presents the saturation indices (SI) of anhydrite, aragonite, calcite, dolomite, gypsum, and halite across groundwater samples (S1 to S49). The results reveal distinct

geochemical behaviors among the major carbonate and evaporite minerals across all sampled groundwater points. Carbonate minerals calcite, aragonite, and dolomite display SI values fluctuating around equilibrium (SI ≈ 0), with several samples showing slight supersaturation (SI > 0). This pattern indicates that the groundwater is either at equilibrium or marginally oversaturated with respect to these minerals, suggesting active carbonate buffering and potential precipitation under existing hydrochemical conditions (Mohammed et al., 2022). Dolomite exhibits more pronounced positive SI peaks compared to calcite and aragonite, reflecting slower reaction kinetics and possible influence of Mg-rich lithologies within the aquifer system.

In contrast, the evaporite minerals anhydrite and gypsum remain consistently undersaturated (SI < 0) in all samples. Persistent undersaturation indicates that groundwater remains chemically capable of dissolving these evaporite minerals, suggesting ongoing water–rock interaction and a continued contribution of sulfate and calcium ions to the hydrochemical system (Kammoun et al., 2022). Halite shows the lowest SI values among all minerals (SI ≈ -7 to -10), indicating strong undersaturation throughout the dataset. It reflects the high solubility of halite and suggests that its dissolution contributes minimally to groundwater chemistry, likely because halite-bearing formations are absent or present only in trace amounts in the study area. The consistently low SI values further confirm that sodium and chloride concentrations arise from other geogenic or anthropogenic sources rather than from halite-equilibrium processes.

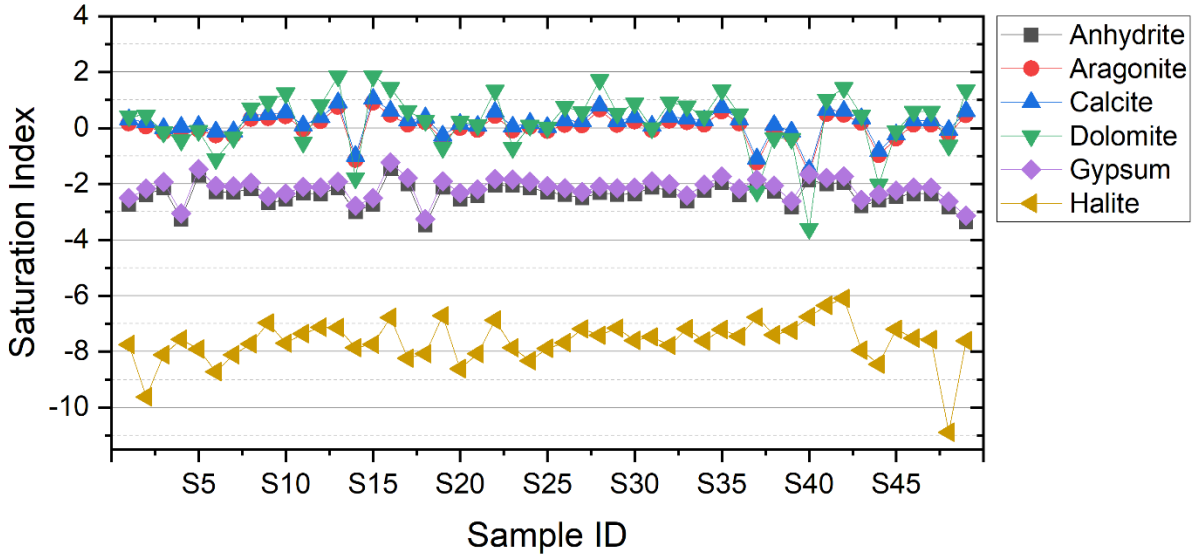

Fig. 34 Saturation Index distribution for major minerals in groundwater

Overall, the saturation index patterns indicate that carbonate equilibrium processes exert the strongest geochemical control on groundwater chemistry, while evaporite minerals contribute mainly through dissolution without reaching saturation. These findings align with typical hydrochemical conditions observed in basaltic and metavolcanic terrains, where

carbonate weathering and secondary mineral formation dominate over evaporitic interactions (Fosu et al., 2025).

4.3.3.4. Pearson correlation matrix

Pairwise correlation analysis of groundwater quality parameters (Fig. 35) reveals significant positive relationships among several key constituents. The correlation matrix reveals strong positive relationships among electrical conductivity (EC), total dissolved solids (TDS), alkalinity (ALKA), total hardness (TH), and the major cations Ca^{2+} and Mg^{2+}. These strong associations indicate that groundwater mineralization in the study area is largely controlled by water-rock interactions, particularly the dissolution of carbonate and silicate minerals.

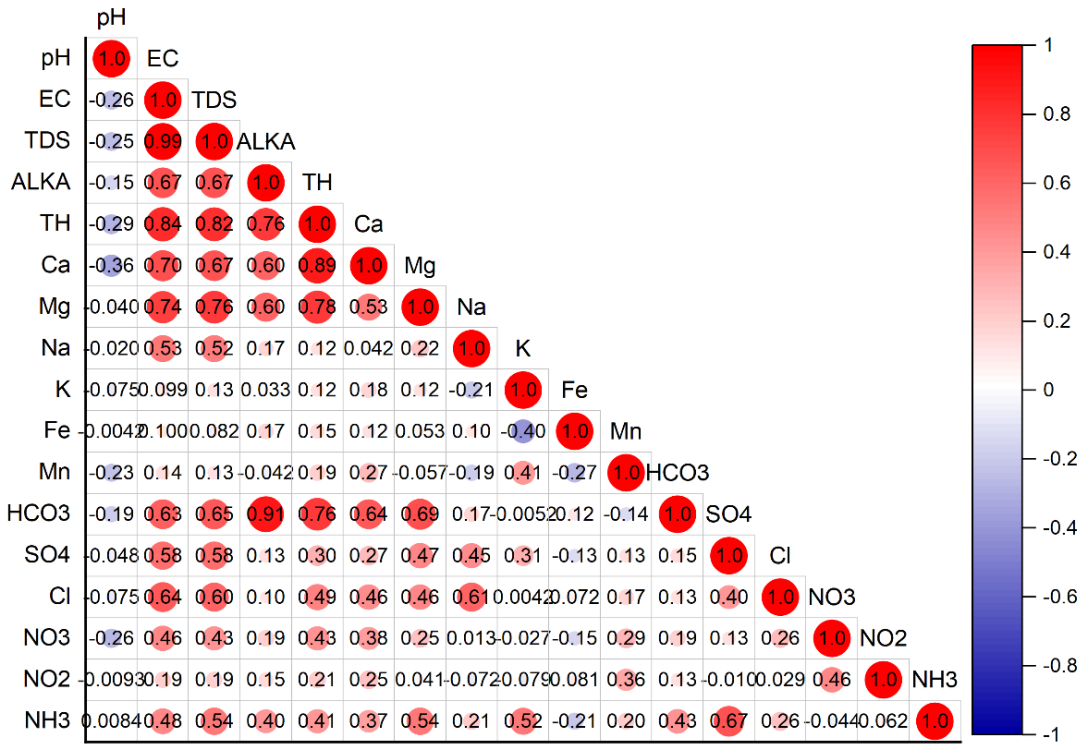

Fig. 35 Pearson correlation matrix showing the association between physicochemical parameters

The very high correlation between EC and TDS (0.99) reflects their mutual dependence on overall ionic strength. Likewise, the strong correlations of Ca^{2+} and Mg^{2+} with TH (0.76 and 0.78) and with HCO_3^- (0.69 and 0.76) support the dominance of carbonate weathering (calcite and dolomite dissolution) as a major geochemical process governing groundwater chemistry. This pattern is consistent with groundwater in crystalline and volcanic terrains, where prolonged interaction with fractured rocks enhances mineral dissolution and leads to elevated hardness and bicarbonate concentrations (P. Kumar et al., 2024).

In contrast, relatively weaker correlations among Na^+, K^+, and anions such as Cl^- and SO_4^{2-} suggest more complex or localized controls, including cation exchange, evaporation effects, or anthropogenic inputs. The moderate Na^+- Cl^- correlation (0.49) may indicate partial halite dissolution or ion exchange reactions, particularly in areas underlain by clay-rich soils or weathered volcanic deposits. Meanwhile, the low correlations among nitrate species (NO_3^-, NO_2^-, NH_3) and major ions imply that these constituents primarily may originate from external sources such as agricultural activities, domestic waste, or surface contamination, rather than from geogenic processes. The weak, negative, or insignificant correlations of trace metals such as Fe and Mn with most major ions further support the notion that redox-controlled mobilization, rather than mineral dissolution, governs their concentrations. Overall, the correlation structure highlights a hydrochemical system dominated by natural geologic controls, with localized anthropogenic influences superimposed on the regional groundwater flow regime.

4.3.3.5.Inter-ionic reaction

The interionic relationship between Na and Cl shows clear trends when compared with the 1:2, 1:1, and 2:1 molar ratio line (Fig. 36a). Most groundwater samples plot above the 1:1 ratio line, and many are also located above the 1:2 line, indicating a relative enrichment of sodium compared to chloride. This pattern suggests that processes beyond simple halite (NaCl) dissolution such as ion exchange or anthropogenic inputs may be responsible for the elevated sodium concentrations (Kong et al., 2025). Only one sample falls below the 2:1 line, while a few outliers appear well above the 1:2 ratio, further supporting the influence of additional geochemical processes on Cl enrichment within the groundwater system.

The interionic relationship between Ca and SO_4 exhibits a distribution pattern comparable to that observed for Na and Cl (Fig. 36b). Most groundwater samples plot above the 1:1 ratio line, with many also positioned above the 1:2 line, indicating a relative enrichment of calcium compared to sulfate. This pattern suggests that processes such as the dissolution of calcium-bearing minerals (e.g., calcite or gypsum) or ion exchange may be contributing to elevated calcium concentrations (Mohammed et al., 2025). Only one sample occurs below the 2:1 line, and several outliers lie well above the 1:2 ratio, further supporting the influence of additional geochemical processes on calcium enrichment in the groundwater.

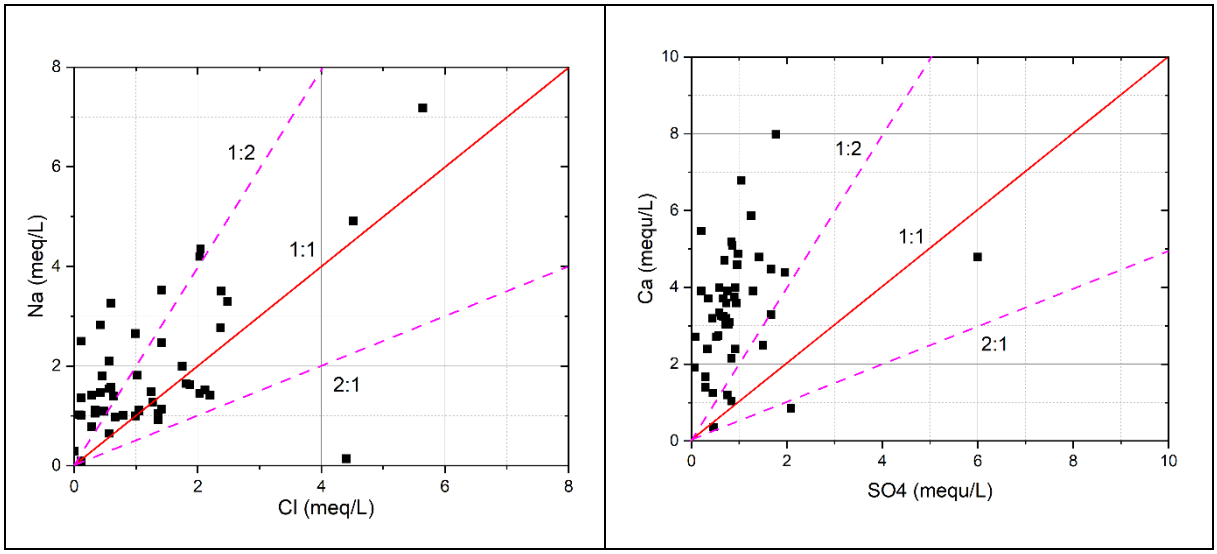

(a) (b)

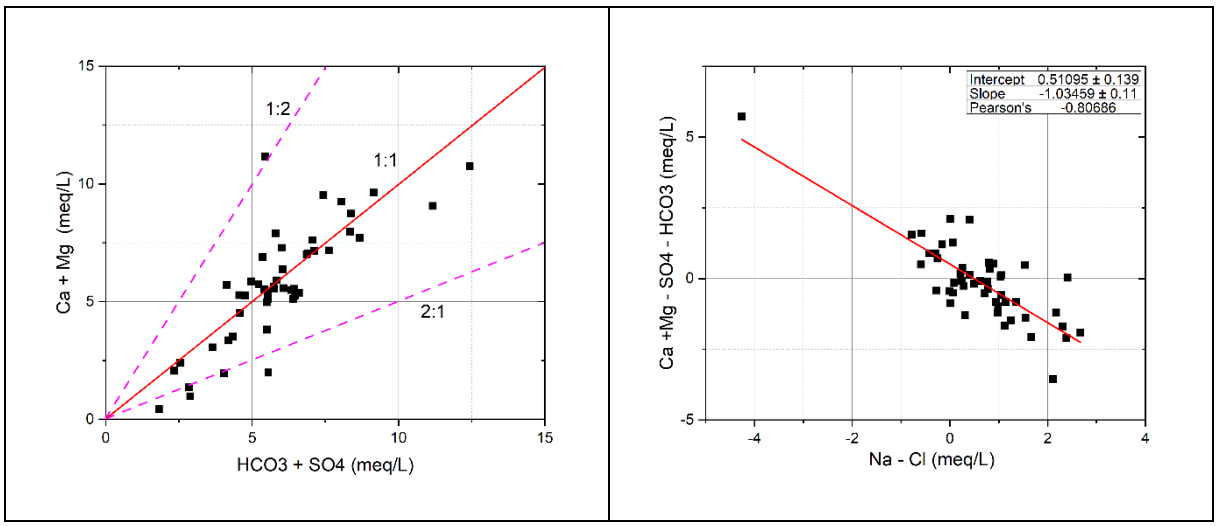

(C) (d)

Fig. 36 Scatter plot showing the interconnection between major ions in the study area

The bivariate plot of Ca^{2+} + Mg^{2+} versus HCO_3- + SO_4^{2-} (meq/L) (Fig. 36c) indicates that groundwater chemistry in the study area is primarily governed by carbonate mineral dissolution. This is because most samples cluster around the 1:1 equilibrium line, reflecting balanced release of divalent cations and corresponding anions during calcite and dolomite weathering. Several points plot above the 1:1 line, suggesting an excess of Ca^{2+} and Mg^{2+} likely caused by silicate weathering, reverse ion exchange, or evaporation concentration effects, which introduce additional cations without equivalent bicarbonate or sulfate. Conversely, samples falling below the line indicate relatively higher HCO_3^- + SO_4^{2-}, a pattern commonly associated with cation exchange processes (where Ca^{2+} and Mg^{2+} are removed from solution and replaced by Na^+). Overall, the distribution of points indicates that carbonate dissolution

dominates, with secondary modification by ion exchange and sulfate sources, consistent with the hydrogeochemical behavior observed in similar hard-rock and mixed-lithological aquifers (Raju et al., 2016).

The ion exchange dynamics were assessed by plotting the difference between (Ca + Mg) and (SO_4 + HCO_3) on the y-axis against the difference between Na and Cl on the x-axis, both expressed in milliequivalents per liter (Fig. 36d). The plot reveals a strong negative linear relationship, with a slope of -1.03 and a Pearson's R^2 value of 0.806. This pronounced inverse correlation indicates an active ion-exchange process within the groundwater system. Wherein calcium and magnesium ions are progressively replaced by sodium ions in the aquifer matrix, most likely through interactions with clay minerals (Salem & Osman, 2017). Samples plotting above the origin (positive y-values) illustrate direct ion exchange, whereas those falling below suggest reverse ion exchange. This pattern is characteristic of aquifers influenced by weathered or clay-rich formations, supporting the interpretation that ion exchange significantly modifies groundwater chemistry in the study area.

The interionic relationships among major ions in the upper Mereb groundwater system collectively indicate that multiple geochemical processes simultaneously influence water chemistry, with carbonate dissolution and ion exchange emerging as the dominant mechanisms. The Na–Cl and Ca–SO4 plots reveal excess sodium and calcium beyond what would be expected from simple halite or gypsum dissolution, pointing to contributions from silicate weathering, reverse ion exchange, and potentially anthropogenic sources. The strong clustering of Ca^{2+} + Mg^{2+} versus HCO_3^- + SO_4^{2-} around the 1:1 equilibrium line further confirms carbonate mineral dissolution as the principal control on groundwater composition, while deviations above and below this line reflect localized effects of evaporation concentration, soil-CO_2 inputs, and cation exchange processes. The ion-exchange bivariate plot, exhibiting a strong negative linear relationship (slope ≈ –1, R^2 = 0.806), provides robust evidence that sodium–calcium–magnesium exchange reactions likely driven by clay-rich lithologies are actively modifying groundwater chemistry across the catchment. Together, these interionic patterns demonstrate a groundwater system shaped by both geological and hydrochemical interactions, underscoring the need for sustained monitoring as zones dominated by ion exchange and high mineralization may pose long-term concerns for drinking water suitability, irrigation performance, and aquifer sustainability.

4.3.4. Classification of groundwater samples

Hierarchical cluster analysis (dendrogram; Fig. 37) partitioned the groundwater samples into three distinct groups, each with coherent hydrochemical signatures. Cluster 1 (the largest group, blue branch) is characterized by moderate to high alkalinity (HCO_3: 201-595 meq/L), moderate electrical conductivity and TDS (EC 587-1202 µS/cm; TDS 425-909 mg/L), and appreciable Ca and Mg (Ca 43.2-160 mg/L; Mg 9.6-51.6 mg/L). This composition is typical of recharge-dominated waters influenced by carbonate weathering and water-rock interaction, producing Ca-Mg-HCO_3 facies (Amit Hasan et al., 2026). The predominance of such signatures in the main cluster indicates that most wells sample relatively unpolluted groundwater that has undergone substantial contact with carbonate-bearing or mafic lithologies, which release Ca and Mg through dissolution reactions.

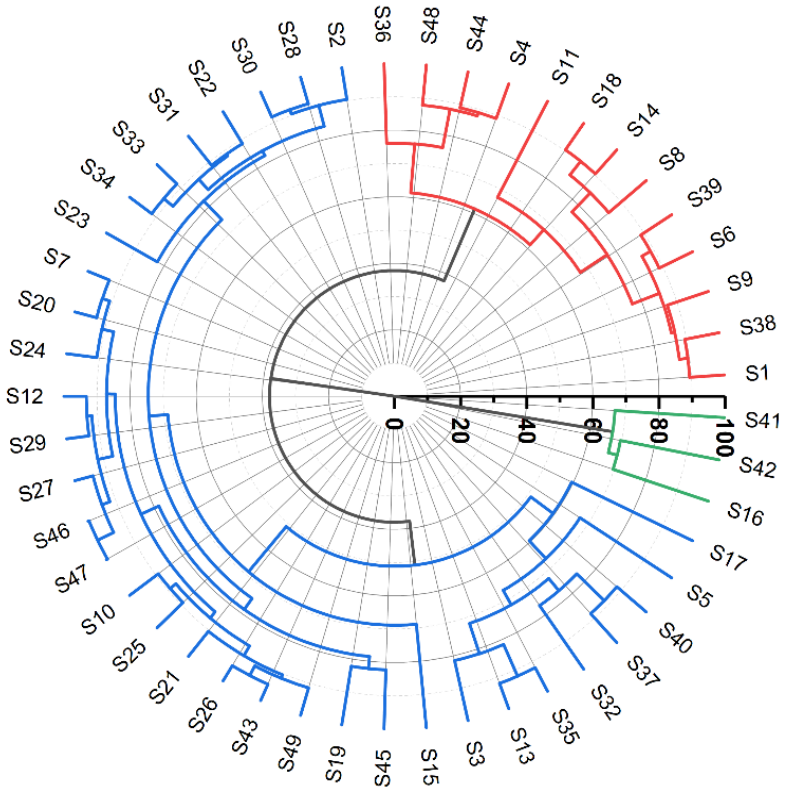

Fig. 37 Cluster dendrogram showing hydrochemical relationships among groundwater samples

Cluster 2 (red branch) includes samples with the lowest mineralization and hardness (EC 135–602 µS/cm; TDS 90–402 mg/L; TH 22–195 mg/L), lower alkalinity (HCO_3: 49–300 mg/L), and generally reduced Ca and Mg concentrations. The chemical pattern of this group points toward groundwater that has undergone comparatively limited solute accumulation or weaker water–rock interaction, as reflected in its dilute nature. Similar low-mineralization

signatures are commonly reported in settings where groundwater exhibits modest chemical evolution or interacts with less reactive lithologies (Bolgov et al., 2024).

Cluster 3 (green branch) is chemically distinct from the other groups, characterized by the highest electrical conductivity and TDS (EC 1362–1649 µS/cm; TDS 912–1105 mg/L), elevated Na (80.5–113 mg/L), Cl (84.5–200 mg/L), and SO_4 (50–94 mg/L), along with high total hardness and alkalinity. The combination of high salinity and a Na–Cl-dominated composition suggests that the groundwater in this cluster may be influenced by processes or lithologies that contribute greater ionic concentrations, such as contact with more soluble mineral phases or interaction with geochemically evolved waters. The markedly elevated Fe (up to 5.5 mg/L) and NH_3 (up to 2.19 mg/L) values indicate conditions that could be shaped by localized reducing environments or specific anthropogenic inputs, although the clustering alone cannot isolate their exact origin. Similar chemical patterns have been reported in aquifers affected by a mixture of geogenic and human-related factors, where both natural mineral dissolution and land-related contributions shape groundwater composition (Kanji et al., 2025). This cluster therefore represents a group of samples with relatively enriched ionic signatures that align with settings where groundwater undergoes stronger chemical modification.

The results of the cluster analysis can also be visualized spatially through GIS, allowing the dendrogram-derived groups to be mapped across the study area (Fig. 38). The spatial pattern shows that Cluster 1 occupies the largest portion of the region (52.1%), stretching broadly from the northwest toward the southwest. Cluster 2 covers 37.2% of the area, extending from the northern part through the central zone and toward the east, with a minor concentration in the south. In contrast, Cluster 3, accounting for 10.7%, is restricted mainly to the northeastern part of the study area. This spatial visualization of cluster map highlights zones of similar groundwater characteristics, enabling faster and more informed decision-making regarding monitoring, management, and resource allocation.

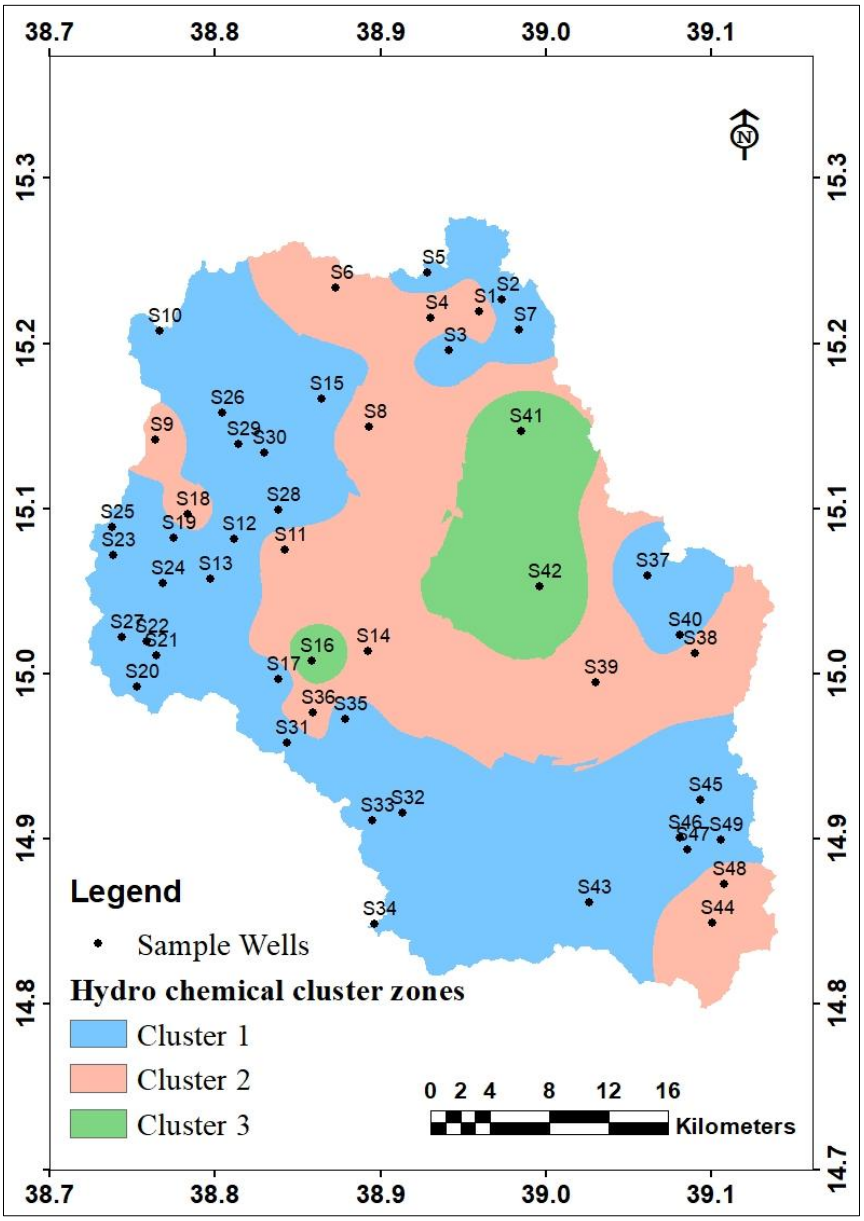

Fig. 38 Distribution Map of Groundwater Cluster Types (C1–C3)

4.3.5. Factors influencing groundwater quality

The Principal Component Analysis (PCA) provides an integrated understanding of the dominant hydrogeochemical processes regulating groundwater quality in the study area. PC1, which accounts for 39.30% (Table 14 and Fig. 39) of the total variance, is characterized by strong positive loadings of EC, TDS, TH, Ca, Mg, HCO_3, and Cl, indicating that mineral weathering, salinity enrichment, and hardness are the major controls on groundwater chemistry (Table 15). This pattern is consistent with the Ca–Mg–HCO_3 facies identified in the Piper diagram and the rock–water interaction mechanisms inferred from the Gibbs plot. These suggest that carbonate and silicate dissolution (El-Rawy et al., 2024), supported by cation exchange reactions, are the primary natural processes governing groundwater evolution. These processes are typical in natural groundwater systems, where geochemistry is largely shaped by

the dissolution of minerals such as calcite and dolomite (Mohammed et al., 2022). The moderate loading of Na further supports the ion exchange trend illustrated by the Na–Cl vs (Ca + Mg) – (HCO_3 + SO_4) plot, which showed a near-stoichiometric negative slope associated with clay–aquifer interactions.

PC2 explains an additional 12.75% of the variance and reflects a combination of redox-sensitive parameters (Fe, Mn, NH_3) and agricultural indicators (NO_3, SO_4, K). The strong negative loading of Fe and positive loadings of Mn and NH_3 indicate spatial variations in redox conditions. Where reducing environments promote the mobilization of Fe and the accumulation of ammoniacal nitrogen. This interpretation aligns with the Cluster 3 groundwater group, which exhibited extremely high Fe and NH_3 levels, pointing to localized zones of stagnation or organic-rich sediments. Simultaneously, the positive loadings of NO_3, K, and SO_4 indicate the influence of agricultural activities or surface recharge, consistent with values observed in Cluster 2. These combined loadings demonstrate that PC2 captures both natural redox processes and anthropogenic contributions to groundwater chemistry.

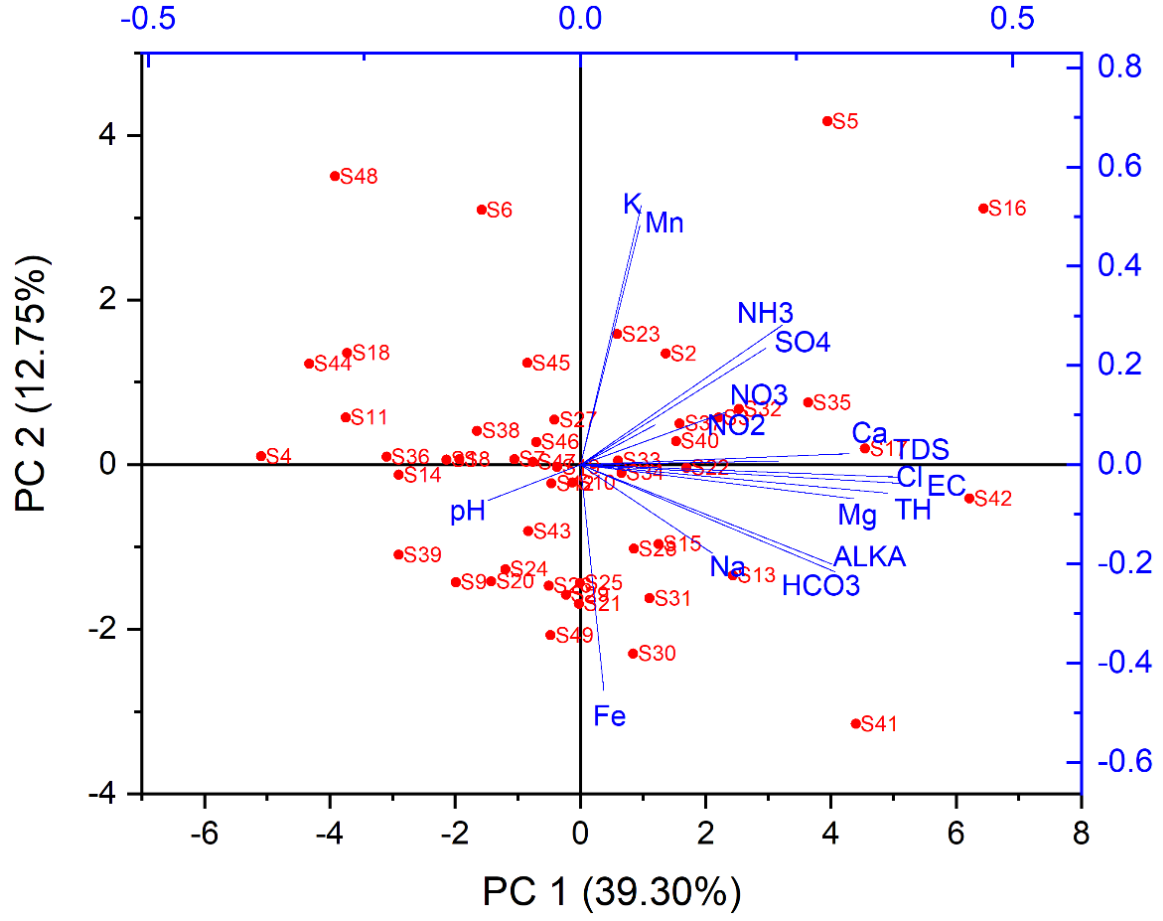

Fig. 39 PCA biplot illustrates the loadings of hydrochemical parameters and the distribution of groundwater samples along PC1 and PC2.

Table 14 Eigenvalues derived from Principal Component Analysis (PCA) of groundwater quality parameters

S.No.	Eigenvalue	Percentage of Variance	Cumulative
1	6.68071	39.30%	39.30%
2	2.16719	12.75%	52.05%
3	1.98512	11.68%	63.72%
4	1.63362	9.61%	73.33%
5	1.04817	6.17%	79.50%
6	0.84345	4.96%	84.46%
7	0.70962	4.17%	88.63%
8	0.55492	3.26%	91.90%
9	0.36641	2.16%	94.05%
10	0.32237	1.90%	95.95%
11	0.28889	1.70%	97.65%
12	0.17819	1.05%	98.70%
13	0.10307	0.61%	99.30%
14	0.06123	0.36%	99.66%
15	0.03486	0.21%	99.87%
16	0.01636	0.10%	99.97%
17	0.00582	0.03%	100.00%

Higher-order components (PC3–PC5; Table 15), although explaining a smaller proportion of the total variance, capture more subtle hydrochemical processes, including ion exchange, localized salinity variations, and nitrogen transformation pathways. When interpreted alongside hydrochemical facies classification, ion-balance analysis, and cluster analysis, the PCA results strengthen the understanding of groundwater evolution. The analysis indicates that groundwater chemistry is predominantly controlled by geogenic processes such as mineral dissolution and ion exchange, with secondary contributions from anthropogenic inputs and redox-related reactions. The strong agreement between PCA groupings and dendrogram clusters further highlights the spatial heterogeneity of the aquifer system. It confirms the combined influence of geology, land use, and hydrochemical evolution on groundwater quality in the study area.

Table 15 PCA extracted loadings

	Coefficients of PC1 (39.30%)	Coefficients of PC2 (12.75%)	Coefficients of PC3 (11.68%)	Coefficients of PC4 (9.61%)	Coefficients of PC5 (6.17%)
PH	-0.10695	-0.07215	0.24787	-0.11945	**0.73867**
EC	**0.36935**	-0.03793	0.06218	0.13536	-0.01989
TDS	**0.36868**	-0.02529	0.07735	0.09219	0.00153
ALKA	**0.29049**	-0.2008	-0.1496	-0.31856	0.05847
TH	**0.3552**	-0.05716	-0.17983	-0.07274	-0.06261
Ca	**0.31098**	0.02218	-0.23391	-0.02828	-0.15138
Mg	**0.31604**	-0.06899	0.09971	-0.16038	0.11117
Na	0.15264	-0.17854	**0.43981**	0.34998	-0.03535
K	0.07025	**0.5226**	0.06899	-0.28826	-0.09992
Fe	0.02712	**-0.45535**	-0.06396	0.07721	0.00525
Mn	0.06893	**0.48283**	-0.24981	0.19399	-0.00215
HCO_3	**0.29448**	-0.21599	-0.12963	-0.3375	0.0252
SO_4	0.21456	0.23452	**0.38763**	0.07865	0.07618
Cl	0.22881	0.00728	0.23536	**0.42232**	-0.08853
NO_3	0.16786	0.10556	-0.33402	**0.36755**	0.11806
NO_2	0.08651	0.08016	-0.37875	0.25429	**0.58322**
NH_3	0.23364	**0.28133**	0.25918	-0.2797	0.17813

4.3.6. Assessment of suitability for drinking

The Water Quality Index (WQI) assessment integrates the weighted influence of key physico-chemical parameters (Table 4) to evaluate the suitability of groundwater for drinking in the upper Mereb catchment. The computed WQI values range from 24 to 127 with a mean of 61.7, categorizing the water into excellent (<50), good (50–100), and poor (100–200) classes (Fig. 40). Most groundwater samples fall within the good quality class (74.19%), indicating that the aquifer is generally suitable for domestic use. Approximately 24.52% of the area exhibits excellent water quality, particularly around S1, S4, S7, S10, S11, S12, S14, S19, S28,

S36, S38, S39, S43, S44, S46, S47, and S48. These zones coincide with Ca–HCO_3 water types characterized by low mineralization and limited anthropogenic influence, as indicated by the Piper diagram and Gibbs plots. In contrast, only two samples (S5 and S41; 1.28%) fall within the poor-quality zone, both located in the northern and eastern parts of the catchment. These locations correspond to high EC, TDS, Fe, NH_3, and NO_3 concentrations, supporting the PCA and HCA interpretations that these zones are influenced by localized contamination and geochemical enrichment.

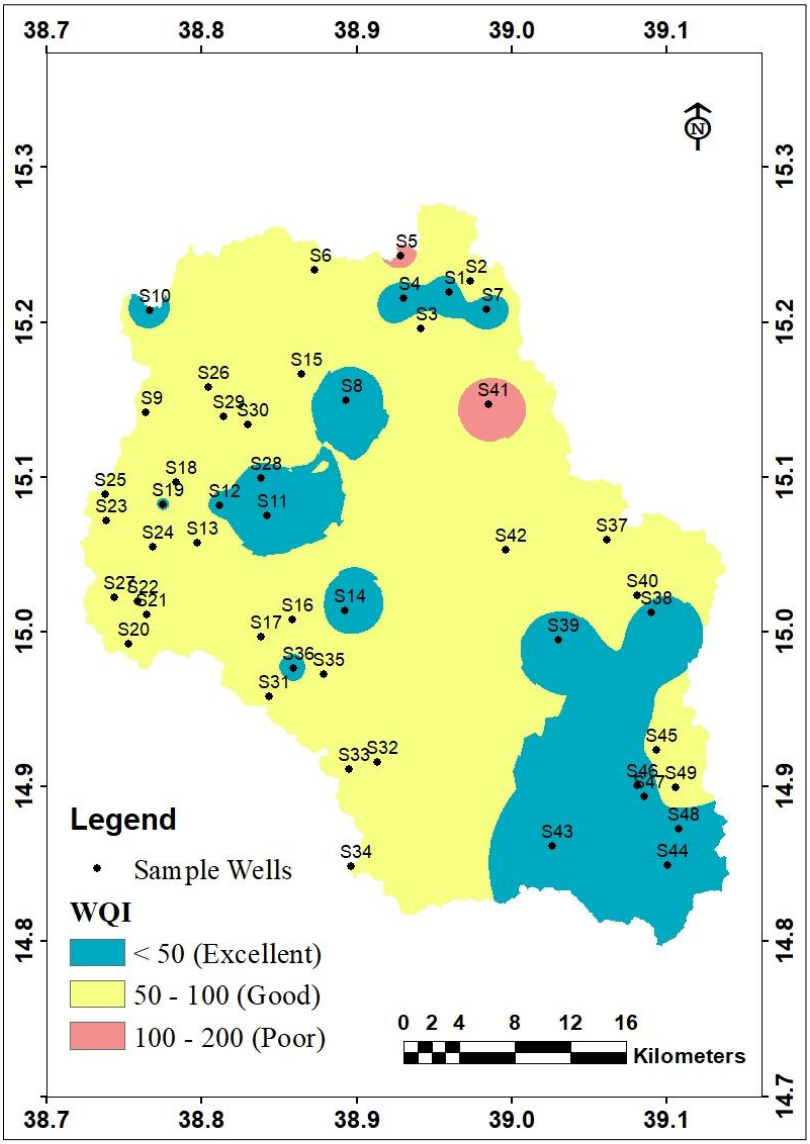

Fig. 40 Spatial distribution of groundwater quality index classes in the study area

The spatial distribution of WQI values (Fig. 40), generated using IDW interpolation, reflects the dominant geochemical processes identified through hydrochemical analyses. Areas classified as poor-quality groundwater correspond to zones where ion exchange and silicate weathering are prominent, indicating that natural mineral–water interactions contribute substantially to elevated ionic concentrations. The high Fe and NH_3 values at S41 and the

elevated TDS and Cl^- at S5, further point to localized reducing conditions and possible anthropogenic influences, consistent with inter-ionic relationship diagrams that suggest cation exchange and secondary inputs. PCA results, in which EC, TDS, Ca, Mg, Cl, and TH strongly load on PC1, represent mineralization and dissolution processes and help explain the spatial decline in groundwater quality within lithologically complex areas.

Overall, the WQI assessment demonstrates that while groundwater in most of the catchment is of good to excellent quality, specific hotspots require management interventions due to natural hydrogeochemical evolution and localized anthropogenic pressures. Integrating the WQI findings with the facies analysis, ion-exchange models, and PCA grouping provides a comprehensive understanding of the controls on groundwater quality. It highlights the need for targeted monitoring in zones prone to contamination or high mineralization. However, it is important to note that spatial interpretation is based on a limited number of sampling points with uneven distribution across the catchment, which may introduce some uncertainty in the delineated patterns. Despite this, the consistency of the observed trends with multiple hydrochemical indicators supports the reliability of the overall interpretation. Future studies incorporating a denser and more evenly distributed sampling network would further improve the accuracy and spatial representation of groundwater quality conditions.

4.3.7. Suitability for irrigation

Groundwater in the upper Mereb area, where farming is the primary livelihood and groundwater is the major irrigation source, generally exhibits favorable sodium-related irrigation quality, as indicated by the Sodium Adsorption Ratio (SAR) and sodium percentage (Na%) (Figs. 41 and 42). The SAR values (0.05–4.66; mean 1.26) place all samples within the S1 low-sodium-hazard class (Fig. 41), indicating minimal risk of soil structural degradation (Alavi et al., 2016). However, most samples fall into the C2–C3 salinity classes of the USSL diagram, demonstrating medium to high salinity. This implies that although sodium hazards are low, salinity may still limit water use for sensitive crops such as tomato, potato, and others (Srivastava, 2019). The Na% values (1.23–82.76%; mean 25.74%) align predominantly within the Excellent to Permissible categories on the Wilcox diagram (Fig. 42), again supporting the general suitability of water for irrigation. Together, both indices confirm that while sodium does not pose a major constraint, salinity remains the principal limiting factor for irrigation in the region.

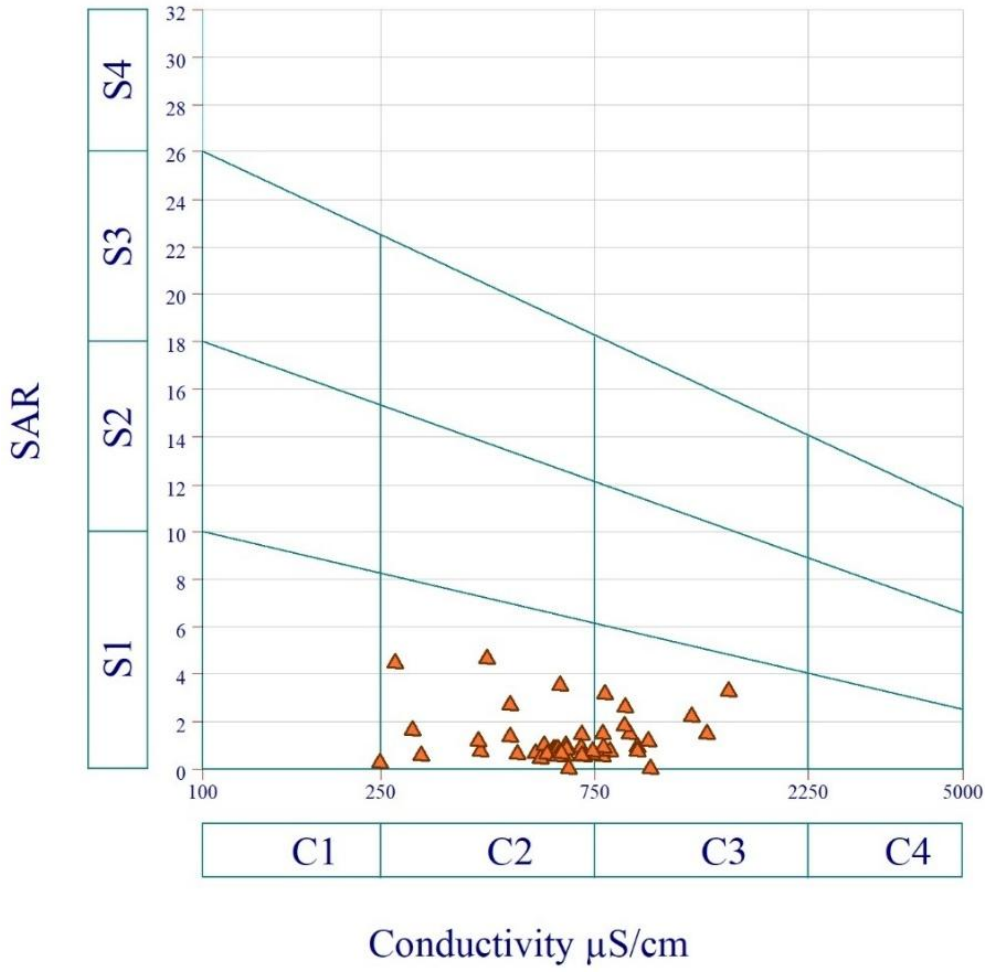

Fig. 41 USSL Diagram for Irrigation Suitability of Groundwater

From a hydrogeological and land-use perspective, the observed salinity patterns are consistent with water–rock interaction, evaporative concentration, and ion-exchange processes typical of semi-arid crystalline terrains (Kanji et al., 2025). In particular, the transition from Ca–Mg–HCO_3 types to more Na–Cl-rich compositions, reflected in some elevated Na% values, may indicate cation exchange and longer groundwater residence times, as reported in comparable studies (Dheeraj et al., 2025). Additionally, localized high Na% values may result from anthropogenic sources, such as agricultural return flows and small-scale domestic inputs, which can concentrate dissolved ions. These interpretations are relevant for decision-makers. It highlights that sustaining irrigation productivity will require different strategies, such as salinity management, crop selection, optimized irrigation scheduling, and regular monitoring of groundwater abstraction to prevent progressive salinization of the aquifer. Overall, the combined use of the USSL and Wilcox diagrams provides a robust assessment framework, highlighting that salinity rather than sodium hazard is the dominant factor limiting the suitability of groundwater for irrigation in the upper Mereb region.

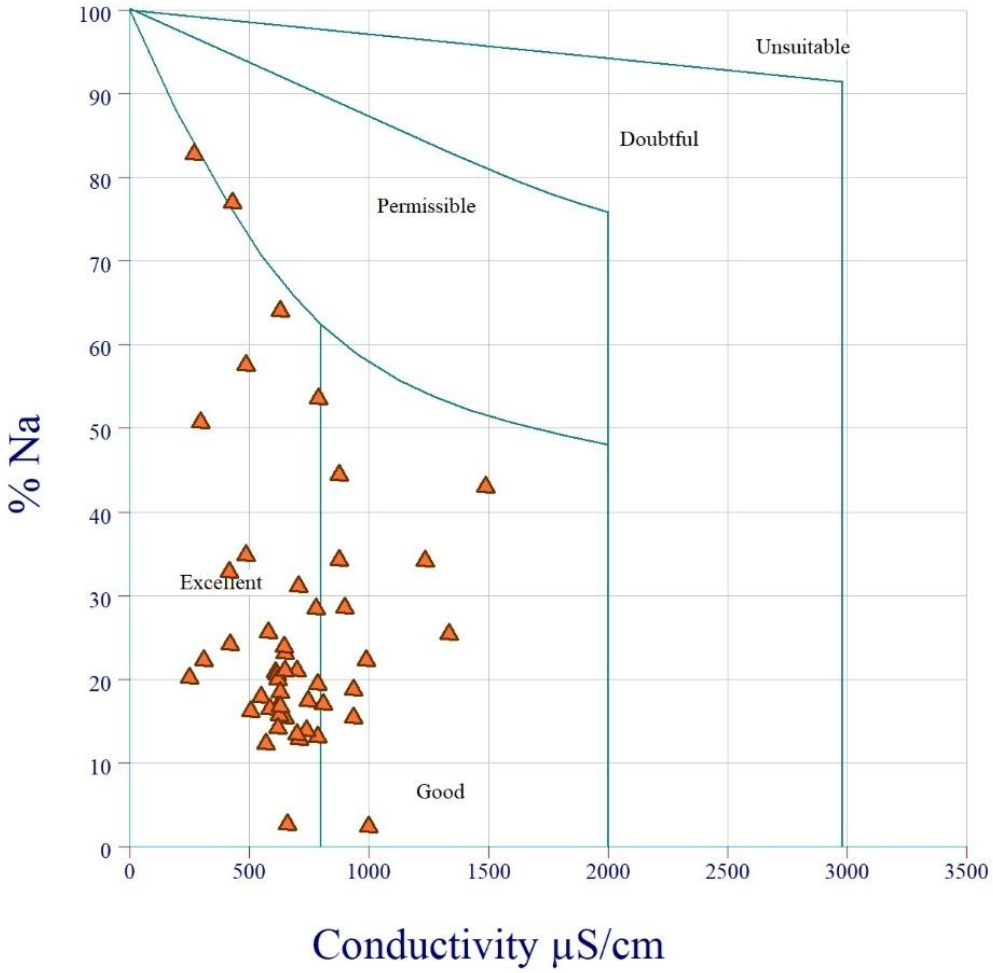

Fig. 42 Irrigation suitability assessment of groundwater based on the Wilcox diagram

5. NEW SCIENTIFIC RESULTS

In my PhD research, I developed a comprehensive hydrogeological framework for assessing groundwater potential and quality in the upper Mereb catchment, based on the integrated interpretation of remote sensing, geological, geophysical, and hydrochemical datasets. As the first systematic investigation of its kind in the study area, this work not only introduces a novel and unified methodological platform but also fills a critical knowledge gap essential for supporting evidence-based decision-making. The major scientific results derived from this research are presented in the following sections.

Thesis 1. Development of litho-structural mapping of upper Mereb area.

I developed litho-structural map of upper Mereb area using integrated remote sensing and geophysical approaches for the purpose of groundwater assessments.

Landsat-9 OLI imagery, satellite gravity data, and DEM-based terrain analysis were combined to establish the framework of the study. Through the application of Principal Component Analysis (PCA), supervised classification, band ratios, and False Color Composite (FCC) techniques, the resulting litho-structural map reveals clear spatial contrasts in lithology across the basin. Basaltic flows dominate the western part of the catchment, whereas metavolcanic, sedimentary, and metasedimentary units are more prevalent in the eastern sectors. Extensive lateritic cover was also identified in both the northern and southern parts of the area, indicating zones of intense weathering that significantly influence surface and subsurface hydrological processes. Structural analysis highlights well-developed lineament systems with dominant NE–SW and NW–SE trends, which are consistent with regional tectonic controls related to Red Sea extension and the interaction between the Arabian and African plates. These structures play a key role in controlling secondary porosity and groundwater movement within the hard-rock terrain. Validation using in-situ geological observations and collected rock samples shows good agreement with the interpreted lithological and structural patterns, increasing confidence in the resulting map. In the Eritrean context, this litho-structural framework provides spatially consistent and cost-effective geological information that supports improved groundwater development planning and also offers potential benefits for broader resource and mineral exploration efforts.

Thesis 2. Enhancement of lithological mapping of upper Mereb area using Machine Learning.

Lithological mapping of the upper Mereb area can be significantly enhanced using Artificial Neural Networks (ANN) and Support Vector Machines (SVM), providing a cost-effective and time-efficient alternative to traditional geological mapping methods.

The training locations were derived from a field-validated lithological map produced from multispectral remote sensing data. Model parameters, including learning rate, number of iterations, and kernel selection, were carefully adjusted to achieve optimal performance in this geologically complex area. The ANN and SVM models achieved nearly similar overall accuracies, indicating consistent and reliable prediction performance. Basalt, metasedimentary, and sedimentary units were classified with high accuracy, while some confusion remained among laterites, metavolcanics, and granitic rocks due to spectral similarities. Despite these challenges, both machine learning approaches effectively delineated the major lithological units across the study area. These results demonstrate that integrating machine learning with remote sensing data can significantly improve lithological mapping, particularly in regions where field data are limited or access is difficult. The enhanced lithological map can serve as a valuable decision-support tool for groundwater exploration, geological investigations, and resource management in Eritrea, and can be adapted to similar geological settings facing comparable data and accessibility constraints.

Thesis 3. Delineation of groundwater potential zones in upper Mereb area using expert and data driven approach.

The Analytical Hierarchy Process (AHP) and the Frequency Ratio (FR)-based groundwater potential mapping revealed that the study area is largely dominated by moderate and low groundwater potential zones, with smaller but significant high and very high potential zones concentrated in the northwestern and northeastern regions.

The two approaches, AHP and FR, classified groundwater potential into five zones ranging from very high to very low, producing broadly consistent spatial patterns across the area. Under the AHP model, moderate-potential zones dominate the catchment (50.04%), mainly occurring in the central and northeastern areas where terrain and soil conditions favor moderate infiltration. Low-potential zones account for 35.61% and are concentrated in the southern and southeastern mountainous regions with steep slopes and shallow soils. High and very high potential zones cover 10.51% and 3.32%, respectively, and are primarily located in

the northwestern part of the catchment, where gentle slopes and favorable lithology enhance recharge, while very low potential zones (0.52%) correspond mainly to steep granitic terrains. Similarly, the FR model identifies moderate (30.98%) and low (30.23%) potential zones as the dominant classes, largely distributed across the central and eastern areas. Higher potential zones (high: 15.31%; very high: 6.22%) are clustered in the northwestern and northeastern regions characterized by fractured rocks and relatively flat terrain, whereas very low potential zones (17.26%) are mainly associated with the steep southern highlands where infiltration is limited. The application of these GIS-based groundwater-potential modelling approaches represents the first methodological introduction of its kind in the study area, demonstrating the value of an integrated framework for delineating groundwater-potential zones. This framework provides a practical and scalable tool that can be applied to other regions of the country, serving as a foundational reference for future groundwater exploration and resource-management initiatives.

Thesis 4. Comparative Evaluation of AHP and Frequency Ratio (FR) models.

I performed a comparative analysis of the AHP and FR output maps to assess their level of consistency, and the results show a strong spatial agreement between the two models, with both consistently identifying similar high- and low-potential zones.

A spatial comparison analysis of the Analytic Hierarchy Process (AHP) and Frequency Ratio (FR) groundwater-potential models was carried out by overlaying their reclassified outputs to evaluate the degree of agreement between the two approaches. The comparison shows that most of the area falls within the non-high-potential category (75.06%), while 14.5% of the area is identified as high potential by only one of the models, and 10.4% represents zones where both models simultaneously predict high groundwater potential. These results reveal a strong correspondence between AHP and FR in delineating both high- and low-potential zones, with both methods consistently mapping low-potential conditions across the southern, higher-relief terrain. Model validation further supports these findings, as the FR method achieves a slightly higher predictive accuracy (AUC = 0.748) compared to AHP (AUC = 0.704), reflecting the advantage of data-driven techniques that incorporate statistically derived relationships between conditioning factors and observed groundwater occurrences. Overall, the combined use of ROC-based validation and spatial overlay comparison demonstrates that both AHP and FR perform reliably and consistently in delineating groundwater-potential zones, offering a sound basis for informed groundwater planning and resource-management decisions.

Thesis 5. Detection of main factors influencing the groundwater quality in the upper Mereb catchment.

I identified the natural and anthropogenic factors that influenced groundwater quality through principal component analysis and hydrochemical methods, where the main result shows that groundwater chemistry is primarily controlled by rock-water interaction processes, with additional influence from agricultural activities and redox conditions.

The Principal Component Analysis (PCA) shows that groundwater quality in the study area is controlled by a combination of natural geological processes and human activities. PC1, which explains the largest share of the variance, reflects the strong influence of rock water interaction process. This was confirmed by Gibbs diagram where most of the samples are projected in the rock dominance zone. The inter-ionic reactions identified that the rock water interactions occurred through carbonate and silicate dissolution, and cation exchange processes. PC2 highlights the joint effect of redox conditions and agricultural inputs, indicating that variations in groundwater chemistry are influenced by both oxidation–reduction processes within the aquifer and nutrients introduced through farming practices, such as nitrate from fertilizers. PC3 to PC5 capture smaller but important processes such as localized salinity changes. When combined, these results show that groundwater evolution is primarily shaped by geogenic controls, with additional contributions from agriculture and redox reactions. The findings provide a clear scientific basis for understanding groundwater quality in the region and offer practical guidance for Eritrea in managing its limited water resources.

Thesis 6. Evaluation of groundwater quality for domestic and agricultural purposes in the upper Mereb catchments.

I assessed groundwater quality in the upper Mereb area for domestic and agricultural purposes using groundwater quality indices and irrigation indices, where the main result shows that groundwater is largely suitable for drinking and irrigation, with minor localized quality issues and salinity as the main limitation for agricultural use.

The Water Quality Index (WQI) shows that groundwater in the upper Mereb catchment is generally suitable for domestic use, with most samples classified as good (74.19%) and a significant portion falling into the excellent category (24.52%). These excellent-quality zones correspond to low mineralization and limited human impact. Only two locations fall into the poor-quality class, where high EC, TDS, Fe, NH_3, and NO_3 values indicate localized

contamination. For agricultural use, irrigation indices show that all samples fall within the low sodium-hazard (S1) category, supported by SAR and Na% values that classify most waters as excellent to permissible. However, the USSL diagram places many samples in the medium to high salinity (C2–C3) classes, indicating that salinity not sodium poses the main limitation for irrigation, especially for salt-sensitive crops. Overall, the combined domestic and irrigation assessments show that groundwater in the upper Mereb region is largely safe for drinking and reasonably suitable for irrigation, but targeted monitoring and salinity-management strategies are needed to protect vulnerable zones. The results provide essential guidance for water managers in Eritrea and offer a useful reference for researchers working in similar semi-arid, data-limited environments.

6. CONCLUSION

This study provided an opportunity to explore how different geospatial and data-driven approaches can be integrated to better understand groundwater systems in a complex and data-limited environment. Working in the upper Mereb catchment demonstrated that no single method is sufficient on its own; rather, the strength of the analysis lies in combining complementary techniques. The consistency observed between structurally derived lineaments, lithological patterns, and groundwater potential zones highlights the value of integrating independent datasets to build confidence in the results. In particular, the use of remote sensing, gravity analysis, and machine learning enabled a more detailed and spatially continuous understanding of subsurface conditions, even in areas where field data are limited. The inclusion of hydrochemical analysis further strengthened the study by providing direct insight into groundwater conditions, helping to connect the assessment of groundwater potential with actual water quality and usability. Together, this integrated approach demonstrates a practical and effective way to support groundwater investigations in similar complex settings. It also highlights the importance of considering both surface and subsurface indicators together, as each dataset contributes a different but complementary perspective on groundwater behavior. Overall, this integration improves the interpretability and reliability of the final outputs in data-scarce regions.

Within the context of Eritrea, this study represents the first application of an integrated hydro-geo-informatics framework for simultaneous groundwater potential and quality assessment. Therefore, it shows its potential as a practical decision-support approach that can be applied in other parts of the country facing similar data limitations. At the same time, the work highlights the importance of data quality and availability in influencing model results, particularly where groundwater occurrence is inferred from indirect indicators and where hydrochemical data coverage is limited. These aspects suggest that the results should be interpreted as supportive tools rather than exact representations. Nevertheless, the framework developed here provides a strong foundation for future research. Where improved datasets, such as detailed productivity well records and expanded water quality sampling, can further refine and validate the findings. Overall, this study shows that groundwater assessment in such environments is a progressive process, where integrated approaches contribute to gradually improving understanding and supporting more informed water resource management.

ACKNOWLEDGEMENT

Throughout my PhD research, I have been privileged to receive invaluable support, guidance, and encouragement from many individuals and institutions whose contributions were essential to the successful completion of this work.

First and foremost, I offer my deepest gratitude to God, whose guidance, strength, and wisdom have enabled me to complete this PhD. I would like also to express my deepest gratitude to my supervisor, Dr. János Vágó, for his continuous guidance, patience, and academic support throughout my PhD journey. His constructive feedback, insightful discussions, and unwavering encouragement have played a central role in shaping both this research and my development as a researcher. I am also sincerely thankful to the Hungarian full Scholarship program, the University of Miskolc, particularly the Faculty of Earth and Environmental Sciences and Engineering and the Institute of Geography and Geoinformatics and government of Eritrea for providing a stimulating academic environment, institutional support, and the facilities necessary to carry out this study. Furthermore, I express my sincere thanks to Dr. Musaab A. A. Mohammed, Abazar M.A. Daoud and Tedros Beyene for the engaging scientific discussions and valuable insights, which contributed to the progress of this research.

My heartfelt appreciation goes to my family, friends, colleagues, and fellow researchers, both at home and abroad, whose knowledge, assistance, and moral support made this demanding journey manageable and rewarding. I am especially grateful to the many Eritrean professionals who generously shared their knowledge and expertise and supported the data collection process. Although too numerous to mention individually, their contributions are deeply appreciated. Special thanks go to governmental institutions, including the Eritrean Higher Education and Research Institutions, Mai-Nefhi College of Engineering and Technology, Mai-Nefhi College of Science, the Eritrean Mapping and Information Center (EMIC), the Asmara Water Resources Department, the Ministry of Agriculture, and the Ministry of Energy and Mines, for their cooperation, data provision, and technical assistance, all of which were essential to the completion of this research.

I am deeply grateful to all who, in one way or another, contributed to this academic endeavor.

LIST OF PUBLICATIONS

Kabral Mogos Asghede, Musaab A. A. Mohammed, János Vágó, Multivariate statistical, hydrochemical, and indexing approaches for groundwater quality evaluation in a semi-arid region: Case study of the Upper Mereb Catchment, Eritrea, the Springer journal of *Discover Applied Sciences*, 2026,
https://link.springer.com/article/10.1007/s42452-026-08345-2

Kabral Mogos Asghede, Abazar M.A. Daoud, Musaab A. A. Mohammed, Woldegabriel Genzebu, Kefela Beyene Kiflay, Péter Pecsmány, János Vágó, Development of a Litho-Structural Map for the Upper Mereb Area, Eritrea, Using Multi-Source Remote Sensing Data and Machine Learning Models, The Elsevier journal of Remote Sensing Applications: Society and Environment, 2025,
https://www.sciencedirect.com/science/article/pii/S2352938525002757

Kabral Mogos Asghede, János Vágó, Geospatial analysis and analytical hierarchy process for delineating groundwater potential zones: a case study in Debarwa catchment, Eritrea, The Journal of Multidisciplinary Sciences, 2025.
https://ojs.uni-miskolc.hu/index.php/multi/article/view/3097/3085

Kabral Mogos Asghede, János Vágó, Comparative analysis of multi-criteria decision-making techniques for groundwater potential mapping in the highlands of Eritrea, The Journal of Geoscience and Engineering, University of Miskolc, 2025.
https://ojs.uni-miskolc.hu/index.php/geosciences/article/view/3920

Kabral Mogos Asghede, Péter Pecsmány, János Vágó, Integrated approach for lineament extraction in assessing groundwater potential: a case study in the highlands of Eritrea, Acta Geographica Debrecina Landscape & Environment series 2024,
https://ojs.lib.unideb.hu/landsenv/article/view/14611/13249

Kabral Mogos Asghede, Dawit Berhane Hagos, János Vágó, Spatial investigation of sulphate in groundwater of Asmara, Eritrea, Journal of Geosciences and Engineering, a publication of the University of Miskolc, December 2023, pp 104 – 113
https://ojs.uni-miskolc.hu/index.php/geosciences/article/view/2476

Kabral Mogos Asghede, Dawit Berhane Hagos, János Vágó, GIS-based prediction map of nitrate in groundwater: a case study of Asmara, Eritrea XXVI. Spring Wind Conference 05 - 07 May 2023, Chapter in book (Conference paper)
https://dosz.hu/fil/0573ad49bdcd00ab4276bf2b315d21641983a4914b84bfe04c2ca5394fb363d7

Martina Zeleňáková; Hany F. Abd-Elhamid; Tatiana Soľáková; Patrik Nagy; **Kabral Mogos Asghede**; Helena Hlavatá; Pavol Purcz, Drought risk assessment in East Slovakia using SPI and RDI at different time scales, Springer Journal, Natural Hazards, 2024.
https://link.springer.com/article/10.1007/s11069-025-07274-4

Tesfamichael Semere Mallu Tumuzghi Tesfay, Shimendi Gde Okbagabir , Teklebrhan Tuemzghi Negash, Berhane Teklesenbet Negassi, Tsegay Bereket Menghis, Tesfit Asrat Medhn, Simon Ghebrehiwet Teklay, Yemane Habtemichael Gebremeskal ,Rezene Habte Tewolde, Kesete Goitom Tewelde , Goitom Kfle Gebremariam, Daniel Brhane, Aklilu Amanuel Tecleab , **Kabral Mogos Asghede**, Ahmedin Hiya Adem, Mulugheta Tesfamichael Solomon, A comprehensive review on finger millet (Eleusine coracana (L.) Gaertn): A gluten-free superfood and feed, Journal of Agriculture and Food Research, 2026
https://doi.org/10.1016/j.jafr.2025.102528

Tesfamichael Semere Mallu Tumuzghi Tesfay, Shimendi Gde Okbagabir , Teklebrhan Tuemzghi Negash, Berhane Teklesenbet Negassi, Tsegay Bereket Menghis, Tesfit Asrat Medhn, Simon Ghebrehiwet Teklay, Yemane Habtemichael Gebremeskal ,Rezene Habte Tewolde, Kesete Goitom Tewelde , Goitom Kfle Gebremariam, Daniel Brhane, Aklilu Amanuel Tecleab , **Kabral Mogos Asghede**, Ahmedin Hiya Adem, Mulugheta Tesfamichael Solomon, The Agronomic, Nutritional, Environmental, and Health Benefits of Teff (Eragrostis tef) as an Underutilized Gluten-Free Superfood and Feed Source, Wiley International Journal of Agronomy Volume 2025, Article ID 6128837, 24 pages
https://doi.org/10.1155/ioa/6128837

List of conference presentations

Kabral Mogos Asghede, Vágó János, Geospatial approach for groundwater quality assessment in Asmara. PhD form (23rd of November 2023),

Kabral Mogos Asghede, Hagos Dawit Berhane, Vágó János; Spatial prediction map of Nitrate in groundwater: a case study of Asmara area; Spring Wind Conference Miskolc, May 5-7, 2023.

Kabral Mogos Asghede, Dr. Vágó János, Hagos Dawit Berhane: Assessment of Magnesium concentration in Groundwater of Asmara, Eritrea Using GIS: Youth Performers Day 2023" event organized by The Department of Geophysics, the Northern Hungary Chapter of the Association of Hungarian Geophysicists, the EAGE Miskolc Student Chapter, the Earth Science Working Committee of Miskolc Chapter of the HAS, and the TEKH (24th of May 2023).

Kabral Mogos Asghede, Vágó János, Spatial variability and prediction of Sulphate concentration in groundwater for sustainable water supply in Asmara, Eritrea Debrecen, Hungary: Debreceni Egyetemi Kiadó (2023) pp. 355-356. , 2 p.

Kabral Mogos Asghede, Vágó János, A GIS Approach for Spatial Prediction and Visualization of Groundwater Pollution by Total Dissolved Solids (TDS) in Asmara, Eritrea. XXIII Conference of PhD Students and Young Scientists, Wroclaw, Poland, 13-15th June 2023.

Kabral Mogos Asghede, Vágó János, Hagos Dawit Berhane, GIS-based assessment of Total Hardness in groundwater: a case study of Asmara, Eritrea. Conference of Technical Science in the North-East Hungary Region, May 22, 2024.

Kabral Mogos Asghede, János Vágó: Integrated approach for lineament extraction in assessing groundwater potential: a case study in the highlands of Eritrea. XV. Geospatial Conference and Exhibition Debrecen, Hungary, May 23-24, 2024.

Kabral Mogos Asghede, János Vágó, Groundwater potential mapping using AHP method in Debarwa catchment area, Eritrea. MultiScience XXXVII. microCAD International Multidisciplinary Scientific Conference University of Miskolc, 30-31 May 2024.

Kabral Mogos Asghede, Vágó János, Delineating groundwater potential recharge zones using Fuzzy-AHP: A case study of Central Highland, Eritrea, PhD form, November 14, 2024.

Kabral Mogos Asghede, Vágó János, GIS based multi criteria decision making (MCDM) comparison for Groundwater potential mapping in Debarwa, Eritrea, GIS day conference November 20, 2024.

Kabral Mogos Asghede, Musaab A. A. Mohammed, János Vágó, GIS-based assessment of groundwater quality for drinking and irrigation in the Upper Mereb catchment, Eritrea. XVI. Geospatial Information Conference and Exhibition, Debrecen May 22-23, 2025.

Kabral Mogos Asghede, János Vágó: Comparative assessment of groundwater potential mapping using statistical and decision-based models in the upper Mereb catchment, Eritrea, PhD Form, 27 November 2025.

REFERENCES

Abd El-Dayem, M., Abd El-Gawad, A., Bedair, S., & Farag, K. S. I. (2023). Groundwater resource evaluation using geoelectrical resistivity survey in the Ghard El-Hunishat area of New Delta project province, North Western Desert, Egypt. *Groundwater for Sustainable Development*, *21*. https://doi.org/10.1016/j.gsd.2023.100918

Abd El-Rahman Hegab, M., Abou El Magd, I., & Hamed Abd El Wahid, K. (2024). Revealing Potential Mineralization Zones Utilizing Landsat-9, ASTER and Airborne Radiometric Data at Elkharaza-Dara Area, North Eastern Desert, Egypt. *Egyptian Journal of Remote Sensing and Space Science*, *27*(4), 716–733. https://doi.org/10.1016/j.ejrs.2024.10.005

Abd El-Wahed, M. A., Kamh, S., Attia, M., & Eldosouky, A. M. (2025). Structural geometry and gold ores along the first outlined N–S dextral shear zone in the Egyptian Nubian Shield, East African orogenic belt: New insights from integrated remote sensing, gravity, magnetic and field studies. *Geomechanics and Geophysics for Geo-Energy and Geo-Resources*, *11*(1). https://doi.org/10.1007/s40948-025-01003-8

Abdelouhed, F., Algouti, A., Algouti, A., Mohammed, I., & Mourabit, Z. (2021). *Contribution of GIS and remote sensing in geological mapping, lineament extractions and hydrothermal alteration minerals mapping using ASTER satellite images: case study of central Jebilets-Morocco* (Vol. 14, Number 1).

Abrams, M., & Yamaguchi, Y. (2019). Twenty years of ASTER contributions to lithologic mapping and mineral exploration. In *Remote Sensing* (Vol. 11, Number 11). MDPI AG. https://doi.org/10.3390/rs11111394

Adesola, G. O., Thamaga, K. H., Gwavava, O., & Pharoe, B. K. (2023). Groundwater Potential Zones Assessment Using Geospatial Models in Semi-Arid Areas of South Africa. *Land*, *12*(10). https://doi.org/10.3390/land12101877

Ahmadi, H., Kaya, O. A., Babadagi, E., Savas, T., & Pekkan, E. (2021). *GIS-Based Groundwater Potentiality Mapping Using AHP and FR Models in Central Antalya, Turkey*. 11. https://doi.org/10.3390/iecg2020-08741

Akbari, H., Rose, L. S., & Taha, H. (2003). Analyzing the land cover of an urban environment using high-resolution orthophotos. In *Landscape and Urban Planning* (Vol. 63).

Akinluyi, F. O., Olorunfemi, M. O., & Bayowa, O. G. (2018). Investigation of the influence of lineaments, lineament intersections and geology on groundwater yield in the basement complex terrain of Ondo State, Southwestern Nigeria. In *Applied Water Science* (Vol. 8, Number 1). Springer Verlag. https://doi.org/10.1007/s13201-018-0686-x

AL-Areeq, A. M., Chowdhury, S., Rahman, M. T., AL-Areeq, N. M., & Quriaa, H. (2023). Assessment of water quality using multivariate statistics and geographical information systems (GIS) of Wadi Aldabab, Taiz, Yemen. *Applied Water Science*, *13*(8). https://doi.org/10.1007/s13201-023-01973-8

Alavi, N., Zaree, E., Hassani, M., Babaei, A. A., Goudarzi, G., Yari, A. R., & Mohammadi, M. J. (2016). Water quality assessment and zoning analysis of Dez eastern aquifer by Schuler and Wilcox diagrams and GIS. *Desalination and Water Treatment*, *57*(50), 23686–23697. https://doi.org/10.1080/19443994.2015.1137786

Alemngus, A., Amlesom, S., & Bovas, J. J. L. (2017). An Overview o f Eritrea ' s Water Resources. *International Journal of Engineering Research and Development*, *13*(3), 74–84.

Ali, K. A., Wilde, S. A., Stern, R. J., Moghazi, A. K. M., & Ameen, S. M. M. (2013). Hf isotopic composition of single zircons from Neoproterozoic arc volcanics and post-collision granites, Eastern Desert of Egypt: Implications for crustal growth and recycling in the Arabian-Nubian Shield. *Precambrian Research*, *239*, 42–55. https://doi.org/10.1016/j.precamres.2013.05.007

Alitane, A., Essahlaoui, A., Ousmana, H., Essahlaoui, N., Hmaidi, A. El, Berrada, M., & Van Griensven, A. (2024). Water quality classification using self-organizing maps and cluster analysis: Case of Meknes-El Hajeb Springs, Morocco. *Environmental Science and Pollution Research*. https://doi.org/10.1007/s11356-024-35633-4

Alrefaee, H. A., Soliman, M. R., & Merghelani, T. A. (2022). Interpretation of the subsurface tectonic setting of the Natrun Basin, north Western Desert, Egypt using Satellite Bouguer gravity and magnetic data. *Journal of African Earth Sciences*, *187*. https://doi.org/10.1016/j.jafrearsci.2022.104450

Aluko, O. E., & Igwe, O. (2018). Automated Geological lineaments mapping for groundwater exploration in the basement complex terrain of Akoko-Edo area, Edo-State Nigeria using remote sensing techniques. *Modeling Earth Systems and Environment*, *4*(4), 1527–1536. https://doi.org/10.1007/s40808-018-0511-4

Alzahrani, H., Basaloom, A., & Mosaad, S. (2025). Geochemical-based appraisal of karst groundwater quality, west Nile Valley, central Egypt, for drinking and irrigation. *Journal of Hydrology: Regional Studies*, *57*. https://doi.org/10.1016/j.ejrh.2024.102152

Amer, R., Ripperdan, R., Wang, T., & Encarnación, J. (2012). Groundwater quality and management in arid and semi-arid regions: Case study, Central Eastern Desert of Egypt. *Journal of African Earth Sciences*, *69*, 13–25. https://doi.org/10.1016/j.jafrearsci.2012.04.002

Amit Hasan, Md., Bipulendu Basak, S., Haque, M. K., & Roy, S. K. (2026). Comprehensive assessment of groundwater quality in Moilakanda, Mymensingh City: Insights from water quality indices and multivariate analysis. *Cleaner Water*, *5*, 100148. https://doi.org/10.1016/j.clwat.2025.100148

Appukuttan, A., & Reghunath, R. (2025). Machine learning-based groundwater potential mapping and factor analysis in tropical lateritic terrains using self-organizing maps and random forest. *Environmental Monitoring and Assessment*, *197*(12). https://doi.org/10.1007/s10661-025-14779-9

Aranguren-Díaz, Y., Galán-Freyle, N. J., Guerra, A., Manares-Romero, A., Pacheco-Londoño, L. C., Romero-Coronado, A., Vidal-Figueroa, N., & Machado-Sierra, E. (2024). Aquifers and Groundwater: Challenges and Opportunities in Water Resource Management in Colombia. In *Water (Switzerland)* (Vol. 16, Number 5). Multidisciplinary Digital Publishing Institute (MDPI). https://doi.org/10.3390/w16050685

Arefin, R. (2020). Groundwater potential zone identification at Plio-Pleistocene elevated tract, Bangladesh: AHP-GIS and remote sensing approach. *Groundwater for Sustainable Development*, *10*. https://doi.org/10.1016/j.gsd.2020.100340

Asghede, K. M., Daoud, A. M. A., Mohammed, M. A. A., Genzebu, W., Kiflay, K. B., Pecsmány, P., & Vágó, J. (2025). Development of a litho-structural map for the Upper Mereb area, Eritrea, using multi-source remote sensing data and machine learning models. *Remote Sensing Applications: Society and Environment*, *40*. https://doi.org/10.1016/j.rsase.2025.101722

Asghede, K. M., Mohammed, M. A. A., & Vágó, J. (2026). Multivariate statistical, hydrochemical, and indexing approaches for groundwater quality evaluation in a semi-arid region: case study of the Upper Mereb Catchment, Eritrea. *Discover Applied Sciences*, *8*(3), 278. https://doi.org/10.1007/s42452-026-08345-2

Asghede, K. M., & Vágó, J. (2025). Geospatial analysis and analytical hierarchy process for delineating groundwater potential zones. *Multidiszciplináris Tudományok*, *15*(2), 3–14. https://doi.org/10.35925/j.multi.2025.2.1

Asghede, K., & Vágó, J. (2025). Comparative analysis of multi-criteria decision-making techniques for groundwater potential mapping in highland of Eritrea. *Geosciences and Engineering*, *12*(2), 109–127. https://doi.org/10.33030/geosciences.2024.02.009

Badrakh, M., Tserendash, N., Choindonjamts, E., & Albert, G. (2025). Potential of random forest machine learning algorithm for geological mapping using PALSAR and Sentinel-2A remote sensing data: A case study of Tsagaan-uul area, southern Mongolia. *Journal of Asian Earth Sciences: X*, *14*. https://doi.org/10.1016/j.jaesx.2025.100204

Bajwa, R. S., Ahsan, N., & Ahmad, S. R. (2020). A Review of Landsat False Color Composite Images for Lithological Mapping of Pre-Cambrian to Recent Rocks: A Case Study of Pail/Padhrar Area in Punjab Province, Pakistan. *Journal of the Indian Society of Remote Sensing*, *48*(5), 721–728. https://doi.org/10.1007/s12524-019-01090-7

Belkendil, A., Habi, M., Yakhlefoune, M., Sarra, A., Mekkaoui, A., Tariq, A., Jemai, S., Zeghmar, A., Bougrine, H., Zouidi, M., Hadjout, S., & Mansouri, Z. (2025). Integrated GIS-based approach for groundwater potential mapping in arid regions: A case study of Kenadsa-Bechar using AHP and frequency ratio methods. *Groundwater for Sustainable Development*, *30*. https://doi.org/10.1016/j.gsd.2025.101461

Benaissi, L., Tarek, A., Tobi, A., Ibouh, H., Zaid, K., Elamari, K., & Hibti, M. (2022). Geological mapping and mining prospecting in the Aouli inlier (Eastern Meseta,

Morocco) based on remote sensing and geographic information systems (GIS). *China Geology*, *5*(4), 614–625. https://doi.org/10.31035/cg2022035

Berhanu, K. G., & Hatiye, S. D. (2020). Identification of Groundwater Potential Zones Using Proxy Data: Case study of Megech Watershed, Ethiopia. *Journal of Hydrology: Regional Studies*, *28*. https://doi.org/10.1016/j.ejrh.2020.100676

Bezák, V., Bielik, M., Marko, F., Zahorec, P., Pašteka, R., Vozár, J., & Papčo, J. (2023). Geological and tectonic interpretation of the new Bouguer gravity anomaly map of Slovakia. *Geologica Carpathica*, *74*(2), 109–122. https://doi.org/10.31577/GeolCarp.2023.08

Bhadran, A., Girishbai, D., Jesiya, N. P., Gopinath, G., Krishnan, R. G., & Vijesh, V. K. (2022). A GIS based Fuzzy-AHP for delineating groundwater potential zones in tropical river basin, southern part of India. *Geosystems and Geoenvironment*, *1*, 93. https://doi.org/10.1016/j.geogeo.2022.10

Bisht, M. S., Kumar, S., Goel, N. K., Arora, M., & Manikanta, V. (2025). Groundwater quality assessment using water quality indices, hydrogeochemical studies and multivariate statistical analysis in Udham Singh Nagar district, Uttarakhand, India. *Environment, Development and Sustainability*. https://doi.org/10.1007/s10668-025-06244-x

Bjørlykke, K. (2014). Relationships between depositional environments, burial history and rock properties. Some principal aspects of diagenetic process in sedimentary basins. In *Sedimentary Geology* (Vol. 301, pp. 1–14). https://doi.org/10.1016/j.sedgeo.2013.12.002

Bosino, A., Pellegrini, L., Omran, A., Bordoni, M., Meisina, C., & Maerker, M. (2019). Litho-structure of the Oltrepo Pavese, Northern Apennines (Italy). *Journal of Maps*, *15*(2), 382–392. https://doi.org/10.1080/17445647.2019.1604438

Bourmada, A., Khammar, H., Ramzi, H., Chaffai, A., Bouchema, N., & Hamida, B. (2024). Integrated assessment of groundwater quality in Algeria's Souk Ahras region: Implications for sustainable and management water for drinking and irrigation purpose. *Desalination and Water Treatment*, *320*. https://doi.org/10.1016/j.dwt.2024.100827

Bowin, C. (1983). Depth of principal mass anomalies contributing to the earth's geoidal undulations and gravity anomalies∗. *Marine Geodesy*, *7*(1–4), 61–100. https://doi.org/10.1080/15210608309379476

Camacho, M., & Alvarez, R. (2021). Geophysical Modeling with Satellite Gravity Data: Eigen-6C4 vs. GGM Plus. *Engineering*, *13*(12), 690–706. https://doi.org/10.4236/eng.2021.1312050

Chaudhari, M. P., George, A., Sanyal, M., & Shrivastav, P. S. (2024). Hydrochemistry and groundwater quality assessment of Gujarat, India: A compendious review. In *Physics and Chemistry of the Earth* (Vol. 135). Elsevier Ltd. https://doi.org/10.1016/j.pce.2024.103635

Chen, X., Warner, T. A., & Campagna, D. J. (2007). Integrating visible, near-infrared and short-wave infrared hyperspectral and multispectral thermal imagery for geological mapping at Cuprite, Nevada. *Remote Sensing of Environment*, *110*(3), 344–356. https://doi.org/10.1016/j.rse.2007.03.015

Chen, Y., Wang, Y., Zhang, F., Dong, Y., Song, Z., & Liu, G. (2023). Remote Sensing for Lithology Mapping in Vegetation-Covered Regions: Methods, Challenges, and Opportunities. In *Minerals* (Vol. 13, Number 9). Multidisciplinary Digital Publishing Institute (MDPI). https://doi.org/10.3390/min13091153

Cracknell, A. P. (2018). The development of remote sensing in the last 40 years. In *International Journal of Remote Sensing* (Vol. 39, Number 23, pp. 8387–8427). Taylor and Francis Ltd. https://doi.org/10.1080/01431161.2018.1550919

Cracknell, M. J., & Reading, A. M. (2014). Geological mapping using remote sensing data: A comparison of five machine learning algorithms, their response to variations in the spatial distribution of training data and the use of explicit spatial information. *Computers and Geosciences*, *63*, 22–33. https://doi.org/10.1016/j.cageo.2013.10.008

Dandge, K. P., & Patil, S. S. (2022). Spatial distribution of ground water quality index using remote sensing and GIS techniques. *Applied Water Science*, *12*(1). https://doi.org/10.1007/s13201-021-01546-7

Daoud, A. M. A., Shebl, A., Abdelkader, M. M., Mohieldain, A. A., Csámer, Á., Satti, A. M. N., & Rózsa, P. (2025). Remote sensing and gravity investigations for barite detection in Neoproterozoic rocks in the Ariab area, Red Sea Hills, Sudan. *Remote Sensing Applications: Society and Environment*, *37*. https://doi.org/10.1016/j.rsase.2024.101416

Daoud, A. M. A., Shebl, A., Nafi, M., Elrasheed, A. A., Csámer, Á., & Rózsa, P. (2025). Machine learning-based lithological mapping and mineral prospecting using hyperspectral and multispectral remote sensing in Wadi Halfa, north Sudan. *Journal of African Earth Sciences*, *232*. https://doi.org/10.1016/j.jafrearsci.2025.105816

Das, S., & Pardeshi, S. D. (2018). Integration of different influencing factors in GIS to delineate groundwater potential areas using IF and FR techniques: a study of Pravara basin, Maharashtra, India. *Applied Water Science*, *8*(7). https://doi.org/10.1007/s13201-018-0848-x

Davamani, V., John, J. E., Poornachandhra, C., Gopalakrishnan, B., Arulmani, S., Parameswari, E., Santhosh, A., Srinivasulu, A., Lal, A., & Naidu, R. (2024). A Critical Review of Climate Change Impacts on Groundwater Resources: A Focus on the Current Status, Future Possibilities, and Role of Simulation Models. In *Atmosphere* (Vol. 15, Number 1). Multidisciplinary Digital Publishing Institute (MDPI). https://doi.org/10.3390/atmos15010122

Demo, A. H., Gemeda, M. K., Abdo, D. R., Guluma, T. N., & Adugna, D. B. (2025). Impact of soil salinity, sodicity, and irrigation water salinity on crop production and coping mechanism in areas of dryland farming. In *Agrosystems, Geosciences and*

Environment (Vol. 8, Number 1). John Wiley and Sons Inc. https://doi.org/10.1002/agg2.70072

Dheeraj, V. P., Singh, C. S., Alam, A., & Sonkar, A. K. (2025). Hydrogeochemical quality investigation of groundwater resource using multivariate statistical methods, water quality indices (WQIs), and health risk assessment in Korba Coalfield Region, India. *Stochastic Environmental Research and Risk Assessment*. https://doi.org/10.1007/s00477-024-02895-w

Díaz-Alcaide, S., & Martínez-Santos, P. (2019). Review: Advances in groundwater potential mapping. In *Hydrogeology Journal* (Vol. 27, Number 7, pp. 2307–2324). Springer Verlag. https://doi.org/10.1007/s10040-019-02001-3

Dongare, P. N., Sharma, K. V., Kumar, V., Gautam, L., & Singh, K. (2024). Enhancing groundwater resource detection in Ahmednagar District through an integrated GIS framework utilizing AHP, SI, and FR models. *Aqua Water Infrastructure, Ecosystems and Society*, *73*(10), 2055–2078. https://doi.org/10.2166/aqua.2024.195

Drury', S. A., Peart, R. J., & Andrews Deller', M. E. (2001). Hydrogeological potential of major fractures in Eritrea. In *Journal of Afrxan Earth Soences* (Vol. 32, Number 2).

Du, Y., Teoh, Y. J., Abir, I. A., Jaya, R. P., & Ulfa, Y. (2025). Lithological distribution using band ratio technique in Southern Langkawi, Kedah, Malaysia. *Environmental Science and Pollution Research*. https://doi.org/10.1007/s11356-025-36465-6

El Fels, A. E. A., & El Ghorfi, M. (2022). Using remote sensing data for geological mapping in semi-arid environment: a machine learning approach. *Earth Science Informatics*, *15*(1), 485–496. https://doi.org/10.1007/s12145-021-00744-w

Eldosouky, A. M., Elkhateeb, S. O., Ali, A., & Kharbish, S. (2020). Enhancing linear features in aeromagnetic data using directional horizontal gradient at Wadi Haimur area, South Eastern Desert, Egypt. *Carpathian Journal of Earth and Environmental Sciences*, *15*(2), 323–326. https://doi.org/10.26471/cjees/2020/015/132

Elewa, H. H., Nosair, A. M., Ibrahim, A., Zelenakova, M., Pietrucha-Urbanik, K., Habib, H. M., Abdel Moneam, N. A., Ragab, R. M., & Ramadan, E. M. (2024). Use of remote sensing, spatial and geophysical modeling, and real recharging capabilities to identify suitable areas for groundwater exploitation in dry coastal areas. *Journal of Environmental Management*, *363*. https://doi.org/10.1016/j.jenvman.2024.121243

El-Omairi, M. A., El Garouani, M., & El Garouani, A. (2025). Enhanced lithological mapping via remote sensing: Employing SVM, random trees, ANN, with MNF and PCA transformations. *Egyptian Journal of Remote Sensing and Space Science*, *28*(1), 34–52. https://doi.org/10.1016/j.ejrs.2024.12.001

El-Rawy, M., Wahba, M., Fathi, H., Alshehri, F., Abdalla, F., & El Attar, R. M. (2024). Assessment of groundwater quality in arid regions utilizing principal component analysis, GIS, and machine learning techniques. *Marine Pollution Bulletin*, *205*. https://doi.org/10.1016/j.marpolbul.2024.116645

Elrinst, T. A. (1950). *THE SECOND DERIVATIVE METHOD OF GRAVITY INTERPRETATION**. http://library.seg.org/

Elsaidy, A., Yimer, E. A., Mogheir, Y., Huysmans, M., Villani, L., & van Griensven, A. (2025). Groundwater drought and anthropogenic amplifiers: A review of assessment and response strategies in arid and semi-arid areas. In *Science of the Total Environment* (Vol. 978). Elsevier B.V. https://doi.org/10.1016/j.scitotenv.2025.179406

Elvis, B. W. W., Arsène, M., Théophile, N. M., Bruno, K. M. E., & Olivier, O. A. (2022). Integration of shannon entropy (SE), frequency ratio (FR) and analytical hierarchy process (AHP) in GIS for suitable groundwater potential zones targeting in the Yoyo river basin, Méiganga area, Adamawa Cameroon. *Journal of Hydrology: Regional Studies*, *39*. https://doi.org/10.1016/j.ejrh.2022.100997

Epuh, E. E., Okolie, C. J., Daramola, O. E., Ogunlade, F. S., Oyatayo, F. J., Akinnusi, S. A., & Emmanuel, E. O. I. (2020). An integrated lineament extraction from satellite imagery and gravity anomaly maps for groundwater exploration in the Gongola Basin. *Remote Sensing Applications: Society and Environment*, *20*. https://doi.org/10.1016/j.rsase.2020.100346

Eslami, F., Yaghmaeian, K., Mohammadi, A., Salari, M., & Faraji, M. (2019). An integrated evaluation of groundwater quality using drinking water quality indices and hydrochemical characteristics: a case study in Jiroft, Iran. *Environmental Earth Sciences*, *78*(10). https://doi.org/10.1007/s12665-019-8321-1

Fagbohun, B. J., Adeoti, B., & Aladejana, O. O. (2017). Litho-structural analysis of eastern part of Ilesha schist belt, Southwestern Nigeria. *Journal of African Earth Sciences*, *133*, 123–137. https://doi.org/10.1016/j.jafrearsci.2017.05.017

Faraji, H., & Shahryari, A. (2024). Assessment of groundwater quality for drinking, irrigation, and industrial purposes using water quality indices and GIS technique in Gorgan aquifer. *Desalination and Water Treatment*, *320*, 100821. https://doi.org/10.1016/j.dwt.2024.100821

Fosu, S., Nuamah-Amonoo, F. M., Sunkari, E. D., Abrokwah, E., & Ndur, S. A. (2025). Hydrogeochemical controls on groundwater salinization in a coastal aquifer, SE Ghana: Implications for seawater mixing and anthropogenic influences. *Scientific African*, *28*. https://doi.org/10.1016/j.sciaf.2025.e02688

Gehbrehiwot, A., & Kozlov, D. (2019). GIUH-Nash based runoff prediction for Debarwa catchment in Eritrea. *E3S Web of Conferences*, *97*. https://doi.org/10.1051/e3sconf/20199705001

Ghannadpour, S. S., Hasiri, M., Jalili, H., & Shahrabi, H. S. (2024). Identifying alterations of Zafarghand porphyry copper system (Isfahan): employing singularity method and false color composite. *International Journal of Mining and Geo-Engineering*, *58*(3), 315–322. https://doi.org/10.22059/IJMGE.2024.376041.595164

Ghebreab, W., Greiling, R. O., & Solomon, S. (2009). Structural setting of Neoproterozoic mineralization, Asmara district, Eritrea. *Journal of African Earth Sciences*, *55*(5), 219–235. https://doi.org/10.1016/j.jafrearsci.2009.05.001

Ghebrehiwot, A. A., & Kozlov, D. V. (2020). Statistical and spatial variability of climate data in the Mareb-Gash river basin in Eritrea. *Vestnik MGSU*, (1), 85–99. https://doi.org/10.22227/1997-0935.2020.1.85-99

Ghezelbash, R., Maghsoudi, A., & Carranza, E. J. M. (2019). Performance evaluation of RBF- and SVM-based machine learning algorithms for predictive mineral prospectivity modeling: integration of S-A multifractal model and mineralization controls. *Earth Science Informatics*, *12*(3), 277–293. https://doi.org/10.1007/s12145-018-00377-6

Ghimire, M., Byanjankar, N., Regmi, T., Jha, R., Joshi, D. R., & Prasai Joshi, T. (2025). Hydrogeochemical characterization of shallow and deep groundwater for drinking and irrigation water quality index of Kathmandu Valley, Nepal. *Environmental Geochemistry and Health*, *47*(3), 61. https://doi.org/10.1007/s10653-025-02372-5

Ghrefat, H., Kahal, A. Y., Abdelrahman, K., Alfaifi, H. J., & Qaysi, S. (2021). Utilization of multispectral landsat-8 remote sensing data for lithological mapping of southwestern Saudi Arabia. *Journal of King Saud University - Science*, *33*(4). https://doi.org/10.1016/j.jksus.2021.101414

Gidafie, D., Nedaw, D., & Azagegn, T. (2024). Integrated remote sensing and geographic information system overlay analysis for groundwater potential evaluation using AHP and fuzzy AHP: Southern sections of the western Afar rift margin and associated rift floor. *Groundwater for Sustainable Development*, *26*. https://doi.org/10.1016/j.gsd.2024.101310

Githinji, T. W., Dindi, E. W., Kuria, Z. N., & Olago, D. O. (2022). Application of analytical hierarchy process and integrated fuzzy-analytical hierarchy process for mapping potential groundwater recharge zone using GIS in the arid areas of Ewaso Ng'iro – Lagh Dera Basin, Kenya. *HydroResearch*, *5*, 22–34. https://doi.org/10.1016/j.hydres.2021.11.001

Gnanachandrasamy, G., Dushiyanthan, C., Jeyavel Rajakumar, T., & Zhou, Y. (2020). Assessment of hydrogeochemical characteristics of groundwater in the lower Vellar river basin: using Geographical Information System (GIS) and Water Quality Index (WQI). *Environment, Development and Sustainability*, *22*(2), 759–789. https://doi.org/10.1007/s10668-018-0219-7

González-Díez, A., Barreda-Argüeso, J. A., Rodríguez-Rodríguez, L., & Fernández-Lozano, J. (2021). The use of filters based on the Fast Fourier Transform applied to DEMs for the objective mapping of karstic features. *Geomorphology*, *385*. https://doi.org/10.1016/j.geomorph.2021.107724

Grauch, V. J. S., & Cordell, L. (1987). Short Note Limitations of determining density or magnetic boundaries from the horizontal gradient of gravity or pseudogravity data. In *GEOPHYSICS* (Vol. 52, Number 1). http://library.seg.org/

Gurmessa, S. K., MacAllister, D. J., White, D., Ourdraog, I., Lapworth, D., & MacDonald, A. (2022). Assessing groundwater salinity across Africa. *Science of the Total Environment*, *828*. https://doi.org/10.1016/j.scitotenv.2022.154283

Guru, B., Seshan, K., & Bera, S. (2017). Frequency ratio model for groundwater potential mapping and its sustainable management in cold desert, India. In *Journal of King Saud University - Science* (Vol. 29, Number 3, pp. 333–347). Elsevier B.V. https://doi.org/10.1016/j.jksus.2016.08.003

Hagage, M., Hewaidy, A. G. A., & Abdulaziz, A. M. (2025). Groundwater quality assessment for drinking, irrigation, aquaculture, and industrial uses in the waterlogged northeastern Nile Delta, Egypt: a multivariate statistical approach and water quality indices. *Modeling Earth Systems and Environment*, *11*(1). https://doi.org/10.1007/s40808-024-02242-6

Hamamin, D. F. (2024). Integration of multi-geostatistical approaches for deciphering groundwater potential zones in complex water-bearing mediums. In *Groundwater for Sustainable Development* (Vol. 26). Elsevier B.V. https://doi.org/10.1016/j.gsd.2024.101208

Hamdan, M. S., Singh, R., Pathak, R., Kumari, S., & Chauhan, V. (2025). Geospatial mapping of groundwater potential zones using multi-criteria decision-making AHP approach: A study of Kadugli district, south Kurdufan, Sudan. *Journal of African Earth Sciences*, *223*. https://doi.org/10.1016/j.jafrearsci.2024.105513

Hamimi, Z., Hagag, W., Fritz, H., Baggazi, H., & Kamh, S. (2022a). The Tectonic Map and Structural Provinces of the Late Neoproterozoic Egyptian Nubian Shield: Implications for Crustal Growth of the Arabian–Nubian Shield (East African Orogen). *Frontiers in Earth Science*, *10*. https://doi.org/10.3389/feart.2022.921521

Hamimi, Z., Hagag, W., Fritz, H., Baggazi, H., & Kamh, S. (2022b). The Tectonic Map and Structural Provinces of the Late Neoproterozoic Egyptian Nubian Shield: Implications for Crustal Growth of the Arabian–Nubian Shield (East African Orogen). *Frontiers in Earth Science*, *10*. https://doi.org/10.3389/feart.2022.921521

Haughton, P., Davis, C., McCaffrey, W., & Barker, S. (2009). Hybrid sediment gravity flow deposits - Classification, origin and significance. *Marine and Petroleum Geology*, *26*(10), 1900–1918. https://doi.org/10.1016/j.marpetgeo.2009.02.012

Horton, R. K. (1965). An index number system for rating water quality. *J Water Pollut Control Fed*, *37*(3), 300–306.

Hosseininia, M., & Hassanzadeh, R. (2023). Groundwater quality assessment for domestic and agricultural purposes using GIS, hydrochemical facies and water quality indices: case study of Rafsanjan plain, Kerman province, Iran. *Applied Water Science*, *13*(3). https://doi.org/10.1007/s13201-023-01891-9

Ingin, Y. P., Mahringer, D., & El-Athman, F. (2024). Hardness properties of calcium and magnesium ions in drinking water. *Applied Food Research*, *4*(2). https://doi.org/10.1016/j.afres.2024.100600

Islam, K. (2024). An assessment and mapping of groundwater potential zones in the Darjeeling Himalayan region using frequency ratio and analytical hierarchy process. *Journal of Earth System Science*, *133*(3). https://doi.org/10.1007/s12040-024-02364-6

Jarray, H., Hamzaoui-Azaza, F., Zammouri, M., Ouessar, M., Barbieri, M., Carrey, R., Soler, A., Gustaldi, E., & Sahal, S. (2023). Geochemical evaluation of groundwater quality and its suitability for drinking and irrigation purposes in arid and semiarid regions: The case of Zeuss-Koutine and a part of Mio-Plio-Quaternary aquifers (SE Tunisia). *Physics and Chemistry of the Earth*, *132*. https://doi.org/10.1016/j.pce.2023.103483

Kammoun, A., Abidi, M., & Zairi, M. (2022). Hydrochemical characteristics and groundwater quality assessment for irrigation and drinking purposes: a case of Enfidha aquifer system, Tunisia. *Environmental Earth Sciences*, *81*(2). https://doi.org/10.1007/s12665-021-10163-1

Kanji, S., Das, S., & Rajak, C. (2025). A comparative hydrochemical assessment of groundwater quality for drinking and irrigation purposes using different statistical and ML models in lower gangetic alluvial plain, eastern India. *Chemosphere*, *372*. https://doi.org/10.1016/j.chemosphere.2025.144074

Karami, S., Madani, H., Katibeh, H., & Fatehi Marj, A. (2018). Assessment and modeling of the groundwater hydrogeochemical quality parameters via geostatistical approaches. *Applied Water Science*, *8*(1). https://doi.org/10.1007/s13201-018-0641-x

Karmegam, U., Chidambaram, S., Prasanna, M. V., Sasidhar, P., Manikandan, S., Johnsonbabu, G., Dheivanayaki, V., Paramaguru, P., Manivannan, R., Srinivasamoorthy, K., & Anandhan, P. (2011). A study on the mixing proportion in groundwater samples by using Piper diagram and Phreeqc model. *Chinese Journal of Geochemistry*, *30*(4), 490–495. https://doi.org/10.1007/s11631-011-0533-3

Keating, P. (1995). A simple technique to identify magnetic anomalies due to kimberlite pipes. *Exploration and Mining Geology*, *4*(2), 121–125.

Kebede, H., Alemu, A., & Nedaw, D. (2021). Mapping geologic structures from Gravity and Digital Elevation Models in the Ziway-Shala Lakes basin; central Main Ethiopian rift. *Heliyon*, *7*(12). https://doi.org/10.1016/j.heliyon.2021.e08604

Khan, M. A., Nakayama, H., & Nakaya, S. (2024). Groundwater resources investigation using geophysical method in crystalline basement and volcanic rock regions of countries belonging to the East African Rift Valley: A review. In *Journal of African Earth Sciences* (Vol. 220). Elsevier Ltd. https://doi.org/10.1016/j.jafrearsci.2024.105432

Khawla, K., & Mohamed, H. (2020). Hydrogeochemical assessment of groundwater quality in greenhouse intensive agricultural areas in coastal zone of Tunisia: Case of Teboulba region. *Groundwater for Sustainable Development*, *10*. https://doi.org/10.1016/j.gsd.2020.100335

Kong, J., Li, P., & Gong, M. (2025). Hydrogeochemical characterization of groundwater quality in the Weining Plain, northwest China. *Physics and Chemistry of the Earth, Parts A/B/C*, *140*, 103994. https://doi.org/10.1016/j.pce.2025.103994

Kouaied, A., Msaddek, M. H., Zghibi, A., Barrek, A., Pistre, S., & Chenini, I. (2025). Groundwater recharge zone mapping in a coastal mediterranean aquifer applying fuzzy and analytical hierarchy process and frequency ratio: A case study of northeast Tunisia. In *Journal of African Earth Sciences* (Vol. 224). Elsevier Ltd. https://doi.org/10.1016/j.jafrearsci.2025.105537

Kpiebaya, P., Amuah, E. E. Y., Shaibu, A. G., Baatuuwie, B. N., Avornyo, V. K., & Dekongmen, B. W. (2022). Spatial assessment of groundwater potential using Quantum GIS and multi-criteria decision analysis (QGIS-AHP) in the Sawla-Tuna-Kalba district of Ghana. *Journal of Hydrology: Regional Studies*, *43*. https://doi.org/10.1016/j.ejrh.2022.101197

Krishnamoorthy, L., & Lakshmanan, V. R. (2024). Hydrogeochemical Evaluation and Multivariate Statistical Analysis of Groundwater for Sustainable Groundwater Quality Management in the Industrial Corridor of Ranipet District, Tamil Nadu, India. *Water, Air, and Soil Pollution*, *235*(10). https://doi.org/10.1007/s11270-024-07443-4

Kumar, M., Singh, P., & Singh, P. (2022). Integrating GIS and remote sensing for delineation of groundwater potential zones in Bundelkhand Region, India. *Egyptian Journal of Remote Sensing and Space Science*, *25*(2), 387–404. https://doi.org/10.1016/j.ejrs.2022.03.003

Kumar, P., Vishwakarma, C. A., Singh, P., asthana, H., Rena, V., mate, C. chinneikim, & Mukherjee, S. (2024). Hydrogeochemical characterization and water quality evaluation for drinking and irrigation purposes of coastal aquifers of Middle Andaman. *Discover Applied Sciences*, *6*(5). https://doi.org/10.1007/s42452-024-05889-z

Lentswe, G. B., & Molwalefhe, L. (2020). Delineation of potential groundwater recharge zones using analytic hierarchy process-guided GIS in the semi-arid Motloutse watershed, eastern Botswana. *Journal of Hydrology: Regional Studies*, *28*. https://doi.org/10.1016/j.ejrh.2020.100674

Lghoul, M., Abd-Elhamid, H. F., Zeleňáková, M., Abdelrahman, K., Fnais, M. S., & Sbihi, K. (2023). Application of enhanced methods of gravity data analysis for mapping the subsurface structure of the bahira basin in Morocco. *Frontiers in Earth Science*, *11*. https://doi.org/10.3389/feart.2023.1225714

Li, X. kun, Chu, Z. rui, Liu, Y. jun, Zhu, M. ting, Yang, L., & Zhang, J. (2013). Molecular characterization of microbial populations in full-scale biofilters treating iron, manganese and ammonia containing groundwater in Harbin, China. *Bioresource Technology*, *147*, 234–239. https://doi.org/10.1016/j.biortech.2013.08.008

Li, Y., Abdelkareem, M., & Al-Arifi, N. (2023). Mapping Potential Water Resource Areas Using GIS-Based Frequency Ratio and Evidential Belief Function. *Water (Switzerland)*, *15*(3). https://doi.org/10.3390/w15030480

Liu, F. X., Xiong, S. Q., Yang, H., Li, F., Jia, Z., Liu, Q., & Fan, Z. (2025). Identifying ultramafic rocks using artificial neural network method based on aeromagnetic data. *Journal of Applied Geophysics*, *237*. https://doi.org/10.1016/j.jappgeo.2025.105688

Liu, F., Zhang, J., Wang, S., Zou, J., & Zhen, P. (2023). Multivariate statistical analysis of chemical and stable isotopic data as indicative of groundwater evolution with reduced exploitation. *Geoscience Frontiers*, *14*(1). https://doi.org/10.1016/j.gsf.2022.101476

Lu, J., Han, L., Liu, L., Wang, J., Xia, Z., Jin, D., & Zha, X. (2023). Lithology classification in semi-arid area combining multi-source remote sensing images using support vector machine optimized by improved particle swarm algorithm. *International Journal of Applied Earth Observation and Geoinformation*, *119*. https://doi.org/10.1016/j.jag.2023.103318

Lu, L., Wang, Z., Wang, Z., Deng, L., Zou, S., Fan, L., & Yang, Y. (2024). Chemical characteristics and water quality assessment of groundwater in the Dongjiang-Hanjiang River Basin, China. *Journal of Environmental Chemical Engineering*, *12*(6). https://doi.org/10.1016/j.jece.2024.114721

Lubis, A. M., Fauzi, H. W., & Akbar, A. J. (2025). Groundwater potential assessment in Pino region, South Bengkulu, Indonesia using geo-investigation, remote sensing, and GIS approaches. *Results in Earth Sciences*, *3*, 100059. https://doi.org/10.1016/j.rines.2025.100059

Measho, S., Chen, B., Pellikka, P., Trisurat, Y., Guo, L., Sun, S., & Zhang, H. (2020). Land Use/Land Cover Changes and Associated Impacts on Water Yield Availability and Variations in the Mereb-Gash River Basin in the Horn of Africa. *Journal of Geophysical Research: Biogeosciences*, *125*(7). https://doi.org/10.1029/2020JG005632

Mehari, A., Schultz, B., & Depeweg, H. (2006). Salinity impact assessment on crop yield for Wadi Laba spate irrigation system in Eritrea. *Agricultural Water Management*, *85*(1–2), 27–37. https://doi.org/10.1016/j.agwat.2006.05.009

Mkilima, T. (2023). Groundwater salinity and irrigation suitability in low-lying coastal areas. A case of Dar es Salaam, Tanzania. *Watershed Ecology and the Environment*, *5*, 173–185. https://doi.org/10.1016/j.wsee.2023.07.002

Mohamed, A., Asmoay, A., Alarifi, S. S., & Mohammed, M. A. A. (2023). Simulation of Surface and Subsurface Water Quality in Hyper-Arid Environments. *Hydrology*.

Mohammed, M. A. A., Eltijani, A., Szabó, N. P., & Szűcs, P. (2023). Hydro-chemometrics of the Nubian Aquifer in Sudan: an integration of groundwater quality index, multivariate statistics, and human health risk assessment. *Discover Water*, *3*(1), 15.

Mohammed, M. A. A., Kaya, F., Mohamed, A., Alari, S. S., Abdelrady, A., Keshavarzi, A., Szabó, N. P., & Sz, P. (2023). Application of GIS-based machine learning algorithms for prediction of irrigational groundwater quality indices. *Frontiers in Earth Science*, (September), 1–19. https://doi.org/10.3389/feart.2023.1274142

Mohammed, M. A. A., Szabó, N. P., Mikita, V., & Szűcs, P. (2025). Tracking the spatiotemporal evolution of groundwater chemistry in the Quaternary aquifer system of Debrecen area, Hungary: integration of classical and unsupervised learning methods. *Environmental Science and Pollution Research*. https://doi.org/10.1007/s11356-025-36175-z

Mohammed, M. A. A., Szabó, N. P., & Szűcs, P. (2022). Multivariate statistical and hydrochemical approaches for evaluation of groundwater quality in north Bahri city-Sudan. *Heliyon*, *8*(11). https://doi.org/10.1016/j.heliyon.2022.e11308

Mono, J. A., Bouba, A., Ngoh, J. D., Amougou, O. U. I. O., Nyam, F. M. E. A., & Mbarga, T. N. (2024). Lineament Mapping in Batie Area (West-Cameroon) Using Landsat-9 Operational Land Imager/Thermal Infrared Sensor and Shuttle Radar Topography Mission Data: Hydrogeological Implication. *Revue Internationale de Géomatique*, *33*(1), 135–154. https://doi.org/10.32604/rig.2024.049966

Moubchir, T., Faouzi, J., Loukili, E. H., Bendaoud, A., Belkhiri, A., Rezouki, S., Eloutassi, N., & Zahir, I. (2024). Investigation of the Hydrochemistry Quality of the Ouichane Groundwater (Morocco) Using Multivariate Statistical Methods and Diagram Analysis. *Moroccan Journal of Chemistry*, *12*(2), 763–775. https://doi.org/10.48317/IMIST.PRSM/morjchem-v12i2.43030

Nagar, S., Farahbakhsh, E., Awange, J., & Chandra, R. (2024). Remote sensing framework for geological mapping via stacked autoencoders and clustering. *Advances in Space Research*. https://doi.org/10.1016/j.asr.2024.09.013

Navarre-Sitchler, A., Steefel, C. I., Yang, L., Tomutsa, L., & Brantley, S. L. (2009). Evolution of porosity and diffusivity associated with chemical weathering of a basalt clast. *Journal of Geophysical Research: Earth Surface*, *114*(2). https://doi.org/10.1029/2008JF001060

Núñez-Demarco, P., Bonilla, A., Sánchez-Bettucci, L., & Prezzi, C. (2023). Potential-Field Filters for Gravity and Magnetic Interpretation: A Review. In *Surveys in Geophysics* (Vol. 44, Number 3, pp. 603–664). Springer Science and Business Media B.V. https://doi.org/10.1007/s10712-022-09752-x

Ogunsanwo, F. O., Ayanda, J. D., Olurin, O. T., Ogundele, O. E., Ogunsanwo, B. T., & Agboola, K. (2024). Physicochemical and geochemical analysis of groundwater quality in Ilaporu, Ogun State, Nigeria, for domestic and agricultural usage. *HydroResearch*, *7*, 225–247. https://doi.org/10.1016/j.hydres.2024.04.003

Oyda, Y., Hatiye, S. D., & Jothimani, M. (2025). Identification of groundwater potential zones using geospatial analysis and frequency ratio model: the case of Kulfo-Hamassa watershed, Rift Valley, Ethiopia. *Discover Applied Sciences*, *7*(6). https://doi.org/10.1007/s42452-025-07092-0

Ozegin, K. O., Ilugbo, S. O., & Ogunseye, T. T. (2023). Groundwater exploration in a landscape with heterogeneous geology: An application of geospatial and analytical hierarchical process (AHP) techniques in the Edo north region, in Nigeria.

Groundwater for Sustainable Development, *20*. https://doi.org/10.1016/j.gsd.2022.100871

Papini, R., Valboa, G., Favilli, F., & L'Abate, G. (2011). Influence of land use on organic carbon pool and chemical properties of Vertic Cambisols in central and southern Italy. *Agriculture, Ecosystems and Environment*, *140*(1–2), 68–79. https://doi.org/10.1016/j.agee.2010.11.013

Paswan, A. K., Agarwal, A., Kumar, V. A., & Verma, S. C. (2025). Multicriteria decision making for sustainable groundwater development and management in basaltic terrain of Upper Bhima basin, Maharashtra, India. *Groundwater for Sustainable Development*, *31*. https://doi.org/10.1016/j.gsd.2025.101511

Pawar, U., Suppawimut, W., & Rathnayake, U. (2024). Mapping of groundwater potential zones in a drought prone Marathwada Region using frequency ratio and statistical index methods, India. *Results in Engineering*, *22*. https://doi.org/10.1016/j.rineng.2024.101994

Perumal, G. (2025). Geo-statistical analysis and hydrochemical characterization of groundwater quality in the Tuticorin coastal region, Tamil Nadu. *Regional Studies in Marine Science*, *92*. https://doi.org/10.1016/j.rsma.2025.104603

Piras, M., Taddia, G., Forno, M. G., Gattiglio, M., Aicardi, I., Dabove, P., Russo, S. Lo, & Lingua, A. (2017). Detailed geological mapping in mountain areas using an unmanned aerial vehicle: application to the Rodoretto Valley, NW Italian Alps. *Geomatics, Natural Hazards and Risk*, *8*(1), 137–149. https://doi.org/10.1080/19475705.2016.1225228

Popalzai, A., Ahmadi, H., Rahmani, A. B., & Pekkan, E. (2023). *Delineation of Groundwater Potential Zones Using Multi-Criteria Decision Analysis: The Case of Balkh Province, Northern Afghanistan*. 41. https://doi.org/10.3390/iecg2022-14817

Prajapati, R., Mukherjee, B., Singh, U. K., & Sain, K. (2024). Machine learning assisted lithology prediction using geophysical logs: A case study from Cambay basin. *Journal of Earth System Science*, *133*(2). https://doi.org/10.1007/s12040-024-02326-y

Raja Shekar, P., & Mathew, A. (2023). Assessing groundwater potential zones and artificial recharge sites in the monsoon-fed Murredu river basin, India: An integrated approach using GIS, AHP, and Fuzzy-AHP. *Groundwater for Sustainable Development*, *23*. https://doi.org/10.1016/j.gsd.2023.100994

Raju, N. J., Patel, P., Reddy, B. C. S. R., Suresh, U., & Reddy, T. V. K. (2016). Identifying source and evaluation of hydrogeochemical processes in the hard rock aquifer system: geostatistical analysis and geochemical modeling techniques. *Environmental Earth Sciences*, *75*(16). https://doi.org/10.1007/s12665-016-5979-5

Ram, A., Tiwari, S. K., Pandey, H. K., Chaurasia, A. K., Singh, S., & Singh, Y. V. (2021). Groundwater quality assessment using water quality index (WQI) under GIS

framework. *Applied Water Science*, *11*(2). https://doi.org/10.1007/s13201-021-01376-7

Razandi, Y., Pourghasemi, H. R., Neisani, N. S., & Rahmati, O. (2015). Application of analytical hierarchy process, frequency ratio, and certainty factor models for groundwater potential mapping using GIS. *Earth Science Informatics*, *8*(4), 867–883. https://doi.org/10.1007/s12145-015-0220-8

Ren, X., Hou, J., Song, S., Liu, Y., Chen, D., Wang, X., & Dou, L. (2019). Lithology identification using well logs: A method by integrating artificial neural networks and sedimentary patterns. *Journal of Petroleum Science and Engineering*, *182*. https://doi.org/10.1016/j.petrol.2019.106336

Richards, L. A. (1954). *Diagnosis and improvement of saline and alkali soils* (Vol. 78, Number 2). LWW.

Saaty, T. L., & Katz, J. M. (1990). How to make a decision: The Analytic Hierarchy Process. In *European Journal of Operational Research* (Vol. 48).

Sadiq, S., Muhammad, U., & Fuchs, M. (2022). Investigation of landslides with natural lineaments derived from integrated manual and automatic techniques applied on geospatial data. *Natural Hazards*, *110*(3), 2141–2162. https://doi.org/10.1007/s11069-021-05028-6

Safiur Rahman, M., Saha, N., Islam, A. R. M. T., Shen, S., & Bodrud-Doza, M. (2017). Evaluation of Water Quality for Sustainable Agriculture in Bangladesh. *Water, Air, and Soil Pollution*, *228*(10). https://doi.org/10.1007/s11270-017-3543-x

Sahoo, A., Subhadarshini, R., & Baliarsingh, F. (2024). Mapping of groundwater potential zones of Khordha District using GIS and AHP approaches. *Cleaner Water*, *1*. https://doi.org/10.1016/j.clwat.2024.100015

Said, C., Youssef, H., Jamal, A., Ouallali, A., Mohamed, E. A., Larbi, B., Assia, I., Zineb, A., Slimane, S., Lahcen, O., Taha, G., Aziza, L., & Moulay Ahmed, B. D. (2023). Litho-structural and hydrothermal alteration mapping for mineral prospection in the Maider basin of Morocco based on remote sensing and field investigations. *Remote Sensing Applications: Society and Environment*, *31*. https://doi.org/10.1016/j.rsase.2023.100980

Salem, Z. E. S., & Osman, O. M. (2017). Use of major ions to evaluate the hydrogeochemistry of groundwater influenced by reclamation and seawater intrusion, West Nile Delta, Egypt. *Environmental Science and Pollution Research*, *24*(4), 3675–3704. https://doi.org/10.1007/s11356-016-8056-4

Samir, K., El-Sharkawi, M., El-Barkooky, A. N., & Hammed, M. S. (2023). Application of Remote Sensing in Lithological Mapping of Umm Tawat Precambrian Rock Assemblage, North Eastern Desert, Egypt. *Journal of Mining and Environment*, *14*(2), 473–491. https://doi.org/10.22044/jme.2023.12857.2333

Sanad, H., Lhaj, M. O., Zouahri, A., Saafadi, L., Dakak, H., & Mouhir, L. (2024). Groundwater pollution by nitrate and salinization in Morocco: a comprehensive review. *Journal of Water and Health*, *22*(10), 1756–1773. https://doi.org/10.2166/wh.2024.024

Satyakumar, A. V., Pandey, A. K., Singh, A. P., & Tiwari, V. M. (2022). Delineation of structural and tectonic features in the Mahanadi basin, eastern India: New insights from remote sensing and land gravity data. *Journal of Asian Earth Sciences*, *227*. https://doi.org/10.1016/j.jseaes.2022.105116

Savari, M., Damaneh, H. E., & Damaneh, H. E. (2025). The role of social capital in sustainable management of groundwater resources in the agricultural sector: a study in arid and semi-arid regions of Iran. *Agricultural Water Management*, *319*. https://doi.org/10.1016/j.agwat.2025.109752

Schoonover, J. E., & Crim, J. F. (2015). An Introduction to Soil Concepts and the Role of Soils in Watershed Management. *Journal of Contemporary Water Research & Education*, *154*(1), 21–47. https://doi.org/10.1111/j.1936-704x.2015.03186.x

Senosy, M. M., Youssef, M. M., & Abdel Zaher, M. (2013). Sedimentary cover in the South Western Desert of Egypt as deduced from Bouguer gravity and drill-hole data. *Journal of African Earth Sciences*, *82*, 1–14. https://doi.org/10.1016/j.jafrearsci.2013.02.001

Shadmehri Toosi, A., Batelaan, O., Shanafield, M., & Guan, H. (2025). Land Use-Land Cover and Hydrological Modeling: A Review. In *Wiley Interdisciplinary Reviews: Water* (Vol. 12, Number 2). John Wiley and Sons Inc. https://doi.org/10.1002/wat2.70013

Shaibur, M. R., Howlader, M., Ahmmed, I., Sarwar, S., & Hussam, A. (2024). Water quality index and health risk assessment for heavy metals in groundwater of Kashiani and Kotalipara upazila, Gopalganj, Bangladesh. *Applied Water Science*, *14*(5). https://doi.org/10.1007/s13201-024-02169-4

Sharma, B., & Pandey, A. A. (2023). Application of geospatial techniques and analytic hierarchy process in delineating ground water potential zones: a case study from the South Eastern part of Bihar, India. *International Journal of Energy and Water Resources*. https://doi.org/10.1007/s42108-023-00260-1

Sharma, M. K., & Kumar, M. (2020). Sulphate contamination in groundwater and its remediation: an overview. In *Environmental Monitoring and Assessment* (Vol. 192, Number 2). Springer. https://doi.org/10.1007/s10661-019-8051-6

Shelar, R. S., Nandgude, S. B., Pande, C. B., Costache, R., El-Hiti, G. A., Tolche, A. D., Son, C. T., & Yadav, K. K. (2023). Unlocking the hidden potential: groundwater zone mapping using AHP, remote sensing and GIS techniques. *Geomatics, Natural Hazards and Risk*, *14*(1). https://doi.org/10.1080/19475705.2023.2264458

Shemsanga, C. (2024). Groundwater Suitability for Domestic, Irrigation, and Livestock Uses in and Around Dodoma City, Tanzania. *Environmental Quality Management*, *34*(1), e22300.

Sikakwe, G. U. (2023). Mineral exploration employing drones, contemporary geological satellite remote sensing and geographical information system (GIS) procedures: A review. In *Remote Sensing Applications: Society and Environment* (Vol. 31). Elsevier B.V. https://doi.org/10.1016/j.rsase.2023.100988

Singh, G., Singh, J., Wani, O. A., Egbueri, J. C., & Agbasi, J. C. (2024). Assessment of groundwater suitability for sustainable irrigation: A comprehensive study using indexical, statistical, and machine learning approaches. *Groundwater for Sustainable Development*, *24*. https://doi.org/10.1016/j.gsd.2023.101059

Sivkov, D. V., Chitalin, A. F., & Dergachev, A. L. (2020). Using Lineament Analysis to Identify Patterns in the Localization of Au Mineralization in the Taryn Gold Field in the Republic of Sakha (Yakutia). *Izvestiya - Atmospheric and Ocean Physics*, *56*(12), 1546–1559. https://doi.org/10.1134/S0001433820120543

Solomon, S., & Ghebreab, W. (2006a). Lineament characterization and their tectonic significance using Landsat TM data and field studies in the central highlands of Eritrea. *Journal of African Earth Sciences*, *46*(4), 371–378. https://doi.org/10.1016/j.jafrearsci.2006.06.007

Solomon, S., & Ghebreab, W. (2006b). Lineament characterization and their tectonic significance using Landsat TM data and field studies in the central highlands of Eritrea. *Journal of African Earth Sciences*, *46*(4), 371–378. https://doi.org/10.1016/j.jafrearsci.2006.06.007

Solomon, S., & Quiel, F. (2003). Integration of remote sensing and GIS for groundwater assessment in Eritrea. In *Geoinformation for European-Wide Integration* (Number April). https://www.researchgate.net/publication/277806620

Solomon, S., & Quiel, F. (2006a). Groundwater study using remote sensing and geographic information systems (GIS) in the central highlands of Eritrea. *Hydrogeology Journal*, *14*(5), 729–741. https://doi.org/10.1007/s10040-005-0477-y

Solomon, S., & Quiel, F. (2006b). Groundwater study using remote sensing and geographic information systems (GIS) in the central highlands of Eritrea. *Hydrogeology Journal*, *14*(5), 729–741. https://doi.org/10.1007/s10040-005-0477-y

Srivastava, S. K. (2019). Assessment of groundwater quality for the suitability of irrigation and its impacts on crop yields in the Guna district, India. *Agricultural Water Management*, *216*, 224–241.

Subba Rao, N., Dinakar, A., & Sun, L. (2022). Estimation of groundwater pollution levels and specific ionic sources in the groundwater, using a comprehensive approach of geochemical ratios, pollution index of groundwater, unmix model and land use/land cover – A case study. *Journal of Contaminant Hydrology*, *248*. https://doi.org/10.1016/j.jconhyd.2022.103990

Sultana, R., Sarker, N. U., Rahman, M. A., Islam, S. M. N., & Mohiuddin, K. M. (2025). Hydrochemical quality assessment of groundwater for drinking and irrigation and associated health risks in a northern district of Bangladesh. *International Journal of Energy and Water Resources*. https://doi.org/10.1007/s42108-025-00362-y

Sun, Z., Deng, Q., Zhang, L., Song, L., Zhao, H., Liu, J., Wu, X., & Mu, J. (2025). Hydrogeochemical analysis and tracing of heavy metal contamination in groundwater using self-organizing mapping. *Environmental Geochemistry and Health*, *47*(6). https://doi.org/10.1007/s10653-025-02534-5

Suryawanshi, S. L., Singh, P. K., Kothari, M., Singh, M., Yadav, K. K., & Gupta, T. (2023). Spatial and decision-making approaches for identifying groundwater potential zones: a review. *Environmental Earth Sciences*, *82*(20). https://doi.org/10.1007/s12665-023-11149-x

Świtoniak, M., Mroczek, P., & Bednarek, R. (2016). Luvisols or Cambisols? Micromorphological study of soil truncation in young morainic landscapes - Case study: Brodnica and Chełmno Lake Districts (North Poland). *Catena*, *137*, 583–595. https://doi.org/10.1016/j.catena.2014.09.005

Teklay, M. (2006). Neoproterozoic arc-back-arc system analog to modern arc-back-arc systems: Evidence from tholeiite-boninite association, serpentinite mudflows and across-arc geochemical trends in Eritrea, southern Arabian-Nubian shield. *Precambrian Research*, *145*(1–2), 81–92. https://doi.org/10.1016/j.precamres.2005.11.015

Teklay, M., Asmerom, Y., & Toulkeridis, T. (2005). Geochemical and Sr-Nd isotope ratios in Cenozoic basalts from Eritrea: Evidence for temporal evolution from low-Ti tholeiitic to high-Ti alkaline basalts in Afro-Arabian continental flood basalt province. *Periodico Di Mineralogia*, *74*(3), 167–182.

Thanh, N. N., Chotpantarat, S., Trung, N. H., Ngu, N. H., & Muoi, L. Van. (2022). Mapping groundwater potential zones in Kanchanaburi Province, Thailand by integrating of analytic hierarchy process, frequency ratio, and random forest. *Ecological Indicators*, *145*. https://doi.org/10.1016/j.ecolind.2022.109591

Thanh Pham, L., Anh Nguyen, D., Eldosouky, A. M., Abdelrahman, K., Van Vu, T., Al-Otaibi, N., Ibrahim, E., & Kharbish, S. (2021). Subsurface structural mapping from high-resolution gravity data using advanced processing methods. *Journal of King Saud University - Science*, *33*(5). https://doi.org/10.1016/j.jksus.2021.101488

Traore, E. M., Olatunji, A. S., Sidibe, M., Ohiani, U. A., Konate, S. I. M., & Kouagou N'dah, N. D. (2025). Discriminating Lithological Units and Alteration Zones of Bougouni Area Using Remote Technology: Implication for Pegmatite Mapping. *Journal of the Indian Society of Remote Sensing*, *53*(7), 2331–2356. https://doi.org/10.1007/s12524-025-02154-7

Tshanga Matthieu, M., Ncube, L., & Thamaga, K. H. (2026). Geological mapping of copper deposits in the democratic republic of Congo through remote sensing data and

machine learning. *Frontiers in Remote Sensing*, *6*. https://doi.org/10.3389/frsen.2025.1678991

Tunio, I. A., Memon, S. A., Kumar, L., Abbasi, H., Ursani, H., & Ghoto, S. M. (2025). Integrated groundwater quality assessment using GIS and statistical analysis techniques at Islamkot subdistrict in the Thar desert area. *Groundwater for Sustainable Development*, *30*. https://doi.org/10.1016/j.gsd.2025.101469

Upwanshi, M., Damry, K., Pathak, D., Tikle, S., & Das, S. (2023). Delineation of potential groundwater recharge zones using remote sensing, GIS, and AHP approaches. *Urban Climate*, *48*. https://doi.org/10.1016/j.uclim.2023.101415

Velis, M., Conti, K. I., & Biermann, F. (2017). Groundwater and human development: synergies and trade-offs within the context of the sustainable development goals. *Sustainability Science*, *12*(6), 1007–1017. https://doi.org/10.1007/s11625-017-0490-9

Verbovšek, T., & Popit, T. (2018). GIS-assisted classification of litho-geomorphological units using Maximum Likelihood Classification, Vipava Valley, SW Slovenia. *Landslides*, *15*(7), 1415–1424. https://doi.org/10.1007/s10346-018-1004-2

Verma, N., & Patel, R. K. (2021). Delineation of groundwater potential zones in lower Rihand River Basin, India using geospatial techniques and AHP. *Egyptian Journal of Remote Sensing and Space Science*, *24*(3), 559–570. https://doi.org/10.1016/j.ejrs.2021.03.005

Voll, E., Silva, A. M., & Pedrosa-Soares, A. C. (2020). Tracking iron-rich rocks beneath Cenozoic tablelands: An integration of geological, airborne geophysical and remote sensing data from northern Minas Gerais State, SE Brazil. *Journal of South American Earth Sciences*, *101*. https://doi.org/10.1016/j.jsames.2020.102604

Wadi, D., Wu, W., Malik, I., Fuad, A., & Thaw, M. M. (2022). Assessment and feasibility of the potential artificial groundwater recharge in semi-arid crystalline rocks context, Biteira district, Sudan. *Scientific African*, *17*. https://doi.org/10.1016/j.sciaf.2022.e01298

Wang, T., Franz, T. E., & Zlotnik, V. A. (2015). Controls of soil hydraulic characteristics on modeling groundwater recharge under different climatic conditions. *Journal of Hydrology*, *521*, 470–481. https://doi.org/10.1016/j.jhydrol.2014.12.040

Wang, W., Xue, C., Zhao, J., Yuan, C., & Tang, J. (2024). Machine learning-based field geological mapping: A new exploration of geological survey data acquisition strategy. *Ore Geology Reviews*, *166*. https://doi.org/10.1016/j.oregeorev.2024.105959

Wang, Z., & Zuo, R. (2025). Intelligent Lithological Mapping: Challenges and Future Prospective. In *Natural Resources Research*. Springer. https://doi.org/10.1007/s11053-025-10563-1

Whitmeyer, S. J., Nicoletti, J., & De Paor, D. G. (2010). The digital revolution in geologic mapping. *GSA Today*, *20*(4–5), 4–10. https://doi.org/10.1130/GSATG70A.1

WHO. (2011). Guidelines for drinking-water quality. *WHO Chronicle*, *38*(4), 104–108.

Wilcox, L. V. (1948). *The quality of water for irrigation use*.

Xiao, K., Jiao, C., Zou, C., Yang, Y., Li, H., Hu, X., Chen, M., Yin, D., Yang, P., & He, R. (2026). Evaluation of machine learning methods for lithology classification of sandstone-type uranium deposit based on well logging data in the Songliao Basin, Northeast China. *Nuclear Engineering and Technology*, *58*(2). https://doi.org/10.1016/j.net.2025.103946

Xu, J., Wen, X., Zhang, H., Luo, D., Li, J., Xu, L., & Yu, M. (2020). Automatic extraction of lineaments based on wavelet edge detection and aided tracking by hillshade. *Advances in Space Research*, *65*(1), 506–517. https://doi.org/10.1016/j.asr.2019.09.045

Yan, Y., Shi, H., Miao, Q., Zhao, Y., Nie, X., Li, Z., Pan, M., Feng, W., Gonçalves, J. M., & Duarte, I. M. (2025). Evolution of chemical characteristics and irrigation suitability of groundwater in arid and semi-arid regions. *Agricultural Water Management*, *311*. https://doi.org/10.1016/j.agwat.2025.109361

Yin, H., Shi, Y., Niu, H., Xie, D., Wei, J., Lefticariu, L., & Xu, S. (2018). A GIS-based model of potential groundwater yield zonation for a sandstone aquifer in the Juye Coalfield, Shangdong, China. *Journal of Hydrology*, *557*, 434–447. https://doi.org/10.1016/j.jhydrol.2017.12.043

Zamani, M. G., Moridi, A., & Yazdi, J. (2022). Groundwater management in arid and semi-arid regions. *Arabian Journal of Geosciences*, *15*(4). https://doi.org/10.1007/s12517-022-09546-w

Zenande, N., Adesola, G. O., Madi, K., & Gwavava, O. (2024). Groundwater potential assessment in the Eastern Cape, South Africa, using analytical hierarchical process (AHP) technique. *Sustainable Water Resources Management*, *10*(6). https://doi.org/10.1007/s40899-024-01166-4

Zerai, H. (1996). Groundwater and geothermal resources of Eritrea with the emphasis on their chemical quality. In *Ournul of African Earth Scimcrs* (Vol. 22, Number 4).

Zhang, Z., Yin, F., Zhu, Y., & Liu, L. (2025). Lithologic Mapping in the Karamaili Ophiolite–Mélange Belt in Xinjiang, China, with Machine Learning and Integration of SDGSAT-1 TIS, Landsat-8 OLI and ASTER-GDEM. *Natural Resources Research*, *34*(3), 1437–1465. https://doi.org/10.1007/s11053-025-10467-0